Abstract

This study presents a comprehensive investigation into volatile organic compounds (VOCs) in indoor environments, with a particular focus on their primary and secondary emission rates. Despite many previous experimental and modeling studies on VOCs, a significant gap remains in applying laboratory findings to actual building environments. This study bridges this gap by quantifying primary and secondary pollutant loads in an indoor environment, utilizing both existing models and novel approaches to estimate model parameters.

In terms of primary emissions, the existing models are well-developed, but there is a need for determining essential model parameters for practical application in real buildings. This study proposed a novel method for estimating the material-to-air partition coefficient of VOCs based on the similarity between moisture and VOC adsorption. This approach employs the Brunauer–Emmett–Teller (BET) models to extract pertinent physical properties of building materials from moisture sorption isotherms, including specific surface area, porosity, and adsorption energy of water. These properties are then used to estimate monolayer adsorption capacity and adsorption energy accounting for the similarity and difference between VOCs and water vapor in sorption and transport in porous medium.

Regarding secondary emissions, experiments were conducted in a test room to characterize emissions, particularly from hydrogen peroxide-based surface disinfection solutions (potential sources of hydroxyl radicals), and electronic air purifiers (sources of both hydroxyl radicals and ozone). An indoor VOC mixture was simulated in the test room, and emission rates of hydrogen peroxide, hydroxyl radicals, and ozone were obtained. These data were used in the IAQ model developed in this study that accounts for the effect of both the secondary and primary emissions.

A model focused on indoor air quality concerns for secondary emissions as well as primary emissions was developed. This model, a simplification of existing models, concentrates on stable and detectable VOCs originating from indoor ozone and hydroxyl radical-initiated chemical reactions. Despite its simplification, the model capably represents primary and secondary emissions in

the test room. Its reduced computational load makes it suitable for scaling up to the building level or integrating with building control systems.

In conclusion, this study advances the understanding of VOCs, especially regarding their emissions, adsorption processes, and secondary emissions. The results contribute the development of a VOC-building material database and provide practical tools to predict VOC pollution load from primary and secondary emissions, which are essential IAQ design and control in buildings.

VOLATILE ORGANIC COMPOUNDS POLLUTION LOADS IN BUILDINGS AND THEIR IMPACTS ON INDOOR AIR QUALITY

by

Zhenlei Liu

B.S., Shandong Jianzhu University, 2012
M.S., Syracuse University, 2017

Dissertation
Submitted in partial fulfillment of the requirements for the degree of
Doctor of Philosophy in Mechanical & Aerospace Engineering.

Syracuse University
August 2023

ACKNOWLEDGEMENTS

I would like to express my deepest gratitude to my advisor, Dr. Jensen Zhang, for his unwavering support, insightful guidance, and encouragement throughout my PhD program. His expertise, feedback, and dedication to my research have been invaluable, and without his mentorship, this thesis would not have been possible. I also want to extend my heartfelt thanks to his wife, Beverly Guo. Her warm and welcoming environment has been a source of comfort and motivation for me.

I would also like to thank my colleagues, Dr. Meng Kong, Dr. Rui Zhang, Jialei Shen and Xin Guo for their support, friendship, and collaboration. I am grateful for the many conversations and discussions that have enriched my research, and for their feedback and encouragement.

Finally, I would like to thank my own family, especially my wife and daughter, for their unwavering support, patience, and understanding throughout this journey. Their love and encouragement have sustained me through the challenges and difficulties of the program, and I am forever grateful for their constant presence in my life.

Thank you to everyone who has supported and encouraged me throughout this journey. Your contributions have been invaluable, and I am honored and humbled to have had you as my advisors, colleagues, and family.

TABLE OF CONTENTS

LIST OF TABLES

LIST OF FIGURES

CHAPTER 1
INTRODUCTION AND BACKGROUND

1.1 Background

Indoor air quality (IAQ) is crucial for maintaining a healthy and comfortable living environment. Poor IAQ can lead to a variety of health problems such as respiratory issues, allergies, and headaches. Prioritizing indoor air quality is particularly important for individuals who spend significant amounts of time indoors, particularly those who may be more susceptible to respiratory issues or allergies [1]. Indoor air pollutant can come from a variety of sources such as building materials, cleaning products, and outdoor pollutants that enter the indoor space. Proper ventilation, air purification systems, and pollutant source control can help improve indoor air quality and promote a healthy living environment for all occupants.

Ventilation and air purification aims to dilute and remove the pollutants from the air, while pollutant source control focuses on controlling the emission sources or emission rates in the indoor environment. In some industrialized countries, the focus of building energy savings has shifted from insulation to reducing ventilation demand to limit space heating energy consumption. To achieve this, energy-saving buildings are constructed to be airtight, and ventilation rates are reduced to a minimum, which can negatively impact indoor air quality. To maintain pollutant concentrations below health thresholds, higher levels of emission control are required. Consequently, low-emission materials are increasingly used in many countries due to growing concerns about sick building syndrome.

The emissions of volatile organic compounds (VOCs) can be divided into primary and secondary emissions. Primary emissions come directly from building materials, furnishings, equipment, occupant, and occupant activities (such as cooking, copying). Secondary emissions are those derived from chemical reactions in indoor air or on surfaces. IAQ is influenced by the activities

of occupants in a complex manner. Over the past years, in response to the COVID-19 pandemic, disinfectants and air purifiers have been extensively used to make indoor air safer and healthier [2]. However, studies have shown that the use of cleaning agents can greatly increase the levels of VOCs in indoor air [3–5], and the use of ionization/ozonolysis in air cleaners can increase ozone concentration [6, 7]. Ozone is a potent oxidant that can react with VOCs in the gas phase, as well as with building materials on surfaces, to form a wide range of VOCs from secondary emissions [8, 9]. For instance, squalene from human skin oil reacts with ozone (O_3), which could come from air purifiers and laser printers, to produce aldehydes and acetone [10].

Many mechanistic models have been developed and utilized characterize indoor VOC emissions. These models are well-established for primary emissions from dry material, wet coating material, and assembly material. However, implementing these models in real buildings is challenging due to a lack of model parameters for many building materials. Approaches that estimate model parameters based on existing laboratory data and transfer them to real buildings are necessary for implementing these models. For secondary emissions, complex models based on comprehensive chemical reaction mechanisms have been developed. However, these models are too complex to be applied for IAQ assessment because the numerous inputs and heavy computation load. It is not necessary to account for all the reactions indoors since not all chemical reactions and species contribute equally to IAQ. To understand secondary emissions from common occupant activities and address IAQ concerns, a simplified model that focuses on the most significant reaction pathways and reaction products of major IAQ concern is needed.

The present research focuses on developing methods to assess the primary VOC emissions from building materials and secondary emissions from the application of indoor cleaning agents and the use of ionization-based air cleaners, and their impact on IAQ.

1.2 Objectives and Scope

As shown in Figure 1.1, the study includes: 1) quantifying the primary and secondary pollution load in an indoor environment with existing models and new approaches to estimate the model

parameters; 2) performing a series of chamber tests to investigate secondary emissions from occupants' activities; 3) developing an IAQ model that integrates IAQ control strategies such as pollution load control, ventilation, and air purification. The results can be utilized for predicting and evaluating IAQ performance in buildings, as well as comparing and rating the performance of low emission materials under realistic indoor conditions. Three specific research tasks were performed in the present study:

1. Developing a similarity approach that estimates the VOC diffusion and partition coefficients of building materials and furnishings based on the materials' moisture transport and storage properties. This helps to expand the database on the pollution loads due to primary emissions from building materials.

2. Conducting full-scale chamber experiments to characterize secondary emissions resulting from hydroxyl radicals and ozone-initiated chemistry. These experiments were conducted under predefined realistic conditions to investigate the effects of housekeeping activities and the use of electronic air purification devices on secondary emission loads.

3. Developing an IAQ model that takes into account the impact of primary and secondary emission sources, ventilation, and air purification. The model incorporated a simplified representation of indoor chemical reaction mechanisms, focusing specifically on reactions initiated by ozone and hydroxyl radicals.

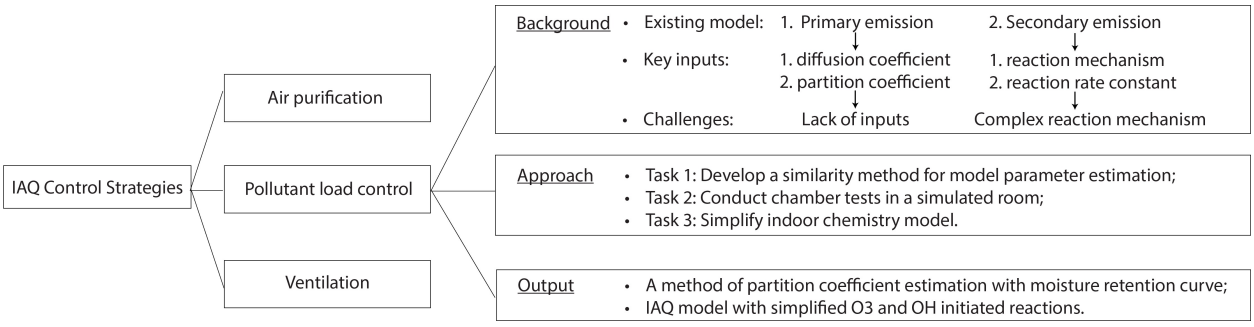

Figure 1.1: IAQ control strategies and scope of this research

CHAPTER 2
LITERATURE REVIEW

2.1 Introduction

This chapter introduces the fundamentals of indoor VOC sources, load, and concentration ranges. It also covers the state of the art in model development for both primary and secondary emissions. To further explain the motivation and specific task of this study, this chapter summarizes the limitations and research gaps in the current understanding of indoor VOC sources and emissions.

2.2 Types and Concentrations of Indoor VOCs

VOCs are a group of molecules that contain carbon and hydrogen atoms (hydrocarbons), and in some cases, oxygen atoms (carbonyl compounds) or chlorine (halogenated compounds). The VOC family includes hundreds of compounds, and their emission sources are numerous and have not been fully characterized to date. VOCs are emitted from a wide range of sources in indoor environments [11]. For example many literatures [12–22] have reported that VOCs can be found in the ambient air, including compounds such as benzene, ethylbenzene, styrene, and toluene. VOCs can also be released by humans, bioeffluents, and hygienic products, including compounds like acrolein, d-limonene, acetaldehyde, and hexanal. Combustion of various types, such as smoking and cooking food, is another significant source of VOCs, with emissions including formaldehyde, acetaldehyde, benzene, naphthalene, and other compounds. Additionally, many cleaning products and room deodorants contain active ingredients, detergents, and/or odorant compounds from the terpene family, such as α-pinene or d-limonene, which are constituents of essential oils extracted from plants or synthesized chemically. Electronic equipment like computers, copiers, and printers can also emit VOCs, with aldehydes like formaldehyde and acetaldehyde, heavy hydrocarbons (e.g., n-decane, n-undecane), and aromatic compounds (e.g., toluene, xylene, and styrene) among

the emissions. Building materials and decoration products are also significant sources of indoor VOCs. The nature of the emitted compounds varies widely depending on the product used, but virtually all materials, including natural materials like wood and wool used for insulation, can release VOCs.

Assessing the impact of VOCs on human health in indoor environments can be complicated due to the number, composition, and high variability of concentrations. The types and quantities of VOCs present indoors are largely determined by the potential sources within the building, resulting in varying levels of VOC compounds and concentrations from one case to another. Figure 2.1 illustrates the distribution of concentration levels of typical air contaminants in residential buildings, based on a review of multiple studies conducted in the U.S., Europe, Asia, and Australia, which included over 20,000 residential building cases in total.

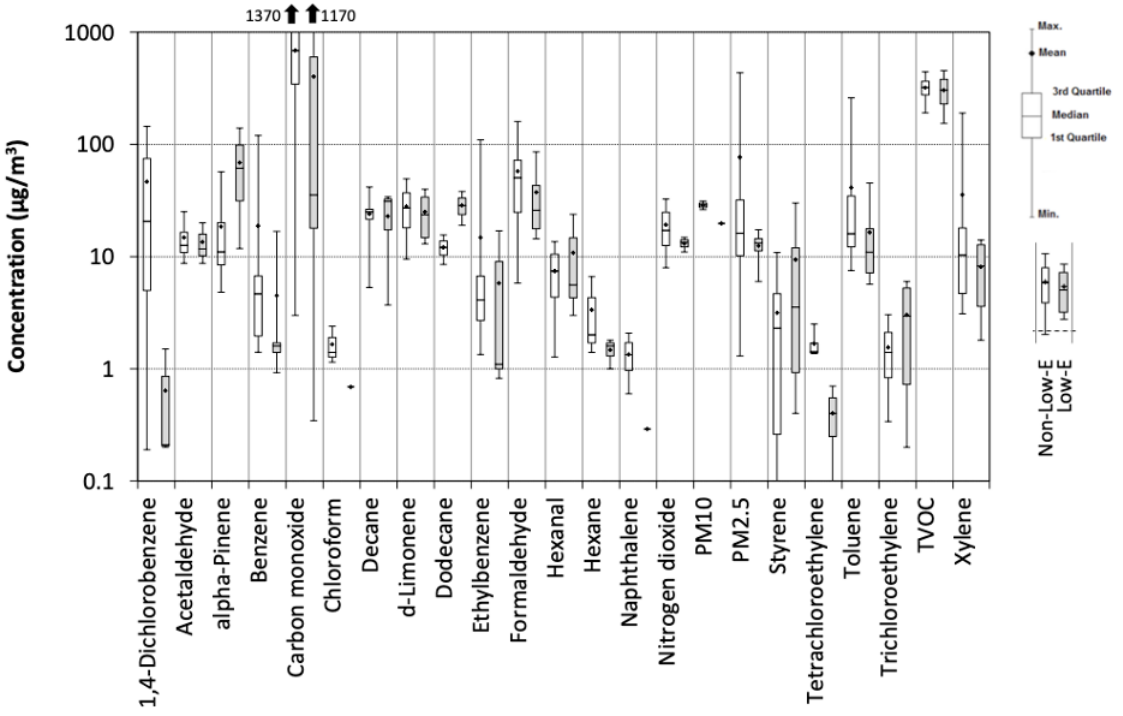

Figure 2.1: Concentration distributions of typical air contaminants measured in the residential buildings based on a review of multiple studies in U.S., Europe, Asia, and Australia (totally over 20 thousand residential buildings studied) [23]. For each pollutant, left unshaded symbols are for non-energy-saving buildings and right shaded symbols correspond to energy-saving residential buildings.

Indoor pollutant concentrations can vary significantly due to a range of factors, including outdoor pollution, indoor sources, ventilation rates, and the use of ventilation systems with specialized filtration and air cleaning technologies. As shown in Figure 2.1, among the 19 VOCs of 23 pollutants studied, 15 showed lower average concentrations in energy-saving residential buildings. Notably, the concentrations of 1,4 dichlorobenzene and toluene were significantly reduced. However, three pollutants showed higher concentrations in energy-saving residential buildings: α-pinene, dodecane, and styrene. Logue's research [24], which mainly drew on data from the USA, revealed that most pollutants had lower concentration levels in energy-saving buildings, with the exceptions of toluene, ethylbenzene, trichloroethylene, and styrene, which were up to 10 times higher in energy-saving buildings. The reduced concentrations of VOCs in energy-saving buildings indicate that controlling VOC emissions from indoor sources can effectively manage VOC levels. Because energy-saving buildings typically have lower ventilation rates than non-energy-saving buildings to reduce energy consumption. However, the less ventilation can result in less fresh air to dilute indoor pollutants emitted from various sources. IAQ issues are often overlooked due to a lack of comprehensive databases, particularly for indoor sources. As a result, accurately predicting IAQ performance can be challenging.

2.3 Primary Emission

Many previous research has been conducted over the past two decades on the primary emission of building materials. However, a major limitation in applying this research to real buildings is the lack of a comprehensive database containing essential parameters for the models. For instance, the diffusion model, which simulates the emission process using an in-material diffusion process and a convective mass transfer over the surface, requires various model parameters. These parameters include the diffusion coefficient (D_m), which is used in Fick's Law to describe the mass flux driven by concentration difference in the material, the partition coefficient (K_{ma}), which describes the equilibrium concentration ratio between pollutant concentration in the material and pollutant concentration in the air, and the initial concentration in the material ($C_m(t = 0)$), which is required

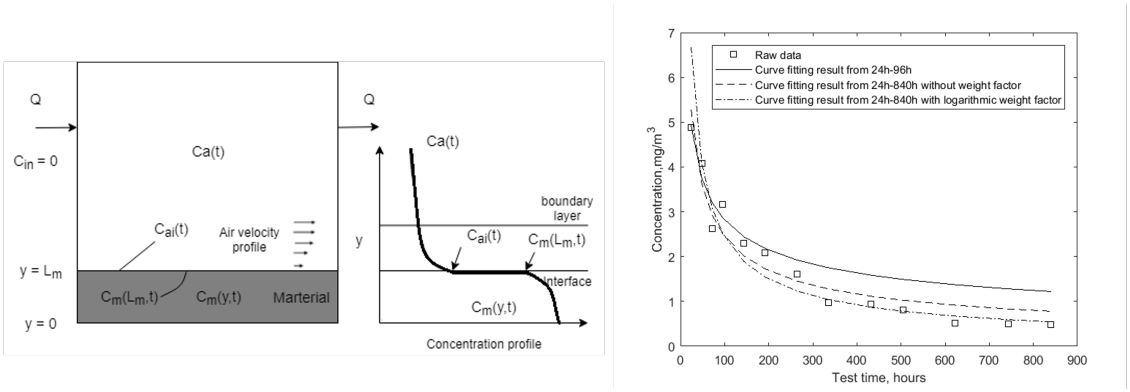

Figure 2.2: A diagram of a dry material emission in a well-mixed single-zone and an example result that collected from a small-scale chamber test [28]

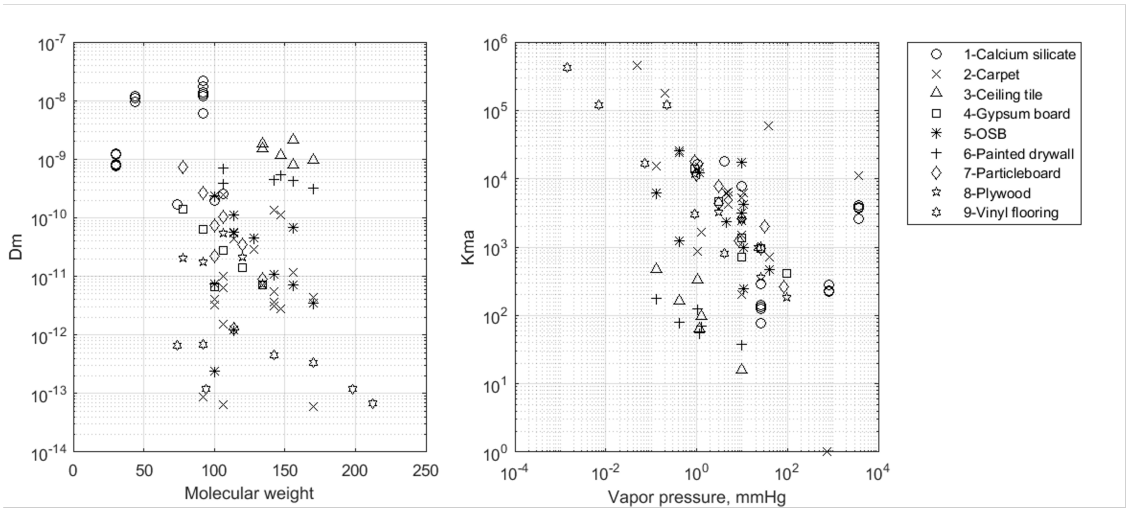

Figure 2.3: Diffusion coefficient (D_m) and partition coefficient (K_{ma}) of VOCs for typical building materials [28]

as an initial boundary condition for the model. Chamber tests have been conducted to measure or estimate these parameters for modeling building material emission and sorption [25–27]. An diagram of a typical small-scale chamber test and example data is shown in Figure 2.2. Nonetheless, the parameters are linked to the characteristics of VOC compounds, such as molecular size and air diffusion coefficient, as well as the properties of materials, like porosity and tortuosity. As indicated in Figure 2.3, there is a significant discrepancy in the values of D_m and K_{ma} among different VOCs (characterized by molecular weight or vapor pressure) and different materials. Establishing a comprehensive database that encompasses all typical materials and major VOCs remains a challenging task.

In this section, this study provided an overview of existing mechanistic models and the advancements in model parameter estimation. Two approaches were discussed: the first involves regression analysis using data from standard chamber tests, while the second is based on the similarity between VOC molecules and water molecules within the same material to estimate VOC properties. In this research, a similarity method will be developed to estimate model parameters by utilizing the available data gathered from chamber tests.

2.3.1 Mass Transfer Model

To assess the impact of VOC emissions from building materials, Little et al. developed a physical mechanistic model based on the equilibrium condition at the air-material interface and Fick's diffusion within the material [25]. By disregarding the convective mass transfer resistance across the air boundary layer on the material surface, they obtained an analytical solution that overestimated early-stage air concentrations from material emissions. Huang and Haghighat took into account convective mass transfer resistance and derived an analytical solution for the model, neglecting VOC concentration in air due to its relatively low value compared to the VOC concentration within the material [29]. They successfully used this model to predict long-term VOC emission rates in chamber tests. Zhang and Xu proposed an enhanced mass transfer model that considered air concentration, although solving for material and air concentrations required the simultaneous use of the finite difference technique [30]. Yang et al. developed a numerical simulation model suitable for dry building materials and applicable to more complex boundary conditions in general [31]. Deng and Kim successfully derived an analytical solution for the model, taking into account both convective mass transfer resistance across the boundary layer and gas phase concentration [32]. Theoretically, this model can be used to assess and predict VOC emissions from homogeneous and porous building materials.

All these models follow the same mass transfer principle, encompassing three key processes: in-material diffusion, which is governed by Fick's law, convective mass transfer across the surface boundary layer over the surface, and partition between the adsorbed phase and gas phase at the

surface. In-material diffusion process is governed by Equation 2.1:

$$\frac{\partial C_m}{\partial t} = D_m \frac{\partial^2 C_m}{\partial y^2} \tag{2.1}$$

Where,

C_m is the concentration of the VOC in the material, μg/m^3.

D_m is the diffusion coefficient of the VOC in the material and is assumed to be constant, m^2/s.

t is the elapsed time, s.

y is the vertical coordinate from the bottom to the top surface of the material, m.

The initial condition of Equation 2.1 is given as follows:

$$C_m(y, 0) = C_m(t = 0) \; at \; 0 \leq y \leq L_m \tag{2.2}$$

Where,

$C_m(t = 0)$ is the initial concentration of the VOC in the material, μg/m^3.

L_m is the thickness of the material, m.

The boundary conditions of Equation 2.1 are:

$$\frac{\partial C_m}{\partial y} = 0 \; at \; y = 0 \tag{2.3}$$

$$-D_m \frac{\partial C_m}{\partial y} = h_m \left(\frac{C_m}{K_{ma}} - C_a\right) at \; y = L_m \tag{2.4}$$

where,

C_a is the concentration of VOC in the chamber air, μg/m^3.

K_{ma} is the partition coefficient.

h_m is the convective mass transfer coefficient of VOC through the top surface, m/s.

For the concentration in the chamber air, the governing equation can be represented as:

$$V \frac{C_a}{dt} = Q(C_o - C_a) + A_m \cdot E \tag{2.5}$$

$$E = h_m(\frac{C_m}{K_{ma}} - C_a) = -D_m\frac{\partial C_m}{\partial y} \tag{2.6}$$

Where,

V is the volume of the chamber, m^3.

A_m is the top surface area of the material, m^2.

Q is the air flow rate, m^3/s.

C_o is the outdoor pollutant concentration, $\mu g/m^3$.

Simulating the VOC transport and emissions using the above equations requires the knowledge of the key model parameters, D_m, K_{ma} and h_m in addition to the parameters representing the material usage or test conditions such as V, A_m, Q and C_o as well as initial condition including $C_a(t = 0)$ and $C_m(t = 0)$. These parameters are influenced by the combined effect of media, environment, and species (MES). Composition and structure of materials directly affect the initial VOC concentration in the material ($C_m(t = 0)$). Factors like porosity, tortuosity and pore size distribution influence both D_m and K_{ma} which are related to the storage and transport of VOCs in the material. Molecular weight was found to correlate with D_m, while vapor pressure was found to correlate with K_{ma}. Additionally, an increased air temperature can escalate the vapor pressure of VOC, which can subsequently influence K_{ma}. Moreover, the higher temperature results in a greater kinetic energy, leading to a higher D_m. The relationship between temperature, D_m and K_{ma} was well established and explored in detail regarding the estimation of D_m and K_{ma} from one reference temperature to others [33]. Therefore, due to the coupled MES effect, particularly regarding material-VOC pairing, the model parameters for real building simulation are not adequate. The following section discusses the approach to obtain D_m, K_{ma}, h_m and $C_m(t = 0)$ for modeling the VOC transport, emission, and adsorption under standard laboratory test conditions. Real building scenarios beyond the standard test condition are discussed separately, as addressed by Zhang et al. [33].

2.3.2 Approaches to Estimate h_m

The convective mass transfer coefficient, h_m, can be predetermined under standard chamber test conditions due to the steady flow patterns in a well-controlled environment. This can be achieved by studying the experimental measurement of a reference VOC compound emission from an activated plasterboard with a 2 mm thick and 20 cm long band of liquid VOC paint [34, 35]. For instance, during the development of the Material Emission Database (MEDB-IAQ) at the National Research Council in Canada, the h_m of two environmental chambers were established to be 1.0 and 1.5 m/h, respectively [34]. Hence, it is possible to independently estimate h_m for the small-scale chamber test, disregarding the specific VOC-material pairing of the chamber. Furthermore, this approach was expanded to be used in a full-scale chamber in a study that examined emissions from "wet" coating materials, which exhibited a stronger response of the VOC emission rate to h_m than dry materials [34].

Besides experiment measurement approach, empirical relationships [29] and Computational Fluid Dynamics (CFD) simulations [27] were also used for the calculation of convective mass transfer coefficient. In the mass boundary layer, the following relationships among Sherwood number (Sh), Reynolds number (Re) and Schmidt number (Sc) exist.

For laminar flow ($Re < 5 \times 10^5$):

$$Sh = 0.664 Sc^{1/3} Re^{1/2} \tag{2.7}$$

For turbulent flow ($Re > 5 \times 10^5$):

$$Sh = 0.037 Sc^{1/3} Re^{4/5} \tag{2.8}$$

Where,

Sh is Sherwood number, $Sh = \frac{h_m}{D_a/l}$. D_a is the diffusion coefficient of the air (m^2/s).

Sc is Schmidt number, $Sc = \frac{\mu}{D_a}$, μ is the kinematic viscosity (m^2/s).

Re is Reynolds number, $Re = \frac{vl}{\mu}$, v is the velocity of the fluid (m/s).

l is the characteristic dimension (m).

Therefore, the convective mass transfer coefficient, h_m, can be calculated independently. When implementing the mass transfer model in a chamber experiment or an actual building, h_m can be predetermined and does not require specific VOC-material pairing. This makes the estimation of h_m straightforward and it is not the central focus of this study.

2.3.3 Regression Analysis Approach to Estimate D_m, K_{ma} and $C_m(t = 0)$

Yang et al. developed a method for determining D_m, K_{ma}, and $C_m(t = 0)$ as an initial boundary condition [31]. They acquired D_m through curve-fitting of normalized experimental data and numerical solutions from standard emission chamber test. K_{ma} was established using a correlation with vapor pressure. $C_m(t = 0)$ was calculated after the process by modifying the initial value to align the peak measured concentration with the predicted highest concentration from the model, using the estimated D_m and K_{ma}. As a result, the accuracy of this correction method heavily relies on the error associated with a single data point, which can be challenging to detect accurately using many sampling techniques. For instance, sorbent samples provide average concentrations over the sampling period, typically requiring 30 minutes to 1 hour to collect a sufficient amount above the detection limit. He et al. devised a non-linear regression technique to obtain D_m, K_{ma}, and $C_m(t = 0)$ using chamber emission test data, and assessed its performance [36, 37]. Their approach utilized Little's model, which overlooks the impact of convective mass transfer through the boundary layer. Xiong et al. developed a linear regression method for estimating D_m and h_m using the analytical solution for the sorption process in a sealed chamber and the wet coating material emission process [38–40]. K_{ma} and C_m were determined based on VOC mass conservation within the chamber and the definition of $K_{ma} = \frac{C_m}{C_a}$ at equilibrium condition. However, the linear regression of the analytical solution only works well in certain cases and not in the emission process of dry building materials [28]. Zhou et al. conducted an experiment to determine K_{ma} and $C_m(t = 0)$ using linear regression of equilibrium state gas phase concentrations across several cy-

cles of sealed and ventilated conditions [41]. This experimental approach shortens the test duration to 48 hours, which is significantly less than many standard chamber tests' periods. However, the emission process in Zhou's study is assumed to occur in a thin layer beneath the surface.

Due to the limitations of existing regression methods, Liu et al. proposed a standardized procedure for obtaining D_m, K_{ma}, and $C_m(t = 0)$ from a standard chamber test [28]. This procedure improved upon previous methods by providing clear description of each steps, such as obtaining a reasonable initial guess and parameter range based on an empirical model. It also investigated the necessary duration of a chamber test and the number of data points required for reliable estimation. Another issue discovered was the iterations stopping at local minimum values, causing the model to fit the chamber test data well but not providing accurate results for year-long simulations. However, with the rapid advancements in machine learning in recent years, regression algorithms have also evolved significantly. The local minimum issue is no longer a major concern, highlighting the potential of machine learning to further enhance regression approaches.

2.3.4 Similarity Approach to Estimate D_m and K_{ma}

Many VOCs or materials may not have adequate chamber test data to apply the regression analysis estimation procedure. To tackle this issue, various approaches have been proposed. For example, Bodalal established an empirical correlation between vapor pressure and partition coefficient [42]. Liu et al. [43] developed a semi-empirical method to connect the partition coefficient with the adsorption potential, which stems from the adsorption potential theory created by Dubinin [44]. However, Dubinin did not provide a clear physical meaning for the adsorption potential, and the adsorption process was described empirically. Some theoretical calculations have been conducted based on microscopic experimental and modeling studies [45, 46]. Although these studies are reliable and comprehensive, transferring them to building material studies is not very practical, considering the costs involved. As a result, a similarity method has been proposed to estimate parameters based on the analogy between water vapor and VOCs on transport and sorption in porous materials . This approach uses well-established data on water vapor for building material

studies.

Xu et al. developed and validated the estimation of D_m using the similarity between water vapor and VOC transport in materials [47, 48]. However, the estimation of K_{ma} using the similarity method has not been explored. From the definition of K_{ma}, the crucial aspect is estimating the concentration of VOCs in the material under the corresponding equilibrium state of a known VOC concentration in the air. Water adsorption isotherms, which provide the adsorption amount of water vapor in a material corresponding to a specific relative humidity, are well-established and widely used in moisture transport models for building materials. Moisture sorption isotherms serve as a suitable candidate for investigating the similarity between water vapor and VOCs adsorption on building materials.

There are some challenges associated with using the similarity approach to estimate partition coefficients, particularly due to the variety of VOC molecules that might require different similarity methods and exhibit distinct interactions with building materials and adsorbed water molecules. For instance, water molecules are polar with strong hydrogen bonds between them. This characteristic might be applicable to formaldehyde, a small polar molecule, but not to methane, a small non-polar molecule. Furthermore, the shape of small molecules can be assumed to be spherical, which may not be an accurate assumption for larger VOC molecules (e.g., decane ($C_{10}H_{22}$) and benzene (C_6H_6), which can be considered as cylindrical and planar molecules, respectively).

In a typical indoor environment, where the concentration of water vapor is significantly higher than that of VOCs, it is crucial to consider the impact of humidity on VOC adsorption. This impact includes: 1) the competition for adsorption at the solid surface, with water vapor being dominant due to its high concentration in the bulk air; and 2) the potential capillary condensation of water vapor within the material's micro-pores. The pores filled with liquid water may no longer contribute, or contribute differently, to the porous transport and storage within the material. Moreover, depending on the solubility of various VOCs in water, the condensed water can either increase or decrease the capacity of VOC adsorption.

2.4 Secondary Emission

2.4.1 Sources of Secondary Emission

Secondary emissions in indoor chemistry refer to the transformations of chemicals and physical processes within indoor spaces. Reactive chemicals in indoor air come from a variety of sources. Pollutants like ozone, nitrogen oxides, particulate matters, and VOCs can enter through ventilation or infiltration via windows, doors, and other openings. Indoor sources of reactive chemicals are numerous, encompassing cleaning products, electronic devices, smoking, combustion appliances, home improvement activities, building materials, furnishings, pesticides, human and pet emissions, and microorganisms such as bacteria and fungi. Numerous sources are associated with occupant activities, like cooking or smoking, which can cause extremely high concentrations of reactive chemicals indoors. For instance, Singer et al. reported a 200-ppb concentration of limonene after indoor cleaning [49], while Kong et al. observed significant amount of particles were generated during the cooking process [50].

The coronavirus disease 2019 (COVID-19) has brought attention to the importance of indoor environments in the spread of respiratory viruses. Research suggested that most COVID-19 outbreaks occurred indoors [51] that the virus can be transmitted through respiratory droplets or aerosols expelled through coughing, speaking, or breathing [2–7]. The fomite route through direct contact with pathogen sources or indirect contact with contaminated surfaces also plays a critical role in the spread of SARS-CoV-2 [8, 9]. Experimental studies have reported long persistence of SARS-CoV-2 (hours to days) on surfaces as well [52, 53], which elevates the transmission risk through fomite route. To reduce the transmission of SARS-CoV-2 indoors, air cleaning devices and surface disinfectants have been suggested to remove virus-laden particles and inactive the virus on surfaces, respectively [54–56]. However, the use of both the air cleaners and surface disinfectants may also generate indoor oxidants which can react with VOCs and lead to the production of secondary emissions. Experiment results indicated that electronic technology-based air cleaner (e.g., electrostatic precipitation, ionization, plasma, UV-PCO) may generate indoor oxi-

dations (e.g., ozone, hydroxyl radicals) that react with VOCs and produce secondary emissions [57–59]. Hydrogen peroxide (H_2O_2) is one of the primary active ingredients in these chemical disinfectants. Hydrogen peroxide used as surface disinfectant, which meets EPA's criteria for against SARS-CoV-2 [55], can vaporize into indoor air and react with gaseous VOCs or deposition on other building surfaces. The surface and gaseous chemical reactions of hydrogen peroxide can generate secondary emissions, which may affect the health of people. The experiment conducted by Zhou et al. [60] suggested that surface deposition dominated gaseous hydrogen peroxide loss. The level of VOCs increased rapidly after surface disinfecting. The presence of sunlight can lead to the photolysis of hydrogen peroxide, which can yield significant hydroxyl radicals (OH) and hydroperoxyl radicals (HO_2). The presence of ozone in air can also react with VOCs or surfaces and yield secondary emissions [61–65].

2.4.2 Modeling Tools of Indoor Chemistry

To better understand the potential secondary emissions that may result from indoor chemical reactions, numerous studies on indoor chemistry, particularly those involving ozone-initiated reactions, have been conducted in recent decades. Additionally, ozone-initiated reactions are sources of hydroxyl radicals and nitrate radicals, which are other two important indoor oxidants [62]. Many studies have investigated the kinetic and mechanisms of reactions between indoor oxidants and other indoor chemicals in both gas-phase and on indoor surfaces [10, 66, 67]. In addition to these kinetic and mechanisms studies, indoor chemical process modeling has also been developed [68–71]. For example, the Indoor Chemistry and Exposure Model (ICEM) and the Detailed Indoor Chemical Model (INCHEM) have been developed based on outdoor atmospheric chemistry models to simulate the transport of pollutant between indoor and outdoor environments, primary emissions from building materials, chemical reactions, and surface deposition [72–74]. INCHEM is a comprehensive model that includes a large number of reactions and species (15,400 reactions and 4,700 species), but it may not be necessary to consider all the reactions or species in evaluating IAQ in a typical indoor environment. It is important to note that gas-phase chemical reactions

must occur on a timescale comparable to or faster than the air exchange rate (AER) in order to significantly impact the indoor environment [11, 62], and that indoor air pollutants can affect human health in different ways. A model that focuses on major indoor chemicals, considers various pollutant sources, and includes simple yet sufficient indoor chemical reaction mechanisms may be more practical for evaluating IAQ.

2.5 Summary and Conclusion

Based on a comprehensive review of existing researches, the concepts of primary and secondary emissions, as well as model development and experimental studies, have been thoroughly examined. The existing gap lies in the transition from laboratory investigations to real-world building applications. The vast number of possible combinations involving VOC species, building materials, building types, lighting conditions, and indoor thermal conditions, which have not been discussed in this section, also affect primary and secondary emissions. The sheer volume of these combinations renders it impossible to study every factor in a laboratory setting. As a consequence, it is crucial to develop reliable and systematic approaches founded on mechanism models, with model parameters derived from laboratory studies, for engineering applications. This will address the existing gap and ensure that the models can operate effectively beyond their standard testing conditions.

CHAPTER 3

SIMILARITY APPROACH TO ESTIMATE PARTITION COEFFICIENT

3.1 Introduction

VOCs are primary contributors to indoor air pollution releasing from various building materials. For a comprehensive understanding of the VOC emission characteristics and an effective control of indoor air pollution, it is crucial to establish accurate measurements and predictions of VOCs emission rates. Parameters like the in-material diffusion coefficients of VOCs (D_m), the material to air partition coefficients (K_{ma}), the convective mass transfer coefficient (h_m), and the initial VOCs concentration in the material ($C_m(t = 0)$) play pivotal roles in quantifying the emission rate of VOCs from building materials. Based on the discussion in Chapter 2, while the estimations of D_m, h_m, and $C_m(t = 0)$ have been well developed, this study primarily focuses on the estimation of K_{ma}. The existing methods of determining K_{ma} present several challenges. For example, the correlation of the partition coefficient with vapor pressure has been established for several specific materials [42]. However, obtaining these correlations is often inconvenient due to the complexity of the experimental methods. Furthermore, these correlations are based purely on experimental data, with little theoretical analysis to back them up.

Various researchers have made attempts to establish prediction formulas for the partition coefficient. For instance, Wang et al. [75] proposed a correlation between the partition coefficient, the liquid density and molar weight of VOCs. However, the applicability of this formula is limited as it may only be effective for VOCs with analogous molecular structures and does not consider influential factors such as temperature and building material parameters. Liu et al. [43] offered an enhancement by deriving a more comprehensive method for predicting partition coefficients, based on the adsorption potential theory by Dubinin [44]. Nevertheless, this approach has its own shortfalls as it fails to elucidate a clear physical meaning for the adsorption potential, and it represents

the adsorption process in an empirical manner.

In this chapter, a novel method was proposed for estimating partition coefficients by assessing the similarity between water molecules and VOC molecules in their characteristics of adsorption by building materials. The moisture sorption isotherm is an effective starting point, offering information on the quantity of adsorbed water at varying humidity levels. This data also helps determine the partition coefficient of moisture for a particular adsorbent in typical RH conditions indoors (30-60% range) where capilary condensation is minimal inside the materials. The similar in the mechanisms of moisture adsorption and VOCs adsorption on an identical adsorbent allows us to calculate the partition coefficient for VOCs.

However, VOCs are various on their molecular structure thus physical and chemical characteristics. But in the same functional group of organic compounds such as alkanes, aldehydes, ketones, and aromatics, VOCs follow certain similarity in their physical characteristics, including latent heat, polarizability, molecular size. There properties contribute to the partition coefficient of VOCs because they can impact the interactions between VOCs molecules and molecules of the adsorbent.

Consequently, the proposed similarity method has been split into two steps: 1) creating a correlation function that can predict the partition coefficient of a reference VOC based on the moisture sorption isotherm data; 2) calculating the partition coefficient of other VOCs using the reference VOCs, based on analogous intermolecular interactions amongst VOCs.

3.2 Partition Coefficient

The partition coefficient is a measure of how a particular chemical compound distributes itself between two different media. In the context of a solid-gas interface, such as VOCs emitting from building materials into the indoor air, the partition coefficient, often denoted by K_{ma}, represents the ratio of the concentration of the VOC in the solid phase (C_m) to its concentration in the gas phase

(C_a) when the system reaches equilibrium (Equation 3.1).

$$K_{ma} = \frac{C_m}{C_a} \tag{3.1}$$

The partition coefficient is an essential parameter in understanding and predicting the emission characteristics of VOCs from building materials. A higher partition coefficient means that the compound prefers to stay in the solid material, and thus it may be slower to emit into the air. Conversely, a lower partition coefficient indicates that the compound readily volatilizes into the air, potentially leading to higher indoor air concentrations.

Several methods have been developed for measuring the partition coefficients for VOCs in solid materials, including the headspace analysis [76], adsorption and desorption tests [26], C-history method [39, 40],and dual-chamber test [47, 48]. However, these measurement methods necessitate laboratory testing for each VOC-material pair, which can be quite expensive. As a result, numerous studies have been conducted to develop various approaches for estimating the K_{ma} of VOCs using existing VOC emission data or VOC sorption test results [28, 36, 37, 39]. This study proposed an approach based on the adsorption isotherm of moisture, leveraging the available databases in studies on moisture and building materials. Based on the definition of K_{ma}, its value can be determined from the adsorption process. As the concentration of VOCs rises in the air, the solid material must adsorb a greater amount of VOCs to restore the system to a new equilibrium state. Consequently, if the amount of VOC adsorption can be quantified under a specific air concentration, K_{ma} can be calculated as per its definition (refer to Equation 3.1).

3.3 Adsorption Models

3.3.1 Langmuir Model

Langmuir developed a model that provides a quantitative description of the volume of gas adsorbed onto an exposed surface [77]. Langmuir model, which is as applicable to localized, monolayer adsorption, includes the following assumptions:

- All the sites of the solid have the same activity for adsorption.
- There is no interaction between adsorbed molecules.
- All of the adsorption occures by the same mechanism that physical adsorption due to the non-specific Van der Waals intermolecular force.
- The extent of adosption is no more than one monolayer on the surface.

The derivation of Langmuir model is achieved by separately accounting for the rates of adsorption and desorption of the adsorbate on the surface. Under equilibrium conditions, the surface is assumed to comprise the fraction Θ, covered by adsorbed molecules, and the bare fraction, $1 - \Theta$. The adsorption rate at the uncovered surface can be expressed as:

$$r_a = k_a p(1 - \Theta) \tag{3.2}$$

Where,

r_a is the adsorption rate, mol/(m^2·s).

p is pressure of adsorbate in gas-phase, Pa.

k_a is the rate constant for adsorption, mol/(m^2·s · Pa), which is a function of temperature and is associated with the rate at which molecules collide with the surface.

$$k_a = \frac{N_A}{(2\pi m_v RT)^{\frac{1}{2}}} \tag{3.3}$$

Where,

N_A is the Avogadro constant, 6.022×10^{23} mol^{-1}.

m_v is molar weight of adsorbate, g/mol.

R is the gas constant, 8.314 J/mol · K.

T is temperature, K.

The desorption rate can be defined as a function of the surface coverage, expressed as:

$$r_d = k_d\Theta \tag{3.4}$$

Where,

r_d is the desorption rate, mol/(m^2·s).

k_d is rate constant of desorption, mol/(m^2·s).

The rate constant of desorption, k_d, can be represented in terms of a factor k_1 and the energy of adsorption, E_1, as:

$$k_d = k_1 e^{\frac{E_1}{RT}} \tag{3.5}$$

As Langmuir model is restricted to monolayer adsorption, Θ can be expressed as the ratio of the amount of adsorption to the monolayer saturation adsorption amount:

$$\Theta = \frac{n_{ads}}{n_m} \tag{3.6}$$

Where,

n_{ads} is adsorption amount on the solid surface, mol/m^2.

n_m is the monolayer saturation adsorption amount, mol/m^2.

At equilibrium, the adsorption and desorption rates achieve a state of dynamic balance.

$$k_a p(1 - \Theta) = k_d\Theta \tag{3.7}$$

By substituting Equation 3.2 - Equation 3.6 into Equation 3.7, the Langmuir model can be articulated as:

$$\frac{n_{ads}}{n_m} = \frac{k_{eq}p}{1 + k_{eq}p} \tag{3.8}$$

$$k_{eq} = \frac{k_a}{k_d} \tag{3.9}$$

Langmuir model, despite its simplicity and specific assumptions, provides a robust framework

to understand the adsorption process at the solid-gas interface. It offers a quantitative relationship between adsorption, gas pressure, and surface coverage, making it a valuable tool in the analysis and prediction of VOC adsorption in building materials.

3.3.2 Brunauer–Emmett–Teller (BET) Model

Because experimental evidence suggested that multilayers adsorption occurred for many adsorbate-adsorbent system, Brunauer et al. [78, 79] extended Langmuir model to account for this phonomennon. Their model, which has come to be known as the BET model, includes the assumptions of the Langmuir model with the exceptions that multilayers adsorption will occur and the heat of adsorption for the first layer will be different from the value for all other layers. The heat of adsorption for all the layers except the first layer is assumed to be the heat of vaporization of the liquid adsorbate.

Assuming that adsorption can occur only from an exposed surface, a consideration of adsorption equilibrium with the bare surface and with the adsorbed monolayer can be used to obtain a general multilayer equation. A picture of how the coverage of each layer is illustrated in Figure 3.1, which denotes the adsorbed molecules in one layer can act as adsorption sites for molecules in the next layer.

$$k_{a,i}\Theta_{i-1} = k_{d,i}\Theta_i \tag{3.10}$$

Where, Θ_i represent the fractions of surface that is covered by i layers of molecules. The sum of the fractions of surfaces equals to unity.

$$\Theta_0 + \Theta_1 + \cdots + \Theta_i + \cdots = 1 \tag{3.11}$$

After integrating and rearranging the terms in the adsorption-desorption equilibrium, final form of BET model can be obtained, which provides a meaningful mathematical relationship between gas pressure, volume of adsorbed gas, and monolayer capacity.

$$\frac{n_{ads}}{n_m} = \frac{C_{BET}\frac{p}{p_s}}{(1-\frac{p}{p_s})(1-\frac{p}{p_s}+C_{BET}\frac{p}{p_s})} \tag{3.12}$$

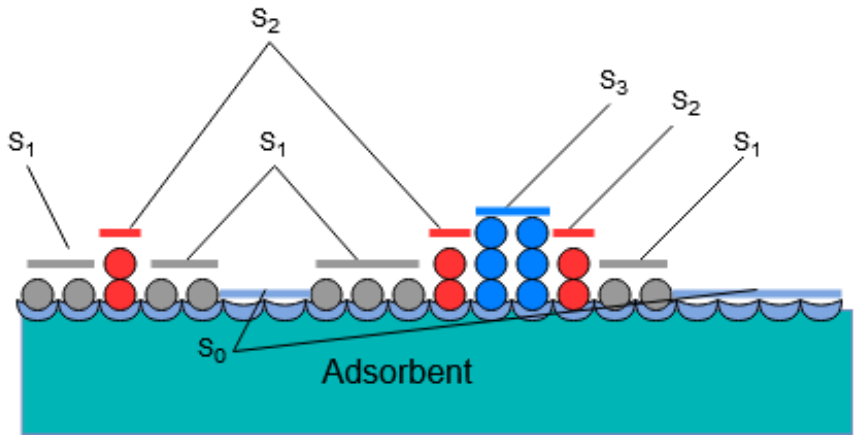

Figure 3.1: Surface coverages of BET model with random stracks of molecules

Where, the BET coefficient, C_{BET}, is commonly assumed to exhibit an exponential relation to the heat of adsorption on first layer minus heat of adsorption on all the other layers, as indicated by the Equation 3.13 [80]:

$$C_{BET} = C_0 e^{\frac{E_1 - E_n}{RT}} = e^{\frac{ln(C_0) + E_1 - E_n}{RT}} = e^{\frac{E_1' - E_n}{RT}} \tag{3.13}$$

Practically, because C_0 is a constant, which is determined by molecular weight and vibration frequency of adsorbent, we can simplify Equation 3.13 by defining an equivalent adsorption energy, E_1'.

BET model serves as an extension of Langmuir model, accommodating multilayers adsorption, and thus, providing a more comprehensive understanding of the adsorption process. By taking into account the interactions between molecules in different layers, it broadens the scope of applicability beyond monolayer adsorption. In the derivations of Langmuir model and BET model, temperature plays a crucial role in the adsorption process. Higher temperature leads to an increase in the kinetic energy of molecules. This enhanced kinetic energy increases the possibility of gas molecule colliding on material's surface. Furthermore, a greater kinetic energy results in a reduced residence time on the surface, due to the accelerated vibration rate caused by higher kinetic energy. This combined effect by temperature was represented by coefficient k_{eq} in Langmuir model and C_{BET} in BET model. The net adsorption energy ($E_1 - E_n$) is generally considered to remain constant, irrespective of temperature [81]. Given a reference temperature, if either $E_1 - E_n$

or C_{BET} is known, then C_{BET} for various temperatures can be determined using Equation 3.13. This method was supported by other studies. For instance, the measured adsorptioin isotherm was compared with model predictions for water, toluene, n-butanol, and iodine on activated carbon and silica gel [81, 82]. Consequently, this study focuses on the standard chamber test condition that both moisture and VOCs adsorptions are happened at a same constant temperature.

3.4 Similarity Approach

3.4.1 Similarity in Adsorption Model

Adsorption models establish a correlation between the concentration of adsorbate in the gas phase and the concentration of adsorbate in the solid phase. This relationship can be used to compute the partition coefficient, K_{ma}, as per its definition. Typically, the concentration of the adsorbate in the gas phase is directly proportional to its partial pressure, denoted by p. The ideal gas law can be utilized to describe the relationship between pressure and concentration in air under conditions of low pressure and temperature substantially below the gas's critical pressure and critical temperature, as represented in Equation 3.14.

$$C_a = \frac{p \cdot m_v}{RT} \tag{3.14}$$

Where,

C_a is concentration of adsorbate in gas-phase, g/m^3.

The amount of adsorbed substance is approximated using the BET model, as shown in Equation 3.12. The quantity of adsorbed substance, denoted by n_{ads}, in the BET equation is measured in moles per unit surface area of the adsorbent. To convert n_{ads} into C_m, it is necessary to multiply by the total surface area of the adsorbent and then divide by the volume of the adsorbent.

$$C_m = n_{ads} \cdot \frac{A_m \cdot m_v}{V_m} \tag{3.15}$$

Where,

A_m is total surface area of adsorbent, m^2.

V_m is volume of adsorbent, m^3.

Hence, the representation of the partition coefficient K_{ma} in the adsorption process, as modeled by the BET model, is illustrated in Equation 3.16.

$$K_{ma} = n_m \cdot \frac{RT}{p} \cdot \frac{A_m m_v}{V_m} \cdot \frac{C_{BET}\frac{p}{p_s}}{(1-\frac{p}{p_s})(1-\frac{p}{p_s}+C_{BET}\frac{p}{p_s})} \tag{3.16}$$

The parameters A_m and V_m are physical properties of the adsorbent, and they are the same for either moisture or VOC adsorption. To predict the partition coefficient K_{ma} for one adsorbate, a from another, b, based on their similarities, the ratio of K_{ma} can be formulated as indicated in Equation 3.17.

$$\frac{K^a_{ma}}{K^b_{ma}} = \frac{n^a_m}{n^b_m} \cdot \frac{p^b m^a_v}{p^a m^b_v} \cdot \frac{\frac{C^a_{BET}\frac{p^a}{p^a_s}}{(1-\frac{p^a}{p^a_s})(1-\frac{p^a}{p^a_s}+C^a_{BET}\frac{p^a}{p^a_s})}}{\frac{C^b_{BET}\frac{p^b}{p^b_s}}{(1-\frac{p^b}{p^b_s})(1-\frac{p^b}{p^b_s}+C_{BET^b}\frac{p^b}{p^b_s})}} \tag{3.17}$$

Two parameters from the BET model, n_m and C_{BET}, require further examination to complete the calculation. In the similarity approach, the first step is to obtain n_m and C_{BET} for moisture adsorption from the moisture sorption isotherm by using BET model to fit the experiment data [80, 83]. Estimations for n_m and C_{BET} for VOCs are derived from the examination of the analogy between moisture adsorption and VOC adsorption on the same adsorbent, and from understanding the properties of water vapor and VOCs and how they impact their respective adsorption characteristics.

3.4.2 Estimation of n_m and C_{BET} Using BET Model for Moisture Isotherm Curve

BET model is a well-established method for characterizing the physical adsorption of gas molecules on a solid surface and serves as the standard for measuring the surface area of materials [80]. This section focuses on using the BET model to fit the moisture isotherm data and estimate parame-

ters n_m and C_{BET}. The moisture isotherm is a curve representing the equilibrium moisture content of a material at various relative humidities (RH) at a constant temperature. Fitting the moisture isotherm data with the BET model can provide the monolayer adsorption capacity, n_m, and the BET constant, C_{BET}, which are parameters critical for understanding moisture adsorption characteristics.

Figure 3.2 provides an example that using BET model to fit the measured adsorption data of moisture on calcium silicate. The parameter n_m represents the amount of moisture that forms a

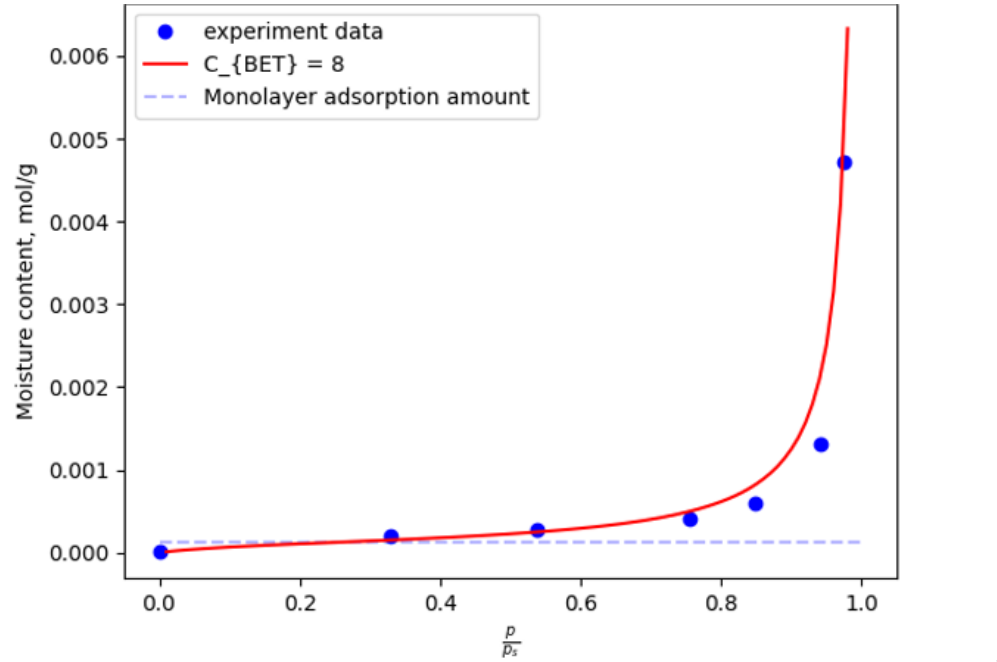

Figure 3.2: Moisture adsorption on calcium silicate with estimted n_m and C_{BET}. Experiment data is from Xu et al. [47].

monolayer on the adsorbent surface. This value is vital to estimate the maximum capacity of the adsorbent. The BET equation is fitted to experimental isotherm data at lower relative humidities where monolayer adsorption predominantly occurs. The C_{BET} parameter is an exponential function of the heat of adsorption for the first layer of molecules adsorbed minus the heat of adsorption for the additional layers of molecules adsorbed on the material as shown in Equation 3.13. C_{BET} offers insight into the strength of the interaction between the moisture and the adsorbent surface.

Fitting the BET model to the moisture isotherm data, and subsequently estimating n_m and C_{BET},

offers valuable information on moisture adsorption. By understanding these parameters, we can estimate the partition coefficients of VOCs, providing a deeper understanding of VOCs adsorption process in the context of moisture adsorption on the same adsorbent.

3.4.3 Estimation of n_m for VOC Adsorption

The parameter n_m represents the saturation adsorption amount at monolayer level, indicating that the adsorbent's surface is fully covered by a single layer of adsorbate molecules. This represents an ideal scenario where the adsorbate molecules are tightly packed without any overlap. The total surface area of the adsorbent can be computed by multiplying the cross-sectional surface area of the adsorbate molecule by the total count of adsorbate molecules (Equation 3.18).

$$A_m = n_m \cdot \alpha \cdot N_A \tag{3.18}$$

Where,

α is effective cross-section surface area of adsorbate molecule, m^2.

N_A is the Avogadro constant, 6.022×10^{23} mol^{-1}.

The ratio of n_m between adsorbate a and b can be represented by Equation 3.19:

$$\frac{n_m^a}{n_m^b} = \frac{\alpha^b}{\alpha^a} \tag{3.19}$$

In Equation 3.18, A_m is assumed to be consistent for both moisture and VOC adsorption. The methodology of measuring specific area through gas adsorption is well-developed. Experimental data reveals slight discrepancies in the specific area of activated carbon and silica when measured by water, nitrogen, and benzene [84]. This variation in measurement can be attributed to the resolution of the adsorption technique, which depends on the size of the adsorbate molecule. Furthermore, these differences can be influenced by various factors such as equipment used, pore dimensions, pore shape, and operational temperature. As a result, the A_m value obtained via moisture adsorption may not accurately represent the true A_m. However, in this study, VOC adsorption

is analogous to moisture adsorption, maintaining a constant adsorption surface for both. As illustrated in Figure 3.3, the pore dimensions of building materials are typically magnitudes larger than the molecular sizes of moisture and VOCs. Consequently, there are no micro-pores that are exclusively accessible to water molecules and not to VOC molecules.

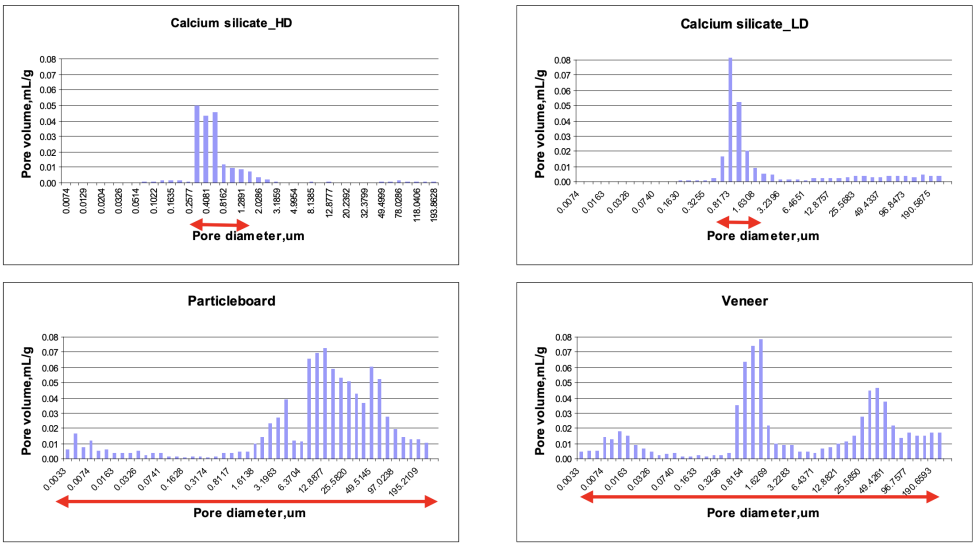

Figure 3.3: Pore volume distribution of high density (HD) calcium silicate, low density (LD) calcium silicate, particleboard, and veneer [48]

A central challenge involves estimating the effective cross-sectional area of different adsorbate molecules. Emmett and Brunauer [85] developed a method assuming that the adsorbate molecules form a hexagonal close-packed arrangement, and the adsorbed molecule is in a liquid phase. From these assumptions, they derived Equation 3.20 to compute the cross-sectional area of the adsorbed molecule.

$$\alpha = f \cdot \left(\frac{m_v}{\rho \cdot N_A} \right)^{2/3} \tag{3.20}$$

Where,

f is the packing factor, which depends on molecular shape and interactions between molecules, such as repulsive steric forces. For hexagonal close-packing f becomes 1.091 [85]. Additional types of packing and shapes of molecule are provided in Table 3.1. In general, molecules in shape of discs and cylinders pack more tightly than molecules in shape of sphere, which results in a higher packing factor. Close packing provides the highest packing factor given less space between

Table 3.1: Maximum packing factors for close packing, random close packing, and random loose packing across spherical, disc, and cylindrical molecules [86]

Shape of molecules	close-packing	random close-packing	random loose-packing
Spheres (3D)	1.091	0.893	0.816
discs, cylinders (2D)	1.135	1.059	1.059

molecules.

ρ is the absolute density of the liquid adsorptive at the operational temperature.

This methodology is commonly applied to estimate the cross-sectional surface area of adsorbed molecules. Nevertheless, Pickering and Eckstrom argued that α is dependent on both the adsorbate and the adsorbent [87]. Substantial evidence supports the argument that the effective value of α is influenced by several factors [80]: (a) the properties of the adsorbate and the chemical composition of the adsorbent which impact the adsorbate-adsorbent and adsorbate-adsorbate interactions; (b) the physical characteristics of the adsorbent surface including roughness, pore shape, and pore size; and (c) the operational temperature. Table 3.2 provides the measured cross-section surface area of 11 adsorbates on different adsorbent and compared with estimated cross-section surface area by Equation 3.20 and Equation 3.21. Equation 3.21 is introduced by Zhao et al. [81] to correlate measured cross-section surface area and the estimation made by Equation 3.20. Because Equation 3.20 may not provide an accurate representation of VOC molecules, particularly for chain-alkanes, which behave more like cylindrical molecules, and aromatic VOCs, which behave more like planar molecules. This is due to Equation 3.20 is oversimplified these VOC molecules as small spherical entities.

$$\alpha' = 1.678\alpha - 0.0616 \tag{3.21}$$

Where, α' is the corrected cross-section surface area of VOCs, which is consistently larger than the estimation of α by Equation 3.20.

As illustrated in Table 3.2, the cross-sectional area of water is the smallest among all the VOCs when adsorbed on the same adsorbents, which is consistent with the smaller molecular size of

water. The surface area of the water cross-section on SiO_2, a hydrophilic substance, varies significantly across the 7 different SiO_2 samples tested at 25 ^oC. This observation is same as ethanol, which is a small polar VOC. Even the glass, which is composed of SiO_2, presents a substantial difference when compared to SiO_2 powder. VOCs (alkane and aromatics) show no significant difference on hydrophobic and hydrophilic substance. Equation 3.20 provides an accurate estimation for water and ethanol on graphitized carbon and on 2 out of the 7 SiO_2 samples. In contrast, Equation 3.21 works well for 2 of the 7 SiO_2 samples, but it tends to overestimate when applied to graphitized carbon. In terms of estimating the cross-section of non-polar VOCs, Equation 3.21 generally yields better results than Equation 3.20, which typically underestimates the cross-section of VOCs.

In the similarity approach, the properties of the adsorbent, such as its chemical composition, surface structure, pore structure, and temperature, are the same for either moisture or VOC adsorption. As a result, information on these factors is imbeded into the n_m and C_{BET} values extracted from the moisture isotherm. Upon estimating the α values for VOCs, their corresponding n_m values can be derived using equation Equation 3.19. These estimated n_m values can then be used in future calculations of K_{ma} in the BET model for VOC adsorption.

3.4.4 Estimation of BET Coefficient for VOCs

The BET coefficient depends on the adsorption energy on the first layer and adsorption energy on other layers. Adsorption energy, when a polar molecule is adsorbed onto a polar or ionic surface, can include a variety of specific interaction contributions. A proposed comprehensive expression for the adsorption energy on the first layer (E_1) at very low surface coverage is formulated as the sum in Equation 3.22 [80]:

$$E_1 = E_D + E_R + E_p + E_{F\mu} + E_Q \tag{3.22}$$

in which E_D and E_R denote the non-specific dispersion and repulsion contributions, and the terms E_p, $E_{F\mu}$, and E_Q represent specific contributions: polarization, field-dipole, and field gradient-quadrupole energies, respectively.

Table 3.2: Cross-section surface areas (in unit nm^2) of some adsorbates estimated by different methods. All literature data are sourced from McClellan et al. [88] unless specifically indicated otherwise.

Compound	Adsorbent	Literature	Volume (nm^3)	Equation 3.20	Equation 3.21
Water	Graphitized carbon	0.105 - 0.106	0.0044	0.105	0.125
	SiO_2	0.108 - 0.187			
	Glass	0.195			
Nitrogen	SiO_2	0.129	0.0056	0.162	0.210
Carbon dioxide	Graphitized carbon	0.142	0.0062	0.170	0.224
Methanol	Graphitized carbon	0.160	0.0097	0.180	0.240
	SiO_2	0.265			
Ethanol	Graphite	0.220	0.0123	0.231	0.326
	SiO_2	0.220 - 0.353			
	Glass	0.200			
Butanol	Graphite	0.353	0.0171	0.312	0.462
Butane	Graphitized carbon	0.397 - 0.425	0.0170	0.323	0.480
	SiO_2	0.370 - 0.560			
	Metal, glass	0.469			
Pentane	Graphitized carbon [80]	0.452	0.0212	0.362	0.542
	Al_2O_3	0.382 - 0.636			
Hextane	Graphitized carbon [89]	0.460 - 0.515	0.0256	0.413	0.631
	SiO_2	0.488 - 0.806			
Benzene	Graphitized carbon	0.400 - 0.483	0.0174	0.320	0.476
	SiO_2	0.360 - 0.527			
Toluene	Graphitized carbon	0.460	0.0225	0.344	0.515
	SiO_2	0.460 - 0.582			

The energy of adsorption is clearly influenced by the characteristics of the adsorption system, which encompasses both the adsorbent and adsorbate. Graphitized carbon, which has a surface structure composed almost entirely of the graphitic basal planes, gives non-specific interactions with a wide range of different adsorbates. When a polar molecule is adsorbed on this surface, $E_D + E_R$ is much larger than $E_p + E_{F\mu} + E_Q$ which is unlikely to contribute more than 10% to the total interaction energy [80]. There is a near consistent linear relationship between E_1 and the carbon count in the same functional group (Figure 3.4). The non-specific interactions between graphitized carbon surfaces and gas molecules, as confirmed by substantial evidence, can be extended to encompass all gas adsorbates [80].

For building materials, there is no sufficient data to proof the linear correlation of E_1. To compute the adsorption energy between complex molecules (VOC molecules and material molecules) is very complex and usually rely on computer simulation such as molecular simulation, density functional theory. Some simplifying assumptions can be applied to highlight similarities between VOCs within the same functional group. This is due to the non-directional and additive nature of dispersion forces, and the similar specific contributions within the same functional group [80]. For example, normal alkanes, of general formula $CH_3 - (CH_2)_n - CH_3$, can be considered as a cylinder. When such alkane molecules interact with adsorbent molecules, the adsorption energy approximately equals to sum of CH_3 groups at the end and every CH_2 groups. As the number of carbon atoms increases, the influence of total CH_2 interactions increased linearly, whereas the interactions of CH_3 groups remain constant. Experimental results demonstrate a good agreement with this simplified assumption for straight-chained alkane, straight-chained alcohols, and carboxylic acids [80]. The next section will introduce a methodology proposed in this research for estimating the adsorption energy of VOCs within the same group using the estimated adsorption energy of water on same building materials.

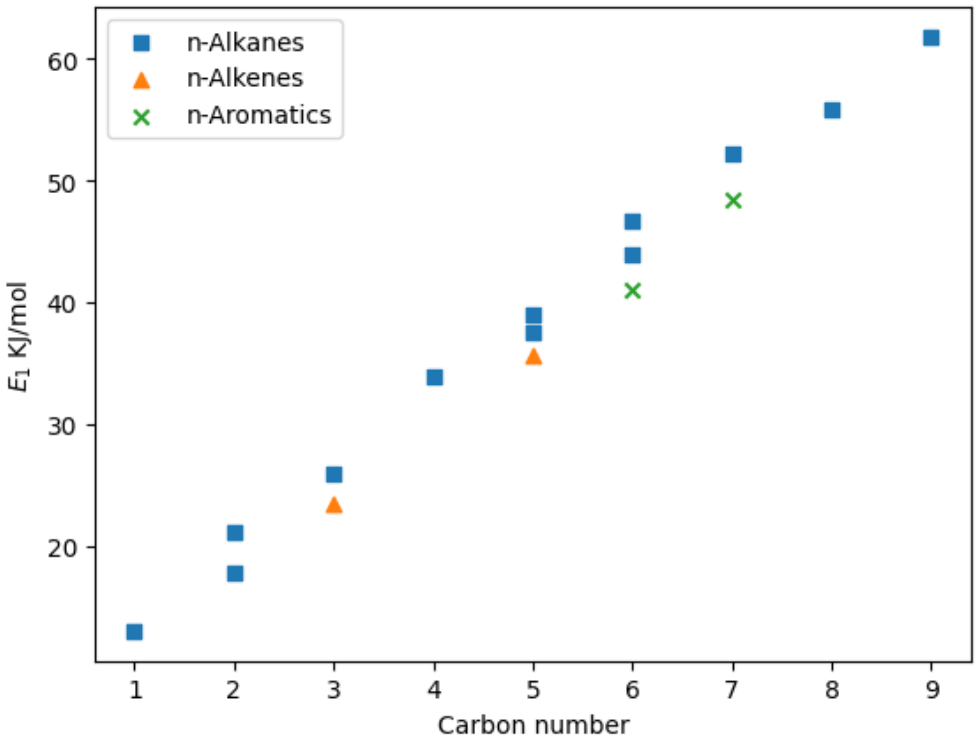

Figure 3.4: Energy of adsorption versus carbon number on graphitized carbon [80]. Alkanes: methane, ethane, propane, butane, pentane, hexane, heptane, octane, nonane. Alkenes: propene, pentene. Aromatics: benzene, toluene.

3.4.5 Estimation of Adsorption Energy for Building Materials

Dubinin et al. [44] expanded their potential theory to incorporate the adsorption of diverse gases on an identical solid. They proposed that the adsorption potential, determined by the interactions between the adsorbate and adsorbent, would retain a consistent ratio for similar compounds. This postulation has gained acceptance and confirmation from subsequent researches [75, 90]. They introduced the concept of an affinity coefficient, γ, derived from Van der Waals forces. The long-range interaction between polar molecules, known as the van der Waals force, is made up of three distinct forces: the induction force, the orientation force, and the dispersion force. Among these, dispersion forces are generally dominant, except in the case of small, highly polar molecules like water, formaldehyde, and acetone. Dispersion forces influence various phenomena, such as adhesion, surface tension, physical adsorption, strengths of solids. London's dispersion interaction energy equation, applicable to two atoms or molecules, associates the dispersion force with ion-

ization energy and polarization of the molecules [86].

Affinity coefficient approximates the ratio of the polarizations of the two molecules, with polarization being proportional to the coefficient that describes the attractive force in Van der Waals forces. Practically, molar volumes of two different molecules in the liquid phase commonly used to estimate γ because molecular weight and liquid density are easy to obtain. Zhao et al. [81] conducted a comparison between estimations made using Van der Waals force and molar volumes for γ. Their results indicated that the molar volume approach proves to be an effective method. Thus, the adsorption energy of an adsorbate can be estimated using γ, given the known adsorption energy of a similar adsorbate to the same adsorbent. This is expressed is Equation 3.23:

$$\frac{E_1^a}{E_1^b} = \frac{\frac{m_v^a}{\rho^a}}{\frac{m_v^b}{\rho^b}} = \gamma \tag{3.23}$$

The approach that is represented by Equation 3.23 tends to oversimplify adsorbate-adsorbent interactions by assuming they can be represented by a single ratio. Notwithstanding, the model's reliance on dispersion forces, a key constituent of Van der Waals forces, can lead to inaccuracies. Although these forces typically dominate, orientation and induction forces can become pivotal when dealing with highly polar molecules like water, formaldehyde and acetone.

The model's oversimplification further manifests when considering the physical properties of the adsorbate molecules. It neglects to account for the influence of molecule size and shape. When dealing with larger or non-spherical molecules, particularly those with complex structures or elongated chains, the simplified assumptions begin to break down. For these larger molecules, the dispersion force operates between the centers of electronic polarization within each molecule, rendering the center-to-center distance between molecules is less important than small molecules. As such, a molecule's shape, size, and orientation can significantly impact its interactions with the adsorbent, subsequently altering the adsorption energy [80].

As a result, the applicability of Equation 3.23 is contingent on the availability of adsorption energy data for a comparable adsorbate on the same adsorbent. The attempt to estimate adsorption

energy solely based on molar volume encounters difficulties, especially when contrasting water with VOCs or VOCs belonging to different groups, such as chain alkanes and aromatics.

The precise computation of adsorption energy often necessitates the employment of sophisticated models such as density functional theory (DFT) within the field of quantum chemistry. DFT typically calculates adsorption energy as the discrepancy between the total energy of the adsorbed system and the cumulative total energies of the unassociated adsorbent and adsorbate [45]. However, such computations fall outside the scope of the present study.

This study suggests an empirical estimation tailored to particular adsorbate-adsorbent combinations. The adsorption energy extracted from moisture isotherms requires adjustment to account for the influence of the molecular structure of a reference VOC and the chemical composition of the adsorbent. Therefore, measured adsorption energy is necessary for both moisture and the reference VOC. Equation 3.23 is applicable for subsequent estimations from the reference VOC to VOCs with similar properties.

Table 3.3 provides the adsorption energy of water, toluene, and formaldehyde for four building materials and activated carbon. In activated carbon, despite its typically larger specific surface area compared to building materials, water displays the lowest E_1 and K_{ma} values. This can be anticipated due to the hydrophobic nature of activated carbon, which makes it less attractive to polar molecules such as water. Consequently, the E_1 for the water-activated carbon pairing is even lower than E_n (44.1 KJ/mol) for water, illustrating that water molecules form stronger bonds among themselves. On the other hand, toluene exhibits the highest E_1 and K_{ma} on activated carbon. This is due to the interaction between the carbon molecules and the aromatic ring in toluene, forming a $\pi - \pi$ bond [45]. The adsorption energy across building materials exhibits consistency, with the exception of particle board. The latter material, due to its composition of wood particles, sawdust, wood chips, and adhesive, presents a more complex structure that affects its adsorption energy profile. Adsorption energy can greatly fluctuate with different adsorbents, leading to significant variations in K_{ma}. This suggests that no straightforward and universal estimation exists for dissimilar molecules. The proposed similarity approach requires both moisture isotherm data as

Table 3.3: Adsorption energy of water, toluene and formaldehyde for four building materials and activated carbon. Experimental data are sourced from [42, 48, 91]

Material	water		toluene		
	K_{ma}	E_1 KJ/mol	K_{ma}	E_1 KJ/mol	$E_{1,H_2O}/E_{1,toluene}$
Activated carbon	84	40.1	7624	53.3	0.75
Calcium silicate	402	45.8	133	41.3	1.11
Gypsum board	4203	47.9	941	52.2	0.91
Plywood	30159	44.1	358	42.8	1.03
Particle board	101571	89.0	968	43.8	2.03

Material	water		formaldehyde		
	K_{ma}	E_1 KJ/mol	K_{ma}	E_1 KJ/mol	$E_{1,H_2O}/E_{1,formaldehyde}$
Calcium silicate	402	45.8	2597	47.1	0.97
Particle board	101571	89.0	28326	47.3	1.88

well as a minimum of one data set for a reference VOC that belongs to the same functional group as the target VOC. The estimation of adsorption energy on building material for a given reference VOC and target VOCs relies on the non-directional and additive nature of dispersion force. As a result, the estimation using affinity coefficient is confined to the same functional group, which is predominantly governed by non-specific interactions with building material. For VOCs associated with multiple functional groups, further studies are needed. For instance, theoretical simulation might be used to determine which functional group is more suited for a particular VOC-material pairing.

3.4.6 Implementation of Similarity Approach in VOCs Groups

The method to estimate K_{ma} using similarity between moisture and VOC adsorption is outlined in Figure 3.5. The estimation of C_{BET} of water to C_{BET} of reference VOC is empirical. The estimation of C_{BET} from the reference VOC to the target VOC relies on the assumed linear correlation of E_1 on building materials. The estimation of n_m draws from the cross-section area of molecules in the adsorbed phase and specific area of the material. The similarity was implemented to and verified by existing literature data.

In Figure 3.6 and Figure 3.7, the estimated values of K_{ma} are compared with the actual measurements and the power law model derived by Bodalal et al., which is based on the fitting of

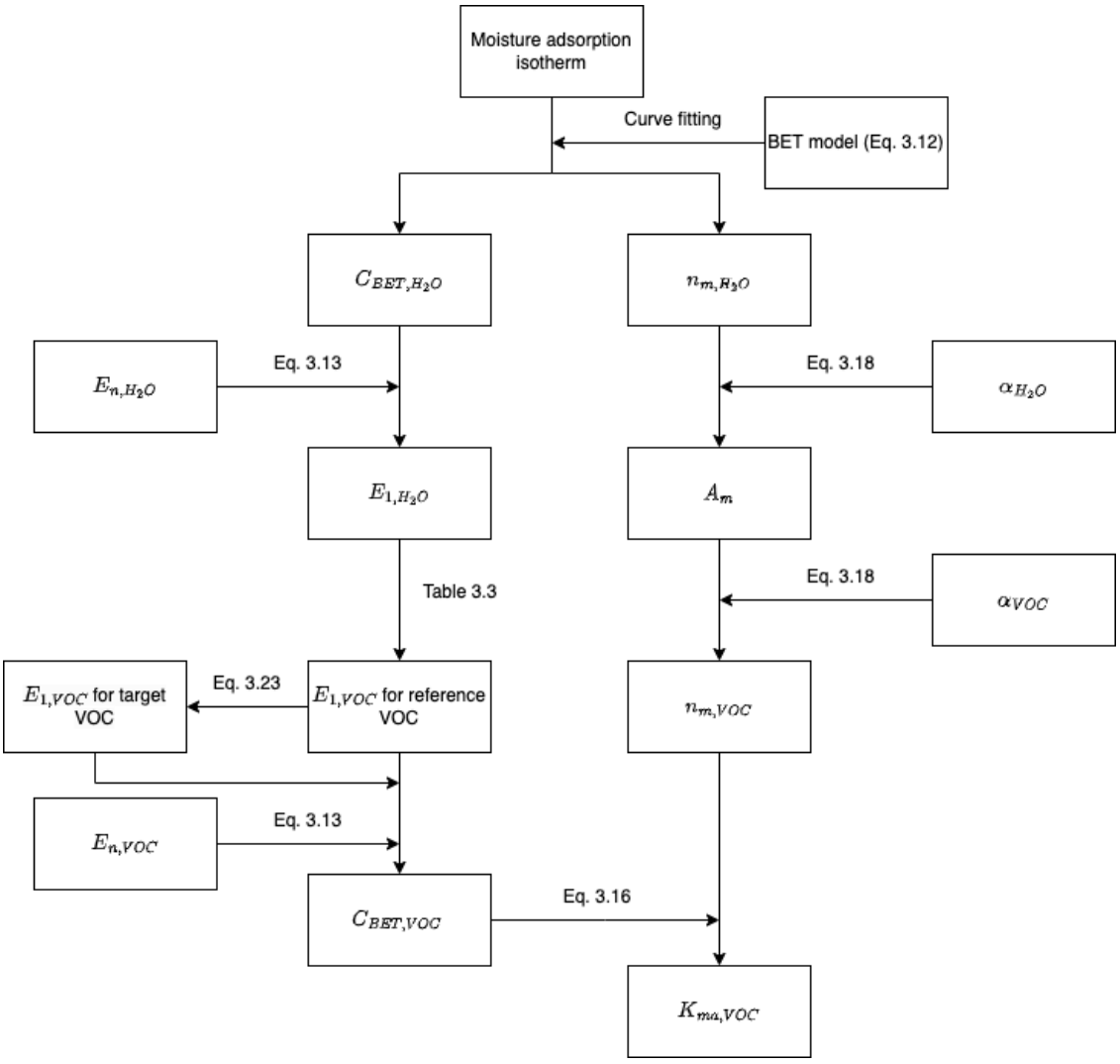

Figure 3.5: Flow chart of estimating K_{ma} of target VOC from moisture adsorption isotherm

measured data [42]. The similarity approach used the data of water and toluene from Table 3.3 to estimate K_{ma} of benzene, ethylbenzene, propylbenzene, and butylbenzene. The estimation has a good agreement on benzene and toluene. However, as moved towards heavier VOCs, the estimations tended to underestimate the values, indicating that the adsorption energies were higher than what was anticipated from the theoretical calculations. In contrast, power law model works better for heavier compound (lower vapor pressure) because these compounds contribute more weighting due to their higher K_{ma} in curve fitting solution.

Estimations for aldehydes was shown in Figure 3.8, the novel similarity approach presents a good agreement with the acutal measured data, which only use the data of pentanal to estimate hexanal, heptanal, octanal.

Nonetheless, the new similarity approach for estimating the partition coefficient of VOCs based on the sorption data of water vapor is capable of describe the trend of K_{ma} for VOCs in the same functional group. Use the similarity approach and the established correlations between K_{ma} and vapor pressure provides an effective approach to expand the database of partition coefficient for VOCs for estimating the emission rates of building materials.

The application of similarity approach need to be carefully investigated. While the similarity approach has been verified for VOCs in aldehydes and aromatics, VOCs associated with multiple functional groups need additional research to establish the viability of this method. Other factors, such contact angle, specific bond (e.g., hydrogen bond, $\pi-\pi$ bond), and polar-polar interactions are oversimplified in the similarity approach. For instance, consider the cases of benzene and butylbenzene. Benzene is symmetric, with similar chemical bonds throughout its structure, making its adsorption process relatively straightforward to predict. Butylbenzene, on the other hand, has an additional alkyl chain attached to the benzene ring, making its structure more complex. The adsorption energy would likely be different depending on whether butylbenzene approaches the solid surface by the benzene ring or by the alkyl chain. Previous researches [45, 46] have highlighted the impact of contact angle on adsorption energy. This study points towards a need for a more nuanced understanding of the adsorption process, specifically accounting for factors like molecular struc-

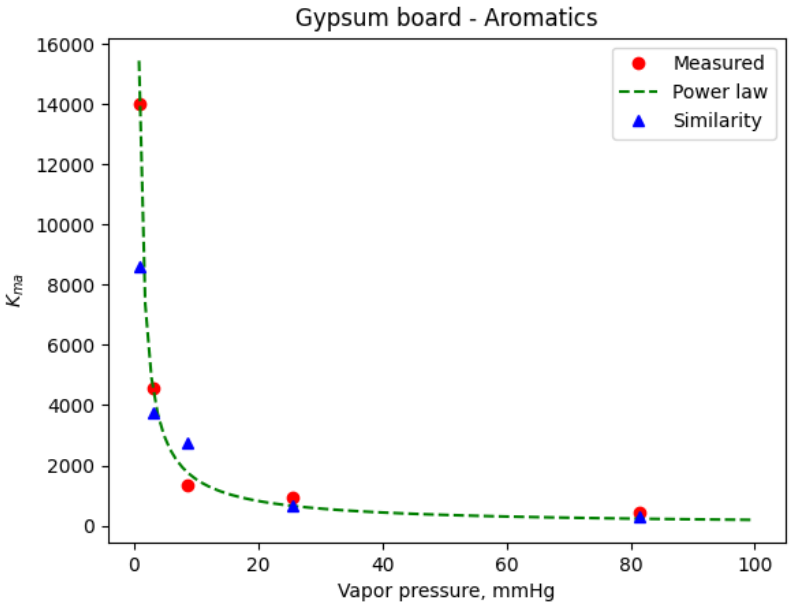

Figure 3.6: Estimation of K_{ma} for aromatics-gypsum board by proposed similarity approach and comparing with power law model for K_{ma} estimation. Measured data and power law model is adopt from Bodalal et al. [42]

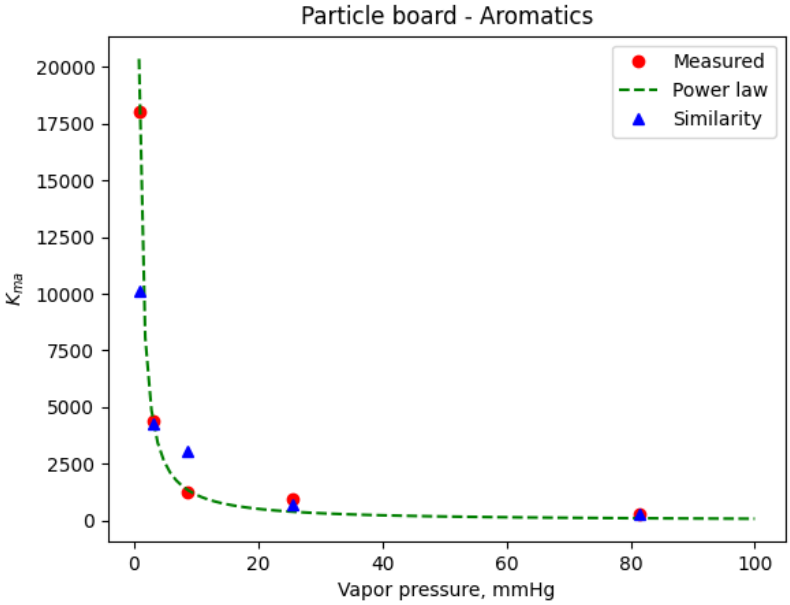

Figure 3.7: Estimation of K_{ma} for aromatics-particle board by proposed similarity approach and comparing with power law model for K_{ma} estimation. Measured data and power law model is adopt from Bodalal et al. [42]

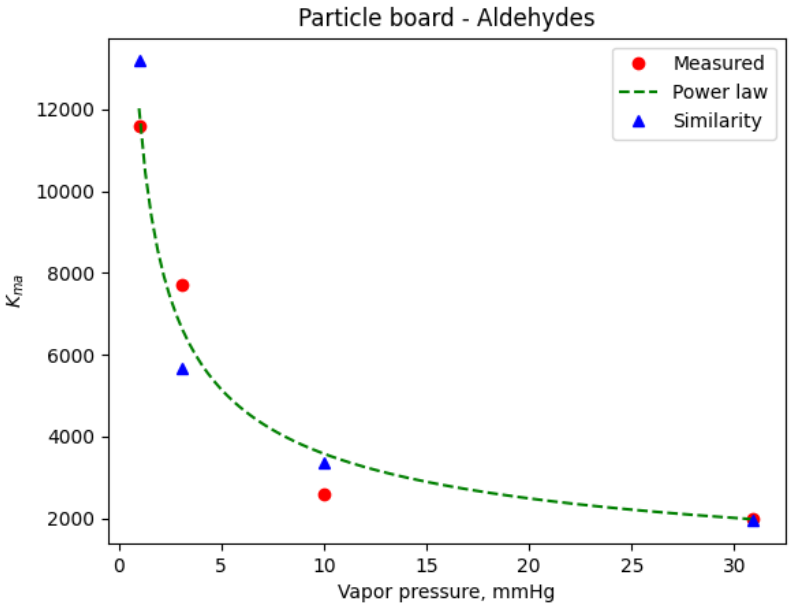

Figure 3.8: Estimation of K_{ma} for aldehydes-particle board by proposed similarity approach and comparing with power law model for K_{ma} estimation. Measured data and power law model is adopt from Bodalal et al. [42]

ture and contact angles, which can significantly influence the adsorption energy and subsequently, the partition coefficients.

3.5 Conclusion

In this study, a novel similarity approach for estimating K_{ma} based on the analogy between moisture adsorption and VOC adsorption on the same adsorbent was developed. This approach requires less information of VOC-material pairing than the established power law model that uses vapor pressure to predict K_{ma}. It only necessitates the moisture isotherm of the same material and the measured K_{ma} or adsorption energy of a reference VOC that belongs to the same functional group as the target VOCs. A correlation between the partition coefficients of various VOCs and their respective liquid molar volumes has been determined for VOCs that exhibit similar functional groups and chemical bonds, given the same material is used in BET model. This correlation is further substantiated by experimental data in the literature. Consequently, this facilitates the prediction or estimation of partition coefficients for certain VOCs based on the known data of similar VOC species in

building materials. In comparison to correlations previously reported between partition coefficients and vapor pressure, the current correlations present here are not purely empirical. Instead, the similarity method offers a theoretical foundation, and the associated parameters can be readily obtained. This establishes an efficient and robust method for estimating the partition coefficients of VOCs, providing a valuable tool for the exploration and understanding of VOC behavior in building materials.

CHAPTER 4
FULL-SCALE CHAMBER EXPERIMENTS TO CHARACTERIZE SECONDARY EMISSION

4.1 Introduction

It has been reported that the COVID-19 pandemic has led to a widespread use of household disinfectants and air purifiers. In order to understand the secondary emissions resulting from the use of these products, a set of chamber tests was conducted to detect and measure the VOCs released during household activities and the use of air cleaners. The tests were carried out in a realistic full-scale test room inside an environmentally controlled chamber. This chapter presents the test facility, methods and procedure, results and major findings.

4.2 Test System and Apparatus

4.2.1 Full-scale Chamber and Test Room

Laboratory testing at full-scale has been established as a dependable approach to evaluate indoor air quality, thermal management, and estimate energy consumption [92, 93]. In this particular study, all tests were carried out in a room built inside an environmental chamber made of polished stainless steel. An HVAC system was utilized to regulate the conditions. Return air temperature was used to represent the chamber air temperature assuming a well-mixed air condition and controlled to within $\pm 1^{o}$C of the set point. To provide well-mixed conditions, a linear air diffuser was built, with the supply air directed towards the wall and distributed throughout the room before being exhausted. A residential room (29.1 m^3) was represented, which had typical wood-framed residential wall and ceiling materials. The walls and ceiling of the room were finished with gypsum wallboard coated with low-VOC paint (Behr Premium Plus Ultra-Pure White Interior Paint). All experiments were performed under controlled air exchange rate (AER), temperature and relative humidity (RH)

conditions. Ventilation was mechanically provided. Supply air drawn from outdoors entered the room through a slot diffuser in the center of the ceiling, and the exhaust port was located at the bottom of one side of a wall. Two axial fans were operated during experiments to promote mixing of room air. For the housekeeping agents' tests, the floor was covered with sheet vinyl flooring since the disinfection agent need to be sprayed to and wiped on the floor. While the test room was not occupied, and thus, there was little accumulation of human-related chemical compounds, such as skin oil/flakes or cooking emissions to isolate the emissions from the housekeeping products. To simulate a small office environment for the air cleaner test, the floor was covered with carpets, and a desk, a laptop, and a heated manikin were placed inside. The manikin was dressed in a soiled T-shirt to provide emissions from human skin. The objective was to replicate an authentic air cleaner usage scenario, where the air cleaner may produce reactive chemicals that can react with indoor VOCs.

4.2.2 VOC Generation

The use of a Dynacalibrator manufactured by VICI metronics, Inc. provided a dependable source of consistent VOC injection into the tested room. To facilitate this, a temperature-controlled glass chamber with permeation tubes was utilized for clean air (carrier flow) to carry VOCs permeated from the tubes. In this project, the Dynacal Permeation tubes, which contain a pure chemical compound in a two-phase equilibrium between its gas phase and its liquid or solid phase, were employed as VOC emission sources. Since the VOC permeation rate from the permeation tube is dependent on temperature, the glass chamber's temperature was regulated to achieve the desired VOC emission rate. The device emitted the compounds at a constant rate through its permeable portion at a constant temperature, which was then carried by the airflow over it for injection into the test chamber. Finally, the carrier flow mixed with the remaining portion of the clean air (dilution flow) to attain the desired VOC concentration level at the outlet of the Dynacalibrator.

4.2.3 VOC Sampling and Analysis

Sorbent tube samples were collected and subjected to Gas Chromatography/Mass Spectrometry (GC/MS) analysis to identify and quantify the VOCs in the test room. In the tests involving formaldehyde injection, 2,4-dinitrophenylhydrazine (DNPH) samples were collected and analyzed via High-Performance Liquid Chromatography (HPLC) to evaluate the formaldehyde concentration and detect potential generation of acetaldehyde and acetone. Proton Transfer Reaction – Mass Spectrometry (PTR-MS) is an optional device that can be utilized to monitor the VOC concentrations inside the chamber at the return air for target compounds such as formaldehyde and toluene, with detection limits in the parts per billion (ppb) range and a sampling interval of no more than 15 seconds per sample. Additionally, the device can monitor background VOCs and any possible O_3 or OH radicals-initiated oxidation products in near real-time, along with continuous monitoring of the O_3 concentration at the return air.

4.2.4 Ozone Sampling

To identify the potential ozone generation, ozone was sampled using the 2B Technologies Model 202 Ozone Monitor, which ranges from 1.5 ppb to 250 ppm and resolution is 0.1 ppb with the accuracy of 1.5 ppb or 2% of reading. The limit for detection of this instrument is 3.0 ppb.

4.3 Test of Hydrogen Peroxide Based Housekeeping Agents

4.3.1 Overview

Activities such as household cleaning can greatly alter the composition of air in indoor environments. Hydrogen peroxide (H_2O_2) based cleaners are common bleach alternatives. Aqueous H_2O_2 is the active ingredient in a number of household non-bleach cleaning products [60]. It is an important oxidant directly related to the hydroxyl (OH) and hydroperoxyl (HO_2) radical pollution load. As illustrated in Table 4.1, H_2O_2 and VOC emissions were monitored from home surface cleaning processes under six distinct scenarios. The purpose of these experiments was to determine the

Table 4.1: Experiment design of H_2O_2-based disinfection agent

Scenarios	Residence time	S/V ratio	Lighting
Regular clean	2 min	Low (2.0)	Dark
Deep clean	60 min	Low	Dark
Median surface	2 min	Median (6.9)	Dark
High surface	2 min	High (11.8)	Dark
Sunlight	2 min	Low	Simulated sunlight
Florescent	2 min	Low	Fluorescent tube

H_2O_2 emission rate over different residence time on the floor, to quantify the deposition rate of H_2O_2 on surfaces, and to identify VOCs emitted from the liquid cleaning solutions used. Zhou et al. has published the outcomes of chamber tests and corresponding simulation in a peer-reviewed article [60]. This current study use the same experimental data but incorporates a newly developed evaporation model and surface deposition model to quantify the emission and deposition rates of H_2O_2 over time. Additionally, a new test was conducted in this study to investigate the changes in the emission rates of ozone and VOCs due to simulated solar radiation. To ensure a comprehensive discussion in this section, the study recaps the results and discussion from the published article and presented the three novel contributions.

4.3.2 Test Method and Procedure

All cleaning experiments were conducted in the test room as shwon in Figure 4.1. The air exchange rate (AER) remained steady at 0.510 ± 0.004 h^{-1}. The room temperature was maintained at 25.7 ± 0.9 ^oC. Room humidity (RH) wasn't regulated and averaged to 25.8 ± 9.5% throughout the experimentation period. The air had a relatively low moisture content, a characteristic owing to the fact that the tests were carried out during the winter season.

For regular cleaning processes, a commercially available non-bleach hydrogen peroxide (H_2O_2) multipurpose cleaner spray with a composition of 0.88% H_2O_2 by volume was used. The cleaner was applied on a section of the vinyl floor (0.75 m^2), in accordance with the manufacturer's guidelines for generic use. The cleaner was sprayed a total roughly 15 mL on the floor. It was then wiped to dryness with clean paper towels twice within a time frame of 1.5 to 2 minutes. For deep

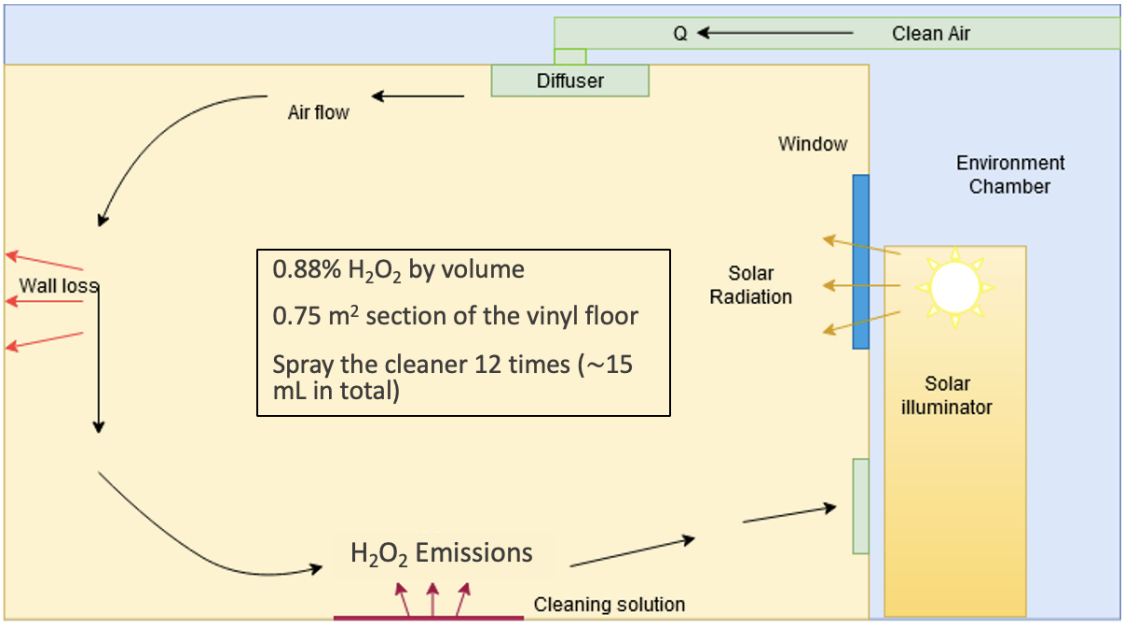

Figure 4.1: Diagram of test room and chamber setup for experiments of H_2O_2-based housekeeping agents

cleaning scenario, the product was left on the floor for more than 1 h before being wiped clean.

In the experiments simulating fluorescent lighting conditions, four exposed fluorescent lights (GE 48" workspace bright white F32 T8 tube) were employed, situated roughly 8 ft above the floor, emulating the lighting conditions of an office. For the experiments mimicking sunlight conditions, a solar illuminator (XE-LUM Large Area Luminaire, Sciencetech Inc., Canada) was positioned outside a window of the residential room, used to imitate the presence of indoor sunlight.

Extra sheets of cardboard measuring 4 ft by 8 ft, coated with the same low-VOC paint used for the room's interior walls, were positioned in the room. The purpose of this was to increase the indoor surface area and consequently alter the surface-to-volume (S/V) ratio, as indicated in reference Table 4.1.

4.3.3 Results and Discussion

Hydrogen Peroxide Emission and Surface Uptake

In the test room, background H_2O_2 levels prior to cleaning activities were 0.64 (±0.43) ppb on average. This level is consistent with that observed in outdoor urban atmospheres (< 1 ppb),

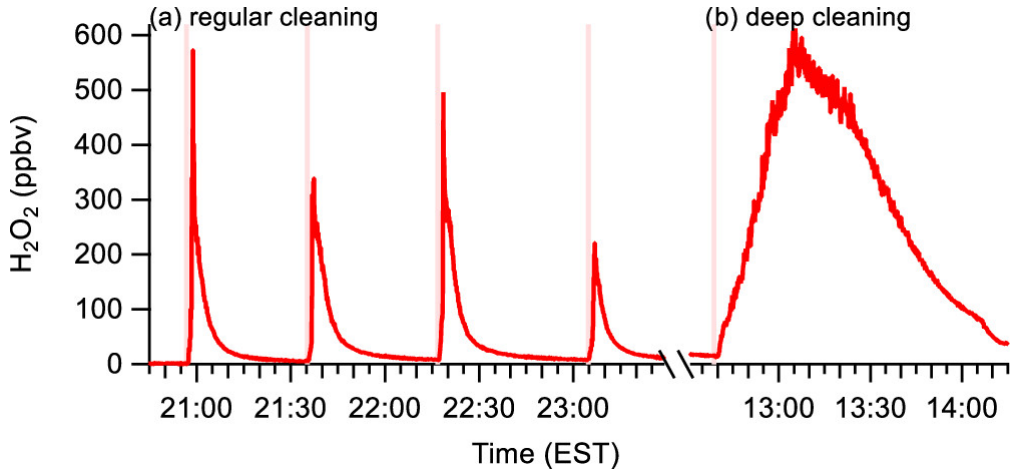

Figure 4.2: H_2O_2 mixing ratios measured during four sequential regular cleaning applications and one deep cleaning application [60]

but higher than in a non-disturbed office [94] and a simulated indoor environment which are not detected [95]. For context, average H_2O_2 levels measured in an undisturbed student office and an engineering laboratory were 1.6 (±1.1) and 2.1 (±0.49) ppb, respectively, possibly due to H_2O_2 formation from ozone-alkene reactions [60].

Significantly elevated H_2O_2 levels were detected in the test room during each consecutive cleaning application as shown in Figure 4.2. Regular cleaning led to a rapid increase in H_2O_2 levels, peaking within 42 (±16) seconds, likely due to H_2O_2 emission from the floor. Peak H_2O_2 levels ranged from 80 to 480 ppb, significantly above the background. Deep cleaning applications showed a slower growth profile and higher peak H_2O_2 levels (570-608 ppb), likely due to prolonged presence of liquid water on the floor.

Deposition of gaseous H_2O_2 onto indoor surfaces significantly influences its airborne levels. Indoor surface-area-to-volume ratio is much higher than outdoors, which leading to a significant effect on H_2O_2 concentration. The surface deposition rate was examined by modifying the area of painted surfaces.

There was a notable decrease in peak H_2O_2 mixing ratios as the S/V ratio increases, underscoring the importance of surface absorption in H_2O_2 reduction (Figure 4.3). Furthermore, there was a 2.8-fold increase in the H_2O_2 removal rate as the surface area increased. This further confirmed that

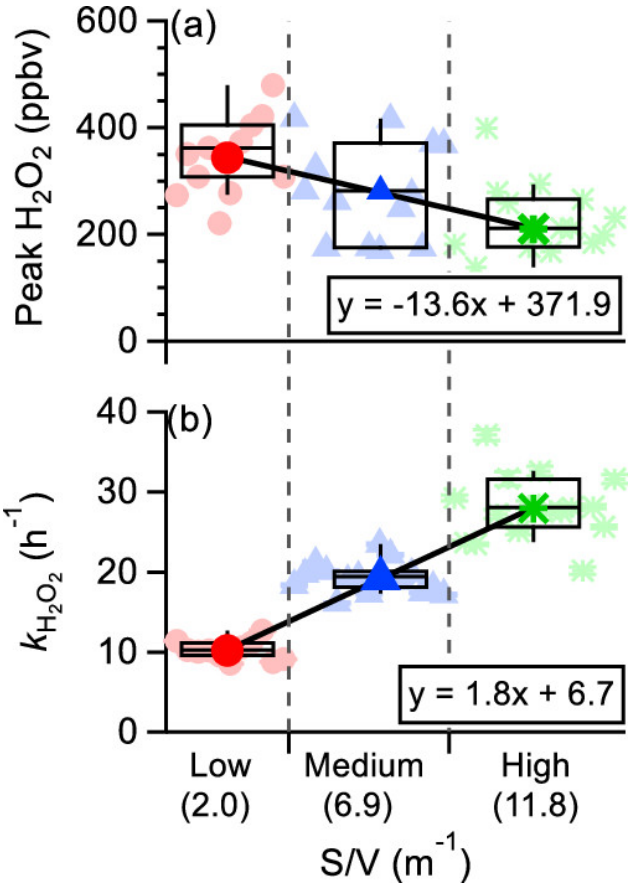

Figure 4.3: Peak H_2O_2 mixing ratios and H_2O_2 exponential decay rate constants observed during regular cleaning events under three surface-area-to-volume (S/V) conditions [60]

surface uptake is a significant sink for indoor H_2O_2 and that indoor surfaces significantly impact both indoor H_2O_2 mixing ratios and residence time.

Experiments flushing the room with outdoor air after cleaning applications suggested that the rapid surface uptake of H_2O_2 is irreversible, pointing to heterogeneous reactions occurring on indoor surfaces, including surface films, indoor building materials, and furnishings. This implies that H_2O_2 may react with components of the paint and wood in the simulated room, demonstrating the potential impact of indoor materials on H_2O_2 levels [96, 97].

In this study, a mass transfer model was developed to characterize the emission rate of H_2O_2 from the cleaning solution. The model was originally reported by Zeh et al. [98] for modeling latex painting on a flat surface. This process bears similarity to the cleaning activities that H_2O_2 was released from a thin aqueous layer on the floor. The mass balance of H_2O_2 concentration in bulk

air was represented by Equation 4.1 taking into account the ventilation dilution, emission from the aqueous solution ($E(t)$), and uptake by room surfaces ($S(t)$).

$$V\frac{dC_{a,H_2O_2}}{dt} = Q_s \cdot (C_{out,H_2O_2} - C_{a,H_2O_2}) + A_l \cdot E - A_m \cdot S \tag{4.1}$$

$$E = h_m \cdot (\frac{C_{l,H_2O_2}}{H} - C_{a,H_2O_2}) \tag{4.2}$$

$$S = \nu_{d,H_2O_2} C_{a,H_2O_2} \tag{4.3}$$

Where,

C_{a,H_2O_2} and C_{out,H_2O_2} is the concentration of H_2O_2 in room air and outdoor air respectively, μg/m^3.

C_{l,H_2O_2} is the concentration of H_2O_2 in cleaning solution, μg/m^3.

V is the volume of test room, m^3.

Q_s is the outdoor air flow rate, m^3/h.

h_m is the convective mass transfer coefficient, m/s.

H is the Henry's law constant, which is a proportionality constant that describes the solubility of a gas in a liquid at a given temperature and pressure.

A_l is the exposure surface area of cleaning solution, m^2.

ν_{d,H_2O_2} is the H_2O_2 deposition velocity of the building material, m/s.

A_m is the surface area of building materials, m^2.

The emission rate of H_2O_2 is dominated by convective mass transfer, considering the diffusion in the liquid within the thin layer is minimal [99, 100]. Given the small volume of aqueous solution applied on the floor, the H_2O_2 concentration in the solution, denoted as C_{l,H_2O_2}, diminishes over time due to the evaporation from the surface. This is modeled by Equation 4.4.

$$V_L\frac{dC_{l,H_2O_2}}{dt} = -A_l \cdot E \tag{4.4}$$

Where,

Table 4.2: Correlation between v_{d,H_2O_2} and surface-area-to-volume (S/V) of regular cleaning events

S/V	Low (2.0)	Medium (6.9)	High (11.8)
v_{d,H_2O_2} m/s	0.00143	0.00077	0.00065

V_l is the volume of cleaning solution, m^3.

The surface deposition of indoor H_2O_2 can be determined by the first-order irreversible surface heterogeneous reaction, which can be quantified by H_2O_2 deposition velocity (v_{d,H_2O_2}). The average value of v_{d,H_2O_2} is estimated from the correlation between the decay of H_2O_2 and S/V ratio in Figure 4.3, where $S/V \cdot v_{d,H_2O_2} = k_{H_2O_2}$. The outcomes of v_{d,H_2O_2} are depicted in Table 4.2, indicating a decrease in v_{d,H_2O_2} as the surface area enlarges. However, v_{d,H_2O_2} should remain constant, irrespective of the surface area. The v_{d,H_2O_2} values in Table 4.2 agree with the values determined for painted gypsum board (0.0069 - 0.00125 m/s) in a 48 L chamber test [101]. H_2O_2 deposition velocity is a mass transfer coefficient governed by the H_2O_2 transport to the surface and uptake by the surface, which is associated with fluid mechanics near the material surface and the chemical reactivity of the material with H_2O_2. The reason of the inconsistent v_{d,H_2O_2} of different S/V conditions is that the additional surfaces used for medium and high surface conditions were vertically hung on a frame in the test room. Given the limited space in the testing room, the gap between each surface is roughly 2-5 cm. This close distance can alter the air flow pattern near the surface, thereby influencing the transport of H_2O_2 to the surface.

Deep clean event was simulated by the model described by Equation 4.1 - Equation 4.4. The simulation illustrates a rise in the concentration of H_2O_2, followed by a decay after approximately 20 minutes. A more gradual decay of the H_2O_2 concentration in the deep clean scenario, as compared to a regular clean, is reflected in the simulation. This is attributable to the off-gassing of aqueous H_2O_2 on the floor. During the test, the surface area reduced, a phenomenon caused by the evaporation of both water and H_2O_2 under relatively dry conditions. However, determining the precise moment at which all liquid has evaporated into the air is challenging, as the floor appeared dry after 2 hours. The evaporation rate of water (major ingredient of the cleaning solution) is con-

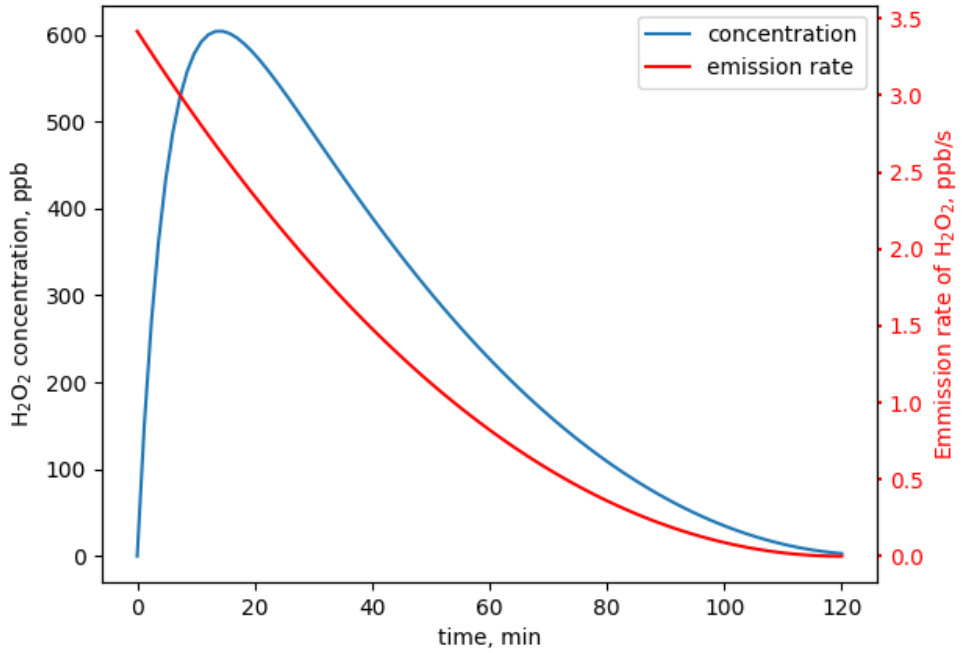

Figure 4.4: Simulated H_2O_2 concentration and evaporation rate of deep clean with low S/V

trolled by temperature, RH, and air velocity, which are constant during the test. The change in surface area is assumed to follow an linear decay if liquid thickness keeps the same and volume is decayed linearly due to the constant evaporation. This reduction in surface area and reduction of dC_{l,H_2O_2} have a significant impact on the emission rate as shown in Figure 4.4.

VOCs Concentration in Regular Cleaning Events

In addition to H_2O_2, cleaning events under low S/V conditions introduced many VOCs into indoor air. The most significant increases were noted for methanol and a mix of glyoxal, propanal, and acetone. Five organic compounds (methanol, acetone, acetic acid, butene, and pentene) detected in the air were also found in the cleaning solution, suggesting direct emissions. Certain VOCs detected in the solution's headspace were not detected in the solution itself, suggesting that they might have formed in the gas phase above the solution or were present at concentrations too low to be detected.

Different VOCs displayed varied temporal trends after cleaning (Figure 4.5). For instance,

Table 4.3: Decay rate constants of indoor VOCs calculated from measurements during several regular cleaning events under the low surface condition with AER = 0.5 h^{-1} [60]

m/z	Mean decay rate constant (h^{-1})	SD decay rate constant (h^{-1})
33	1.84	0.86
47	1.18	0.14
51	1.19	0.73
57	1.88	0.53
59	1.67	1.17
69	1.19	0.40
84	1.44	2.03
105	1.88	0.33
139	0.95	0.50

methanol (m/z 33), isoprene (m/z 69), methyl chloride (m/z 51), and either formic acid or ethanol (m/z 47) levels surged immediately after cleaning and peaked within a few minutes. Conversely, compounds such as acrolein or butene (m/z 57), and a mix of glyoxal, propanal, and acetone (m/z 59), showed slower growth and peaked after approximately 20 minutes. Some VOCs decreased initially due to air mixing from opening the door and then recovered to pre-cleaning levels. The differing profiles are likely related to physical properties like air-surface partitioning coefficients and Henry's law constants.

The study found that first-order decay rate constants for nine ions from PTR-MS measurements (Table 4.3) that showed clear decay lower than H_2O_2 but higher than the air change rate. The observations of decay rates that higher than air exchange rate, suggesting that besides direct emissions and ventilation, chemical reactions played a role in the loss of VOCs introduced by cleaning. The removal of these compounds from ventilation accounting for 14-86% of total removal and possibly chemical reactions in the gas phase and on surfaces contribute to the rest [60].

Indoor Ozone and Hydroxyl Radicals Concentration

The primary oxidants in indoor environments without cleaning events are typically ozone and hydroxyl radicals. Ozone was injected into the test room to simulate the transport of outdoor ozone to indoor through ventilation. The injected ozone concentration was set at 20±1.1 ppb, reflecting the typical outdoor ozone concentration [11]. As shown in Figure 4.6, due to surface deposition on

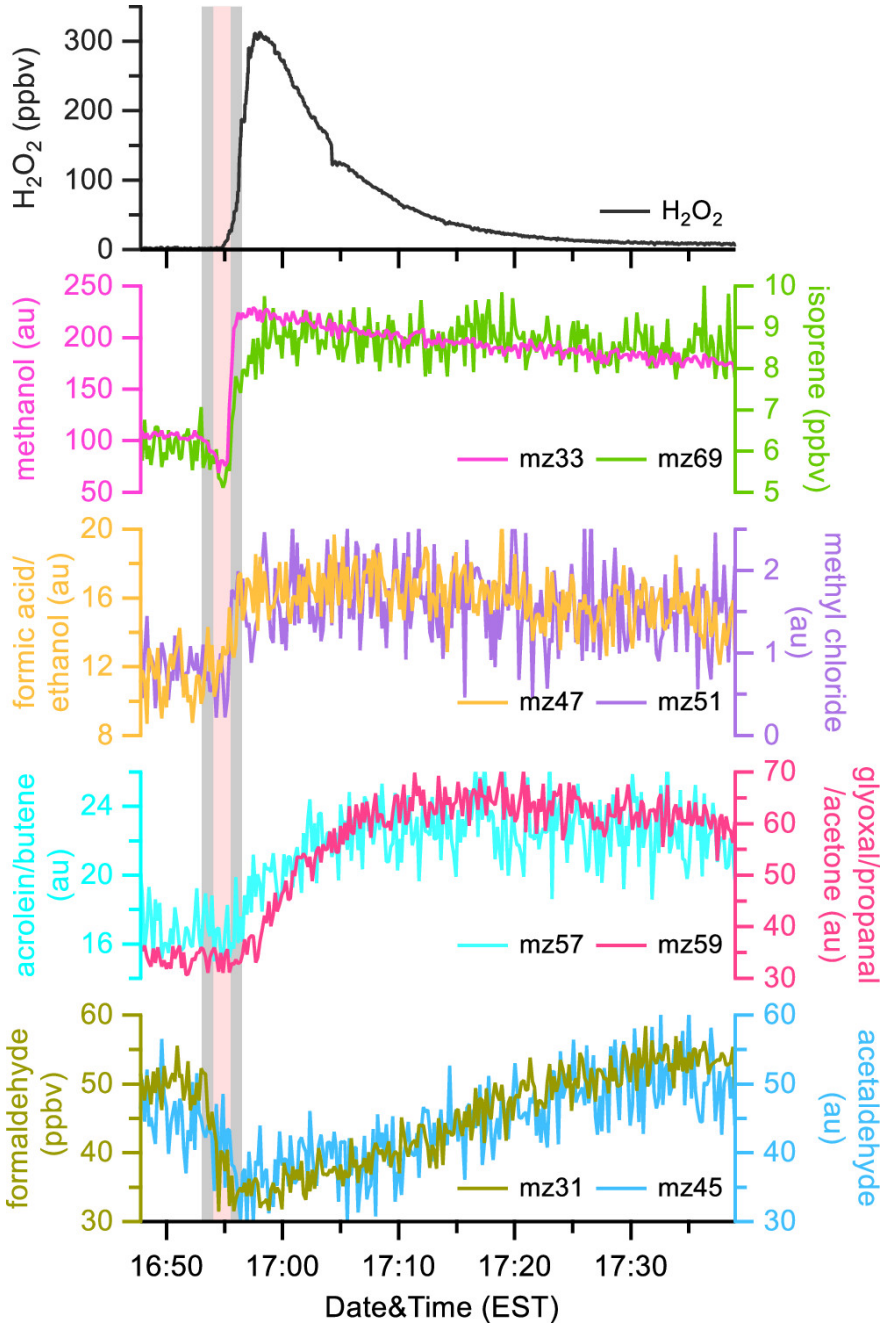

Figure 4.5: Time series of H_2O_2 and select VOCs (m/z) during a regular cleaning event under the low-surface-area condition [60]

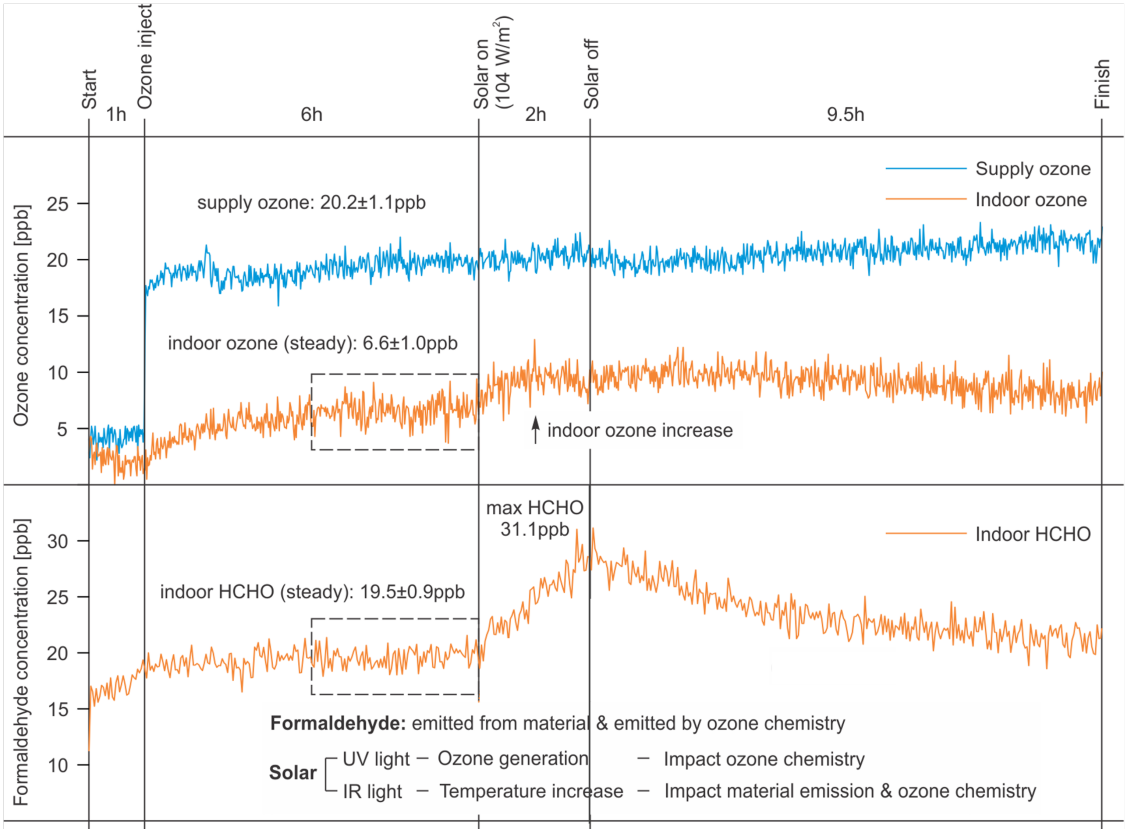

Figure 4.6: Ozone and formaldehyde concentration in the test room with and without simulated solar radiation

building materials, the steady-state ozone concentration measured was 6.6 ± 1.0 ppb. Following two hours of exposure to simulated solar light, the ozone concentration rose to 10 ppb. In the mean while, formaldehyde concentration increased 50% in the presence of ozone, which is attributed to the ozone and OH radicals-initiated reactions and enhanced primary emission by the 2.5 °C temperature increase in air and material surface due to the simulated solar radiation. The observed fluctuation in the formaldehyde concentration that measured by PTR-MS can be attributed to its high resolution (< 1 ppb) and quick response (< 15 s). The standard deviation of formaldehyde concentration at steady state is 0.9 ppb. This suggests that the average concentration over a longer time span remains consistent. After turning off the simulated solar, both ozone and formaldehyde returned to their steady state concentrations in 9.5 h.

Hydroxyl radicals were generated via O_3-alkene reactions and photolysis of H_2O_2 and H_2O. Ozone-alkene reactions are only important with ozone present, as discussed above, and photolysis

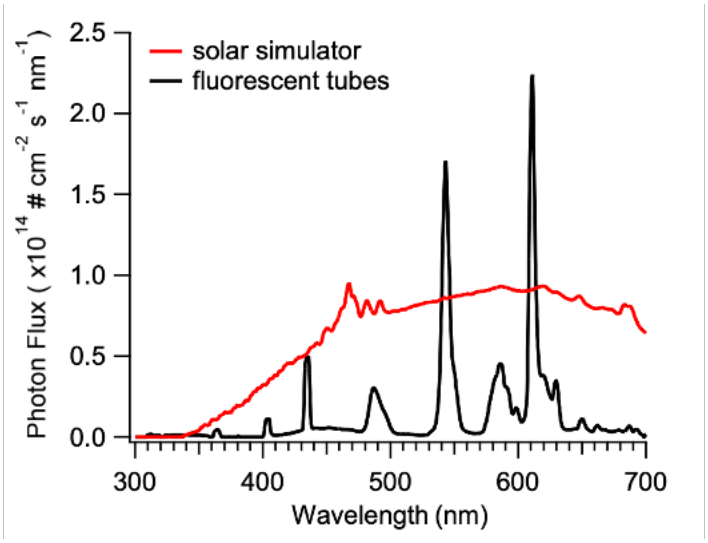

Figure 4.7: Wavelength-resolved photon fluxes from two light sources near the sampling port in the test room [60]

is only important under illuminated condition. Due to their short lifetime, estimated at 42 ms by Weschler and Shield in a simulated VOCs mixture replicating a real indoor environment [102], hydroxyl radicals are difficult to detect. Therefore, the concentration of hydroxyl radicals was not directly measured during the tests. The generation of hydroxyl radicals was simulated using the INdoor Detailed Chemical Model (INDCM), a near-explicit zero-dimensional photochemical box model constructed based on a comprehensive chemical mechanism [74]. The photon fluxes from the two light sources were measured near the sampling ports, which were in the center of the room (Figure 4.7). The measurement were used to calculate the average photolysis rate constant of H_2O_2 as 8.08×10^{-8} s^{-1} for fluorescent tube and 6.66×10^{-8} s^{-1} for simulated sunlight [60].

The simulation outcomes, as shown in Figure 4.8, reveal that the average OH concentration under dark conditions was lower than the levels commonly found in urban outdoor environments, but similar to outdoor levels during nighttime [103]. Upon exposure to sunlight, the concentration of OH increased, and the levels of other radicals, namely HO_2 and RO_2, also escalated due to photolysis reactions with VOCs.

Throughout cleaning activities, the simulations indicate that without light, the use of H_2O_2-based cleaners does not significantly increase the concentration of radicals. Nevertheless, in illu-

minated conditions, cleaning can contribute to increased radical levels due to H_2O_2 photolysis.

4.3.4 Conclusion

Hydrogen peroxide is widely used as a cleaning agent and disinfectant in residential and non-residential buildings. Although measured H_2O_2 levels were always below the occupational exposure limits, there's speculation that higher concentrations might be observed when larger areas are cleaned, more cleaner is applied, or cleaning solutions with a higher H_2O_2 content are used.

The emission and deposition processes of H_2O_2 were modeled using a mass transfer model developed in this study. The emission rate of H_2O_2 correlates with its concentration in the cleaning solution, which diminishes over time due to evaporation. The average emission rate of H_2O_2 was determined as 4.41 $\mu g/(m^3 \cdot s)$, leading to a peak concentration of H_2O_2 of 600 ppb.

The deposition velocity of H_2O_2 on a painted surface was found to be 1.43×10^{-3} m/s, which is equivalent to an air change rate of 10.3 h^{-1} for diluting H_2O_2. The photolysis of H_2O_2, a significant source of hydroxyl and hydroperoxyl radicals, was modeled by the INDCM using the photolysis rate constants measured in the experiment: 8.08×10^{-8} s^{-1} for a fluorescent tube and 6.66×10^{-8} s^{-1} for simulated sunlight.

4.4 Test of an Electrostatic Precipitation and an Ultraviolet Lamp Based Air Cleaning Device

4.4.1 Overview

This study conducted comprehensive chamber tests of two distinct air cleaning systems, one relying on ultraviolet (UV) light, and the other, on electrostatic precipitation. Both UV irradiation and corona discharge, intrinsic to these air cleaners, could potentially generate ozone and OH radicals.

Ozone and OH radicals, as strong indoor oxidants, pose a risk for the secondary emission of VOCs through chemical reactions. The chamber tests assessed the generation rates of ozone and OH radicals attributed to these two air purifying devices. Moreover, the experiment characterized and quantified the stable VOC by-products resulted from ozone and OH radical-initiated reactions.

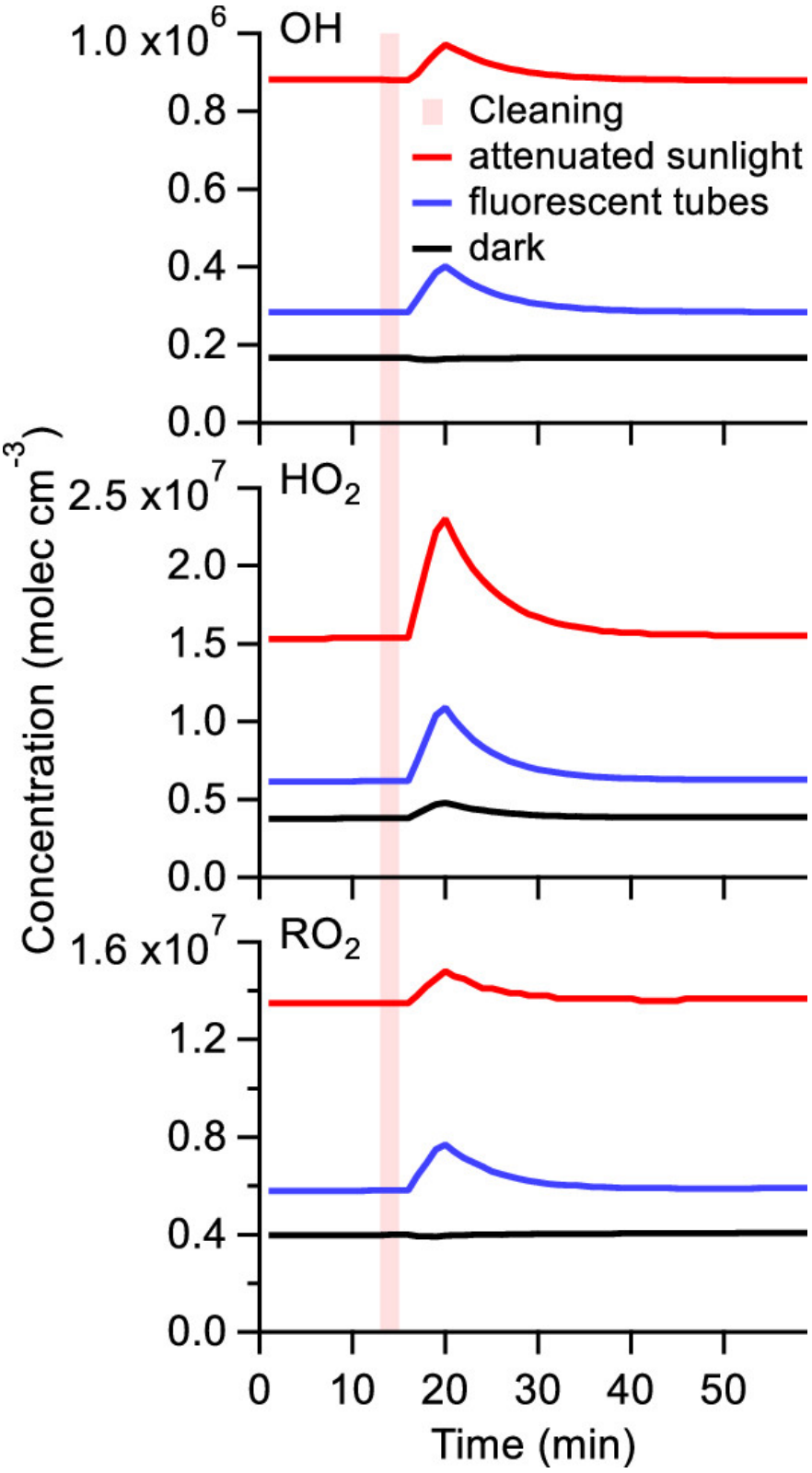

Figure 4.8: Estimated radical concentrations under different lighting conditions during regular cleaning under the low surface condition [60]

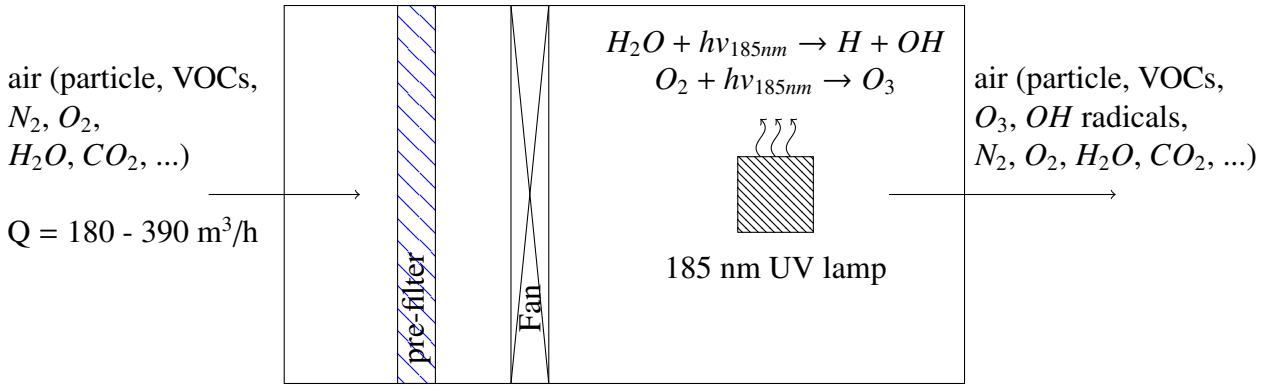

Figure 4.9: Diagram of the UV lamp-based air cleaner (AC-1)

4.4.2 Air Cleaning Device

The tested UV lamp-based air cleaner (AC-1) is a prototype device that aims to decompose VOCs through reactions initiated by ozone and OH radicals. It has a prefilter to remove large particles that could damage the device, and a 185 nm UV lamp that producing hydroxyl radicals and ozone which are strong indoor oxidants can react with VOCs (Figure 4.9). The mechanism of ozone and OH radicals generation and reactions with VOCs will be discussed in the next chapter as part of the indoor air chemistry model.

The electrostatic precipitation-based air cleaner (AC-2) has two segments (Figure 4.10): the first aims to remove particles by charging them in the incoming flow and then collecting them using an oppositely charged collector. The second segment consists of UV light that uniformly irradiates the incoming flow to inactivate any micro-organisms and decompose VOCs. Ozone and OH radicals are not generated by the 254 nm UV lamp, but are produced by the corona discharge from the electrostatic charger.

4.4.3 Test Method and Procedure

The tests were conducted inside the test room in which a manikin wearing soiled T-shirt was used to test if the O_3 generated from the air cleaner would react with the skin oil on the T-shirt and result in significant secondary emissions (Figure 4.11). As mentioned above, the test room was

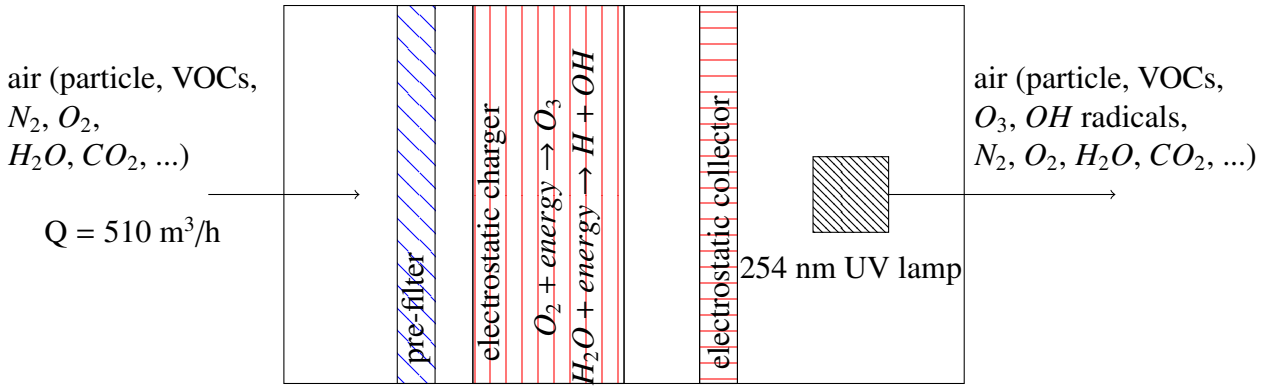

Figure 4.10: Diagram of the electrostatic precipitation-based air cleaner (AC-2)

covered by typical indoor surfaces, such as carpet and painted gypsum board to mimic the real usage condition of an air cleaner.

Certain chemical by-products may not naturally occur indoors and could be difficult to detect due to their short lifetimes. These chemicals, created via indoor air chemistry, include transient radical species such as hydroxyl (OH), hydroperoxy (HO_2), organic peroxy (denoted as RO_2, representing the sum of all existing peroxy radicals), and nitrate (NO_3) radicals. When ozone interacts with common indoor unsaturated VOCs like terpenes, it forms Criegee intermediates. Other significant species include secondary ozonides, nitrated and oxygenated VOCs (such as organic nitrates, carbonyls, dicarbonyls, and hydroxy carbonyls), and secondary organic aerosol (SOA).

This study primarily aims to concentrate on species that substantially impact IAQ. As a result, the VOCs of interest in this study should remain stable during steady-state conditions. The study involved the collection of VOC samples in steady state, both with and without the deployment of an air cleaner. These two samples account for conditions of only primary emissions, and primary plus secondary emissions, respectively. This approach enables the quantification and identification of VOCs originating from primary or secondary emissions. This is based on the assumption that primary emissions decay very slowly and can be regarded as constant during the test duration (12-18 hours). Once the air cleaner is activated, ozone is actively monitored.

The test procedure has 3 main steps:

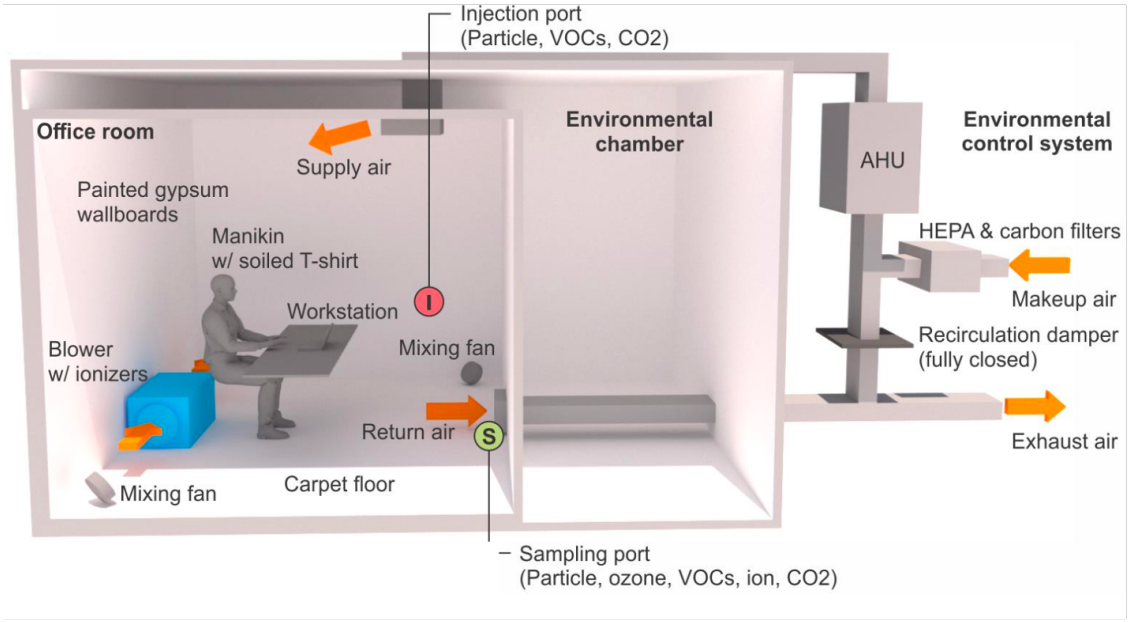

Figure 4.11: Schematic of experiment setup for investigating VOCs secondary emissions from air purification devices

1. Baseline condition monitoring: monitor the baseline condition at the return air with the air cleaner off until a steady state is achieved (6 hours minimum), and then take sorbent samples.

2. Steady-state concentration measurements with the air cleaner off: start the injection of formaldehyde and toluene with the air cleaner off until a steady state is achieved (6 hours minimum), and then take a sorbent sample with a duplicate for GC/MS analysis for identification of VOC species in the air, and a DNPH cartridge sample for aldehydes identification and quantification.

3. Steady-state concentration measurements with the air cleaner on: turn on the air cleaner until a steady state is achieved (6 hours minimum), and then take a sorbent sample with a duplicate for GC/MS analysis for identification of VOC species in the air, a DNPH cartridge sample for aldehydes identification and quantification.

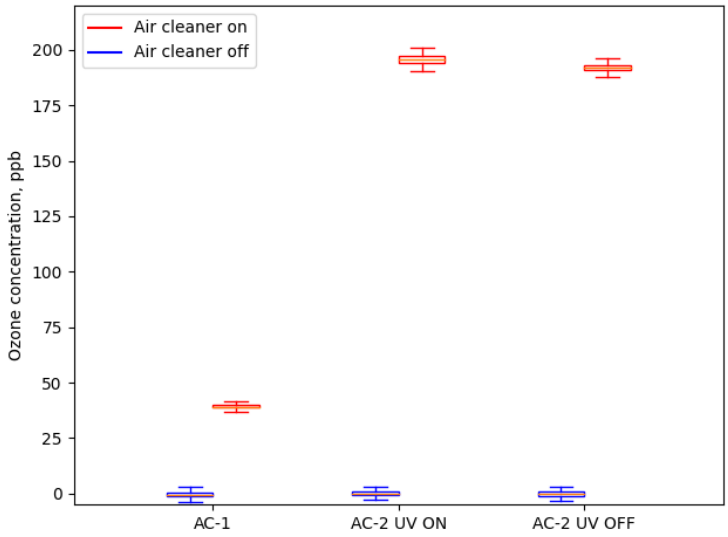

Figure 4.12: Steady state concentration of ozone during the AC-1 and AC-2 chamber test

4.4.4 Results and Discussion

Ozone Generation

Ozone was produced from both AC-1 and AC-2 air cleaners through the processes of UV light irradiation and corona discharge in the electrostatic charger, as depicted in diagrams Figure 4.9 and Figure 4.10. The specific mechanism of ozone formation will be elaborated on in the following chapter.

In chamber tests for both AC-1 and AC-2, the presence of ozone was detected. As soon as the air cleaners were switched on, ozone concentrations rose promptly. The steady-state concentration achieved was about 40 ppb for AC-1 and roughly 200 ppb for AC-2, both considerably higher than the background levels, which were less than 1 ppb. For AC-2, tests were conducted under two conditions: with the 254 nm UV light turned on and off, demonstrating that the major source of ozone is the electrostatic charger instead of the UV lamp.

The ozone generation rates from AC-1 and AC-2 were quantified and will be incorporated into the Indoor Air Quality (IAQ) model in the next chapter for further investigation. The ozone generation rates were found to be 12.9 mg/h for AC-1 and 31.1 mg/h for AC-2.

VOCs from Primary and Secondary Emissions

The simulated small office room shares common major compounds found in a real building, making the background level realistic compared to the total volatile organic compound (TVOC) level in a typical office with required ventilation rates [104]. The conditions of the tests were deemed realistic, reflecting typical background levels in office buildings. According to the standard furniture emission testing method BIFMA M7.1 (2016), the lower limit of quantitation (LOQ) is usually set at 2 $\mu g/m^3$ for individual target VOCs and 20 $\mu g/m^3$ for TVOCs. Consequently, major compounds have been defined as those having a measured concentration equal to or higher than 2 $\mu g/m^3$ in at least one of the collected air samples.

Most VOCs found in the chamber background had concentration levels near the LOQ, with a few exceptions identified in Figure 4.13 and Figure 4.14. Formaldehyde and toluene were introduced into the room to simulate higher, yet realistic concentrations. The background concentration of 2-Ethylhexyl acrylate, the contaminant with the highest concentration, could have originated from the use of tapes for air sealing in the test room, as it has been detected in adhesives [105]. The 2-Ethylhexyl acrylate was not detectable in AC-2 tests which took place approximately six months after the AC-1 test, indicating a slow release of the compound.

The operation of the air purifier resulted in increased concentrations of several VOCs, most of which were aldehydes like hexanal, benzaldehyde, octanal, nonanal, (E)-2-nonenal, decanal, formaldehyde, acetaldehyde, as well as ketones, alcohol and alkane. These VOCs likely originated from O_3 reactions with skin oil, a phenomenon observed in a previous experiment [106]. Some of the VOCs could also be the result of reactions between OH radicals and individual VOCs, such as the reaction of OH radicals with toluene, aldehydes, and α-pinene to form formaldehyde. A decrease in toluene and α-pinene concentration, and increases in the concentrations of formaldehyde, acetaldehyde, and acetone were observed during the chamber test. Phenol, which increased when the UV lamp was on, could have been produced from reactions between toluene and hydroxyl radicals. The reactions initiated by both ozone and OH radicals had a significant impact on IAQ, particularly the reactions between toluene, aldehydes, α-pinene, and skin oil.

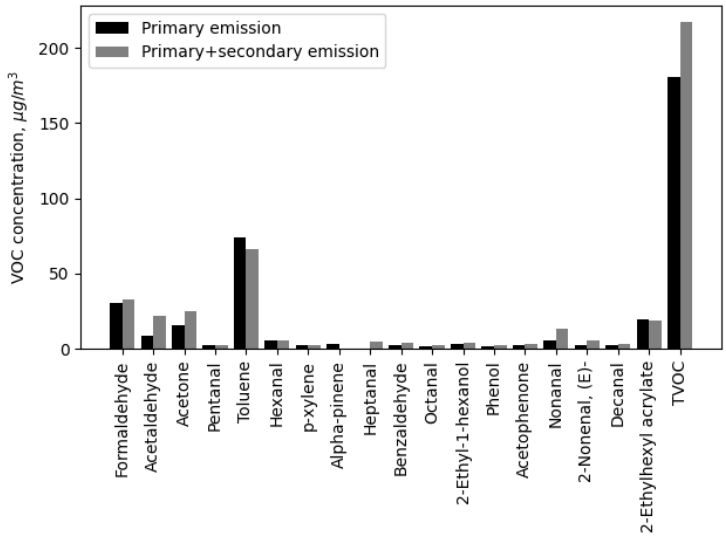

Figure 4.13: Detectable VOCs in the chamber during AC-1 test

The TVOC concentrations in AC-1 and AC-2 tests increased significantly, showing that while toluene was removed by AC-1 and AC-2, noteworthy VOC by-products were generated during the operation of AC-1 and AC-2.

4.4.5 Conclusion

In conclusion, the comprehensive chamber tests carried out on AC-1 and AC-2 have shed light on the significant secondary emissions stemming from the use of the 185 nm UV lamp and corona discharge generated by electrostatic precipitation technology. These tests underscore the importance of understanding the potential implications of indoor air purifier use, particularly with devices such as AC-1 and AC-2.

Key findings of the study highlight the generation of major indoor oxidants, ozone, and OH radicals, primarily produced through UV irradiation and an electric field. The subsequent chemical reactions led to the production of several VOCs, including but not limited to formaldehyde, acetaldehyde, acetone, phenol, and benzaldehyde.

Significantly, the generated ozone concentrations in the test room from AC-1 and AC-2 were 40 ppb and 200 ppb, respectively. These levels are in proximity to or exceed the recommended

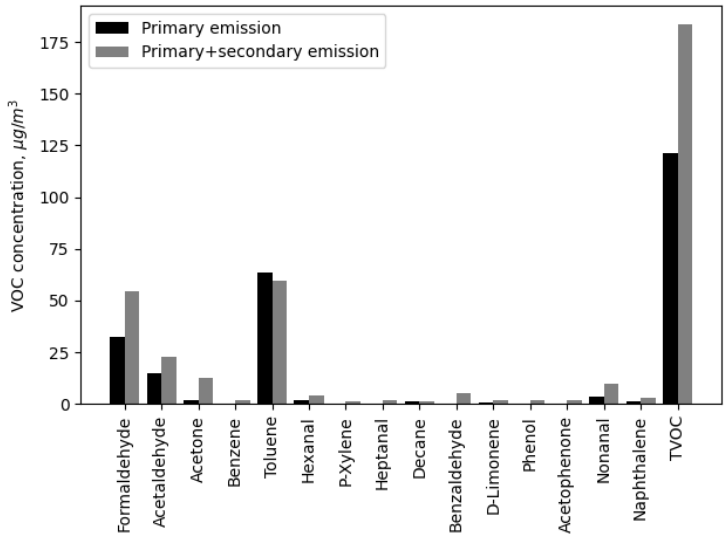

Figure 4.14: Detectable VOCs in the chamber during AC-2 test

threshold limit of 50 ppb, as set by the World Health Organization. These findings raise potential public health concerns, especially in confined indoor spaces.

However, it is essential to note that the test room, simulating a small single office room, represents a smaller environment than the designed usage condition of AC-1 and AC-2. This discrepancy indicates the necessary of an IAQ evaluation model for investigating air cleaners under real usage conditions that beyond the standard chamber test condition. Such a model would not only provide a more realistic scenario for assessing the effectiveness and safety of these devices, but it could also enhance our understanding of the indoor chemical reactions involving ozone and hydroxyl radicals.

4.5 Conclusion

In summary, hydrogen peroxide-based housekeeping agents and indoor air purifiers such as AC-1 and AC-2 have the potential in improving air quality. However, it is essential to be mindful of their usage due to potential by-products that may detrimentally affect indoor air quality and human health.

Hydrogen peroxide (H_2O_2) has been pinpointed as a significant pollutant emitted from H_2O_2-

based cleaning products. This study has suggested surface uptake as the primary removal mechanism of H_2O_2, accounting for 94% according to a model simulation. The model was developed in this study for simulating cleaning activities by taking into account the dilution by ventilation, emission from aqueous H_2O_2 and surface deposition of H_2O_2 on building materials. The investigation under diverse lighting conditions implied that photolysis constitutes a primary source of ozone and OH radical generation, during both non-cleaning and cleaning periods involving H_2O_2.

In tests involving air purification devices, UV light and electric fields emerged as significant sources of ozone and OH radicals. A decline in toluene levels due to reactions with OH radicals was noted. Conversely, aldehydes, particularly formaldehyde and acetaldehyde, showed an increase as products of OH radical and ozone-initiated reactions.

Moving forward, an IAQ model will be discussed in the next chapter that assesses the impact of secondary VOC emissions beyond the test conditions. This comprehensive evaluation is crucial for developing effective strategies to maintain optimal IAQ and safeguard human health.

CHAPTER 5

MODEL OF SECONDARY EMISSIONS FROM ULTRAVIOLET LAMP AND ELECTROSTATIC PRECIPITATION BASED AIR CLEANING DEVICE

5.1 Mechanism of Ozone and Hydroxyl Radicals Formation from Ultraviolet Radiation and Corona Discharge

5.1.1 AC-1: Ozone and Hydroxyl Radicals Formation from Ultraviolet Radiation

During the testing of AC-1, the sources of indoor oxidants such as ozone and hydroxyl radicals were generated through chemical reactions initiated by the 185 nm UV lamp. Water molecules (H_2O) absorb UV light with wavelength between 175 and 190 nm and break the hydrogen-oxygen bond to generate H and OH radicals [107–110].

$$H_2O + h\nu_{185nm} \rightarrow H + OH \tag{5.1}$$

$$H + O_2 + M \rightarrow HO_2 + M \tag{5.2}$$

Where, M represents an arbitrary neutral species (e.g., N_2, O_2, CO_2) in the ambient air which could absorb the kinetic energy released from the changing of electron configurations [110, 111].

The hydroperoxyl (HO_2) radicals can react with O_3 that is generated from UV irradiation and produce OH radicals.

$$HO_2 + O_3 \rightarrow OH + 2O_2 \tag{5.3}$$

The theoretical maximum rate, which assumed that O_2 and O_3 are sufficient in the reactions, of formation of OH radicals from Equation 5.1 - Equation 5.3 can be calculated as Equation 5.4.

$$\frac{dC_{OH}}{dt} = 2I_{185nm}\sigma_{H_2O}C_{H_2O} \tag{5.4}$$

Where,

$\frac{dC_{OH}}{dt}$ is the rate of formation OH radicals, molec/(cm^3 · s).

I_{185nm} is the intensity of 185 nm UV light, photons/(cm^2 · s). The measured total output of this 185 nm UV light is reported as 1.07×10^{18} photons/s [110].

σ_{H_2O} is the cross-section area for adsorption by water at 185 nm, cm^2. The adsorption cross-section of a molecule describes the effective target area for adsorption of the incident radiation. It represents the probability that a molecule will absorb a photon of a particular wavelength when it is exposed to a beam of light. σ_{H_2O} is measured and reported as 7.22×10^{-20} cm^2 for 185 nm UV light [112].

C_{H_2O} is the concentration of water molecules, molec/cm^3.

The factor 2 in the Equation 5.4 denotes from the process describe by Equation 5.1 - Equation 5.3, there are two OH radicals formed for each H_2O photolyzed.

When high-energy UV radiation with wavelength up to 254 nm hits an oxygen molecule (O_2), it can cause the oxygen molecule to split into two individual oxygen atoms (O), which are O(^{3}P) or O(^{1}D). O(^{3}P) and O(^{1}D) are two different excited states of the oxygen molecule (O_2) that are formed during the reactions that produce O_3. O(^{3}P) represents the triplet state of the atomic oxygen, with two unpaired electrons in 2p energy orbitals. O(^{1}D) represents the first excited state of atomic oxygen, where the atom has one electron promoted to a higher energy level. In this case, the notation "^{1}D" signifies that the electron configuration corresponds to the 1D state.

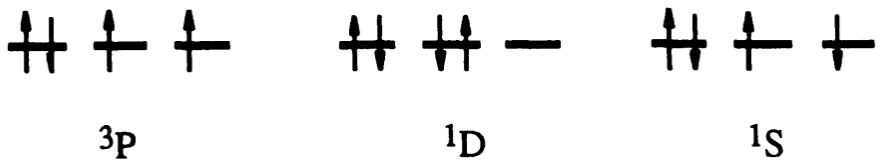

Figure 5.1: Three possible electron configurations in the partially filled 2p orbitals of atomic oxygen. Under each configuration is the corresponding term symbol. [113]

Ozone is formed from the photolysis of O_2 by the UV radiation.

$$O_2 + hv_{185nm} \rightarrow O(^1D) + O(^3P) \tag{5.5}$$

$$O_2 + hv_{185nm} \rightarrow O\left(^3P\right) + O\left(^3P\right) \tag{5.6}$$

The reaction in Equation 5.5 only occurs at the UV wavelength lower than 175 nm [114]. Therefore, only reactions expressed by Equation 5.6 happened in the chamber test with a 185 nm UV light. Both excited states are highly reactive and can participate in a variety of chemical reactions that are important in atmospheric chemistry. O(^{3}P) can react with other oxygen molecules to form ozone through a chain reaction:

$$O(^3P) + O_2 + M \rightarrow O_3 + M \tag{5.7}$$

The calculation of theoretical maximum formation rate of O_3 from Equation 5.6 – Equation 5.7 is similar to Equation 5.4 and express as Equation 5.8.

$$\frac{dC_{O_3}}{dt} = 2I_{185nm}\sigma_{O_2}C_{O_2} \tag{5.8}$$

Where,

σ_{O_2} is the cross section for adsorption by oxygen at 185 nm, cm^2, which is reported as 1.2×10^{-20} cm^2 [112].

C_{O_2} is the concentration of oxygen molecules, molec/cm^3.

However, many studies reported that the measured ozone concentration is about one order of magnitude below the theoretically achievable ozone concentration at 172 nm [115] and 185 nm UV [114]. The adsorption of UV radiation by ozone molecule can cause the split of oxygen atoms as well.

$$hv_{185nm} + O_3 \rightarrow O\left(^1D\right) + O_2 \tag{5.9}$$

In the meanwhile, OH radicals and HO_2 radicals can convert to each other with presence of ozone with reactions in Equation 5.10 and Equation 5.3.

$$OH + O_3 \rightarrow HO_2 + O_2 \tag{5.10}$$

$$O\left(^1D\right) + H_2O \rightarrow OH + OH \tag{5.11}$$

The efficiency of ozone generation by UV radiation depends very strongly upon wavelength because of the wavelength dependence of oxygen molecular absorption and ozone molecule adsorption [116]. As shown in Figure 5.2, the peak adsorption efficiency of oxygen is happened at 160 nm, the beginning of the fast decay region. The peak adsorption efficiency of ozone in Schumann-Runge Bands is at 254 nm, where leads to a decomposition of ozone. At 185 nm, ozone was generated since the high UV adsorption by oxygen and low UV adsorption by existing ozone. HO_2

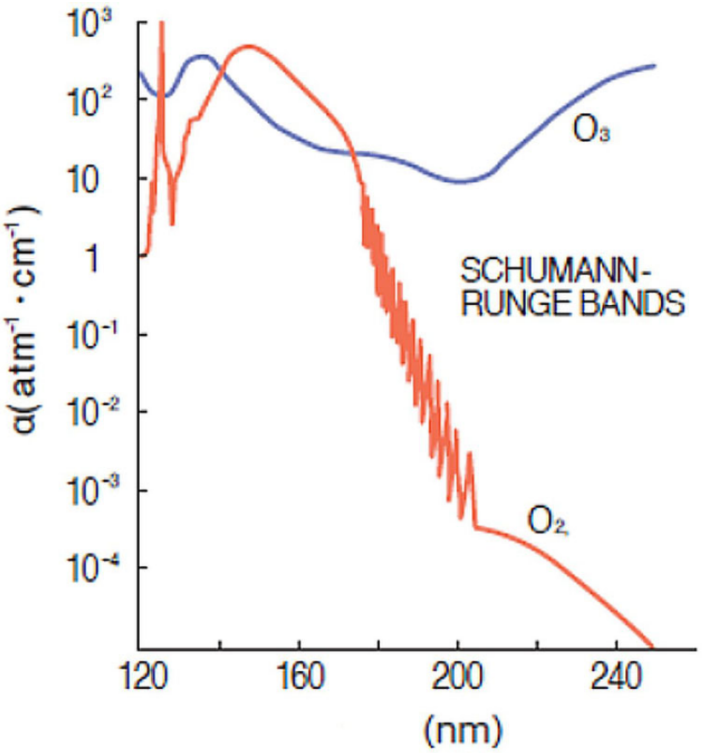

Figure 5.2: Wavelength of dependence of oxygen and ozone adsorption. [117]

radicals can further removed by reaction Equation 5.12 to generate hydrogen peroxide, which can be photolysis to OH radicals.

$$HO_2 + HO_2 \rightarrow H_2O_2 + O_2 \tag{5.12}$$

$$H_2O_2 + hv_{185nm} \rightarrow OH + OH \tag{5.13}$$

The process is summarized in Figure 5.3. From the above analysis, the generation rate of ozone

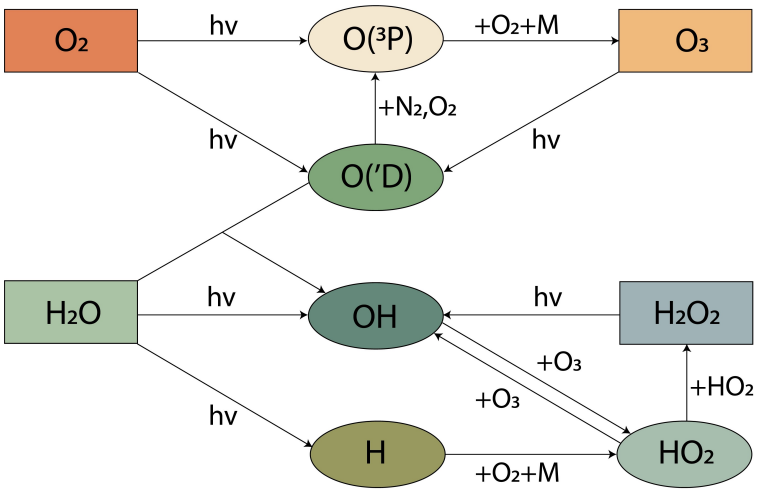

Figure 5.3: Major reactions affecting O_3 and OH radicals by UV light in the chamber test.

from a photochemical process associated with the wavelength of UV and concentration of oxygen. Moisture can produce OH and HO_2 radicals which introducing a new ozone loss mechanism.

5.1.2 AC-2: Ozone and Hydroxyl Radicals Formation from Corona Discharge

Electrostatic precipitator (ESP) and plasma are air purification technologies used to remove particles and gaseous pollutants. An electrostatic precipitator uses a high-voltage electric field to charge particles in the gas stream, which are then attracted to oppositely charged plates or collectors. The ionizer-assisted/plasma air filter is an alternative solution, that ionizes the incoming air and breaks the chemical bonds of the molecules. Particles in the inflow air are attached by ions and collected either on oppositely charged collectors or become attracted to other surfaces. In addition to particulate matter, the ionizer/plasma can inactivate the airborne micro-organisms and chemically transform gaseous pollutants by breaking the chemical bonds of gas molecules.

A high voltage is applied to a dielectric material, which ionizes the surrounding air and creates a corona discharge, which is a type of electrical discharge that occurs in a gas when the electric field exceeds the dielectric strength of air. Ozone can be generated by a corona discharge, where the discharge breaks down oxygen molecules in the air and forms ozone molecules. Water molecules can be destructed in the corona discharge as well, which generate OH radicals and HO_2 radicals. The process is same as the mechanism of ozone and OH radicals generation by UV irradiation

[118, 119]. The only difference is in the type of energy carriers, electrons in the case of electric fields and photons when it comes to UV irradiation.

5.2 Indoor Air Quality Model

To effectively address the issue of IAQ in buildings, it is crucial to understand the factors that contribute to poor IAQ and how to model and predict it. One of the primary factors that can impact IAQ is the presence of indoor pollutants, which can release from various sources such as furniture, building materials, cleaning products, and cooking fumes. In order to accurately model and predict IAQ, it is necessary to consider the sources and types of pollutants that exist in a particular space. However, the interactions between different VOCs are often neglected in existing models of VOCs emission from and sorption on building materials [28, 32]. To address this issue, this study considered the chemical reactions between VOCs and indoor oxidants in the model to account for the secondary emissions of VOCs. Ventilation and air purification are also crucial factors for good IAQ, as they facilitate the removal of pollutants and supply fresh outdoor/clean air. As such, this study developed an IAQ model that considered the transport of pollutants via ventilation, air purification using an air cleaner, sources and sinks of indoor pollutants, and indoor chemical reactions between different pollutants. The governing equation (Equation 5.14) that shows in the mass balance of species i in the bulk air.

$$\frac{dC_i}{dt} = \frac{Q_s}{V}(C_{is} - C_i) - \frac{P_i}{V} + \frac{E_i}{V} - \frac{D_i}{V} + \frac{R_i}{V} \tag{5.14}$$

Where,

C_i is concentration of pollutants i in the bulk air, $\mu g/m^3$.

Q_s is airflow rate of supply air, $\mu g/m^3$.

V is volume of the single zone space, m^3.

$C_{i,s}$ is concentration of pollutants i in the supply air, $\mu g/m^3$.

P_i is the term to describe the removal rate of pollutants i by the air purification system, $\mu g/s$.

E_i is total primary emission rate of pollutants i from all the indoor sources except the secondary emissions from indoor chemical reactions, μg/s.
D_i is adsorption rate of pollutants i to all the indoor sinks except the air purification system and consumed by indoor chemical reactions, μg/s.
R_i is the net formation rate of pollutants i from indoor chemical reactions, μg/s.

In this study, the AC-1 and AC-2 removed particle and virus from the air in the chamber test. The removal rate was modeled with single-pass efficiency (η) by Equation 5.15. The gaseous pollutants were removed by the chemical reactions, therefore the η of VOC equals to zero for AC-1 and AC-2.

$$P_i = Q_r \eta_i C_i \tag{5.15}$$

Where,
Q_r is the airflow rate recirculating through the air cleaner, m^3/s.
η_i is the single-pass removal efficiency of pollutant i, %.

In the chamber test, the background VOCs were emitted from the building materials, furnishings, and soiled T-shirt to mimic the emissions from a human. VOC can be adsorbed by the indoor surfaces if the concentration of VOCs in the bulk air is high. The emissions and adsorption process of a porous media was governed by diffusion in the media and convection mass transfer on the exposures surfaces. The diffusion in the media is modeled by Fick's law, which is associate with the diffusion coefficient. Typically, the diffusion in the material is much lower than the diffusion in the air and convection mass transfer at the air-solid interface. Therefore, the diffusion coefficient limits the transport of VOCs in the media and affect the rate of emission and adsorption. The emission and adsorption rates of VOCs of the building materials and furnishings were assumed as a constant during the chamber test. The emissions from human was simulated by a soiled T-shirt wearing on a heated manikin, which is designed in the experiment to make sure the emission rate can be assumed as a constant during the test. Therefore, considering all the sources and sinks in

the test room, the emission rate and adsorption rates of VOCs were assumed as constants during the chamber tests. The net emission rate was obtained from the chamber test results without using the air cleaners.

The chemical reactions was modeled by reaction rate constant of a first-order reaction.

$$\frac{R_i}{V} = \sum_{x,j} k_{x,j} C_x C_j - \sum_{y} k_{y,i} C_y C_i \tag{5.16}$$

Where,

x, y, j denote another gaseous chemicals that participate in the chemical reactions associated with i.

$k_{x,j}$ (or $k_{y,i}$) is reaction rate constant of reaction between chemical x and j (or y and i), $(\mu g/m^3)^{-1}s^{-1}$.

$\sum_{x,j} k_{x,j} C_x C_j$ and $\sum_{y} k_{y,i} C_y C_i$ represents all the chemical reactions that can produce and consume compound i, respectively.

5.2.1 Estimation of Model Parameter from Model-Based Testing Method

Primary Emission Rate

The primary emission rate was obtained from the challenge concentration that measured in the chamber right before turning on the air cleaner. With assuming the chemical reactions were induced by O_3 and OH, there is no indoor chemical reactions before turning on the air cleaner. The samples were collected at a steady state, when the concentration in the chamber did not change over time. The Equation 5.14 can be rewritten as Equation 5.17.

$$\frac{dC_i}{dt} = 0 = \frac{Q_s}{V}(C_{is} - C_i) + \frac{E_i}{V} - \frac{D_i}{V} \tag{5.17}$$

The net emission rate of pollutant i is obtained from Equation 5.18 with measured ventilation rate, concentration of species in the chamber, and concentration of species in the supply air.

$$E_{i,net} = E_i - D_i = Q_s(C_i - C_{is}) \tag{5.18}$$

Where,

$E_{i,net}$ is the net emission rate of pollutant i, μg/s.

Generation Rate of Ozone

The level of indoor ozone concentration depends on the outdoor ozone concentration, air change rate, indoor emission rate, surface removal rate, and reaction between ozone and other chemicals in air [120]. The mass balance equation of O_3 was defined as Equation 5.19.

$$\frac{dO_3}{dt} = \frac{Q}{V}(C_{O_3,s} - C_{O_3}) + \frac{E_{O_3}}{V} - \frac{D_{O_3}}{V} + \frac{R_{O_3}}{V} \tag{5.19}$$

The O_3 generation rates were obtained by the regression analysis to fit the measured O_3 concentration. The generation rates of O_3 were reported as 12.9 mg/h and 31.1 mg/h for AC-1 and AC-2, respectively. ozone generation is associated with wavelength and intensity of UV light, voltage of electric field, oxygen and water molecule concentrations. Oxygen and moisture are stable and sufficient for the chemical reactions of ozone formation. Therefore, constant generation rate of O_3 can be applied for AC-1 and AC-2.

However, the decay of O_3 is more complex, because ozone is reactive and can react with many indoor surfaces and VOCs. The term of O_3 natural decay on surfaces can be expressed as a first-order decay model [63].

$$D_{O_3} = \sum_m \frac{A_{i,m} v_{O_3,m} C_{O_3}}{V} \tag{5.20}$$

Where,

$\sum_m \frac{A_{i,m} v_{O_3,m}}{V}$ is the ozone removal rate by indoor surfaces, s^{-1}.

$v_{O_3,m}$ is the ozone deposition velocity of the indoor surface m, m/s.

The gaseous chemical reactions of ozone can be expressed as:

$$\frac{R_{O_3}}{V} = -\sum_i k_{O_3,i} C_i C_{O_3} \tag{5.21}$$

Table 5.1: List of VOCs react with OH radicals and reaction rate constant

VOCs	k_{OH}	reference
toluene	5.65×10^{-12}	[121]
alpha-pinene	5.37×10^{-11}	[66]
formaldehyde	8.64×10^{-12}	[121]
acetaldehyde	1.47×10^{-11}	[121]
pentanal	2.82×10^{-11}	[121]
hexanal	2.92×10^{-11}	[121]
heptanal	2.96×10^{-11}	[122]
octanal	2.86×10^{-11}	[123]
nonanal	3.20×10^{-11}	[124]
decanal	3.14×10^{-11}	[123]
acetone	1.69×10^{-12}	[121]
p-xylene	1.43×10^{-11}	[68]
benzaldehyde	5.90×10^{-12}	[68]

To accurately determine the rate of ozone generation in the air, we substituted the variables R_{O_3} and D_{O_3} into the governing equation and employed it to fit the measured O_3 concentration during the chamber test. Through this methodology, the O_3 generation rate under the given experimental conditions was obtained, which is essential for developing further models of the impact of O_3 generation on IAQ.

Generation Rate of Hydroxyl Radicals

The concentration of OH radicals was not directly measured in the chamber test. The generation rate of OH radicals can be estimated if the concentration of OH radicals at steady state and the reaction rate of all the chemical reactions with VOCs are known.

$$\frac{dC_{OH}}{dt} = \frac{Q}{V}(C_{OH,s} - C_{OH}) + \frac{E_{OH,net}}{V} - \sum_m k_{m,OH} C_m C_{OH} \tag{5.22}$$

As shown in Equation 5.22, $\frac{dC_{OH}}{dt} = 0$ because of steady state and $C_{OH,s} = 0$ because of the high reactive OH radicals can be fully removed by the filtration system of the chamber. The reaction rate constant and corresponding VOCs that react with OH radicals are listed in the Table 5.1. The two unknowns in Equation 5.22 are the concentration in air and net generation rate of OH radicals.

The steady state concentration of OH radicals can be estimated with the toluene reduction. AC-1 and AC-2 does not have any other air cleaning technologies to removal gaseous pollutants except ionization, which remove the pollutants by chemical reactions. According to the data from literature [68, 121], toluene does not react with O_3. And there is no known chemical reactions with detected VOCs in the chamber to produce toluene. Therefore, the toluene reduction is purely from the chemical reactions with OH in the chamber test.

$$air\ cleaner\ off:\ \frac{Q}{V}(C_{toluene,s} - C_{toluene}) + \frac{E_{toluene,net}}{V} = 0 \tag{5.23}$$

$$air\ cleaner\ on:\ \frac{Q}{V}(C_{toluene,s} - C_{toluene}) + \frac{E_{toluene,net}}{V} - k_{toluene,OH}C_{toluene}C_{OH} = 0 \tag{5.24}$$

Using the toluene concentrations displayed in Figure 4.13 and Figure 4.14, along with the reaction rate found in Table 5.1, the estimated steady state concentrations of OH radicals are 4.08×10^6 molec/cm^3 and 2.32×10^6 molec/cm^3 during the AC-1 and AC-2 chamber tests, respectively. The corresponding generation rates are 7.87×10^7 molec/(cm^{3}s) and 4.48×10^7 molec/(cm^{3}s) for AC-1 and AC-2, respectively, which are approximately 20% of the theoretical calculation by Equation 5.4 under the same humidity level. However, the theoretical calculation assumed a perfect formation of OH radicals, which did not consider other factors in a indoor condition, such as shading of UV light, trade off between OH and HO_2 radicals, and surface uptake of OH radicals. The estimated generation rate of OH radicals agreed with the measured data by a tracer gas method that using the same UV lamp [110]. This study provided an approach to estimate the steady state and generation rate of OH radicals when the direct measurement is not available. The quantification of OH radicals is challenging due to the high reactivity of OH radicals and a complex indoor chemical mixtures.

5.3 Simplified Modeling of the Chemical Reactions in Indoor Air

In order to apply the IAQ model to real-world situations, it is important to gather information about the primary emission, adsorption, and reaction rate constants of each pollutant. However, it

should be noted that some pollutants, particularly certain short-lived VOC compounds or organic radicals, may not be well understood. To address this, it is necessary to identify the specific VOCs of interest in a typical indoor environment and focus on pollutants that have a measurable impact on IAQ. This study will explore how to model these specific VOCs and their related reactions using a simplified approach, and evaluate the performance of the simplified model in assessing the issue of secondary emissions and IAQ.

5.3.1 Define Target VOCs of Interest and Related Indoor Chemical Reactions

The indoor concentration and types of VOC compounds can vary significantly based on the presence of potential indoor sources. Therefore, each case may have unique VOC profiles and concentrations. Annex 68 project has set up the metrics to access the performance of low-energy buildings as regards indoor air quality combining the aspirations to achieve high energy performance without compromising indoor environmental quality. The Annex 68 project compared the measured VOC concentrations in Asia, Europe, North America, and Africa, along with the exposure limitations set in these regions. The IAQ evaluation in this study targeted specific VOCs of interest by combining the measured VOCs in the chamber with the suggested VOCs from Annex 68 project (Table 5.2). Based on this analysis, the project selected specific VOCs of interest to create a reference for comparison between regions with varying levels of development and climates. The chamber test simulated realistic conditions, where the background VOCs were similar to those typically found in actual buildings. The defined target VOCs of interest include toluene, acetaldehyde, formaldehyde and α-pinene. Since the chemical reactions of other C4-C9 aldehydes are a significant source of formaldehyde and acetaldehyde, all measured aldehydes were included as target VOCs in this modeling study.

5.3.2 Major or Representative OH Radical Induced Reactions Modeled

The Master Chemical Mechanism (MCM version 3.2) is a comprehensive modeling and simulation software for predicting the dynamics of reactants and reaction products in a gas mixture including

Table 5.2: List of detected VOCs and selected target pollutants for Annex 68 with their respective concentration and exposure limits

VOCs	Concentration μg/m^3	Annex 68 target	Long-term exposure limit μg/m^3
Formaldehyde	30.2	Yes	9
Acetaldehyde	8.6	Yes	48
Acetone	15.5		
Pentanal	2.1		
Toluene	73.9	Yes	250
Hexanal	5.2		
p-xylene	2.6		
α-pinene	2.8	Yes	200
Benzaldehyde	2.3		
Octanal	1.3		
2-Ethyl-1-hexanol	3.4		
Phenol	1.5		
Acetophenone	2.4		
Nonanal	5.6		
2-Nonnal,(E)	2.3		
Decanal	2.2		
2-Ethylhexyl acrylate	19.1		

intermediate reaction products. For the test chamber condition of the present study, it can include hundreds or even thousands of chemical species. Predicting the concentrations of all the species present is also unnecessary since only a few are of interest from IAQ perspective. This study focuses on modeling the target compounds of interest to IAQ that are significantly present at the steady state without modeling the intermediate species and those with lower concentrations than background levels before the air cleaner was turned on.

NO_3 is an essential indoor oxidant that can initiate many reactions with VOCs results in various radicals and stable compounds, such as formaldehyde, acetaldehyde and acetone. NO_3 is produced when O_3 reacts with NO_2, leading to the formation of NO_3 and O_2. Recent studies pointed out the photolysis of HONO, which is produced from combustion or NO_2 hydrolysis on indoor surfaces, as a source of indoor OH. Without combustion appliances, the indoor concentration of NO_2 is typically around half of outdoor concentration, which ranges from 45 to 65 ppb in the U.S. from 2000 - 2015 [125, 126]. Measuring NO_3 proves challenging, but model-based approaches and

inference experiments have estimated concentrations with an upper bound of 10^{-3} ppb [121]. Given this upper bound for NO_3, only reactions with alpha-pinene need to be considered. This is because the reaction rate between NO_3 and alpha-pinene surpasses that of reactions with aldehydes and toluene by 4-5 orders of magnitude. This difference in reaction rate means only the interaction between NO_3 and alpha-pinene significantly influences on IAQ.

During the chamber test, the conditions had reduced NO_2 (5.7 ppb) and NO_3 levels due to the absence of combustion and photolysis in the test room. Therefore, this project only considers reactions initiated by ozone and OH radicals. However, if other reactions, such as NO_3/alpha-pinene, O_3/NO_2, HONO photolysis, are considered in different conditions, the principles outlined in Equation 5.14, target VOCs selection, and the simplified indoor chemical reaction model remain applicable. Adjustments to the chemical reaction model would be necessary to accurately capture real-world conditions in simulations.

Toluene

The reaction between toluene and hydroxyl radicals in the gas phase is an important process in atmospheric chemistry. The reaction between toluene and hydroxyl radicals in the gas phase is a complex process and can be grouped in four routes as shown in Figure 5.4.

One of the pathways involved in the interaction between toluene and OH radicals in the gas phase is the hydrogen abstraction (H-abstraction) mechanism. This mechanism entails the OH radical extracting a hydrogen atom from toluene, resulting in the formation of a benzylperoxy radical.

$$C_7H_8\ (toluene) + OH \rightarrow C_7H_7O_2 \tag{5.25}$$

The benzylperoxy radical is a highly reactive species that can undergo self-destruction or react with various indoor oxidants such as OH, HO_2, NO, and NO_3. This leads to the production of several oxidized products, including benzaldehyde, benzyloxy radicals, nitrooxymethyl-benzene, and benzyl alcohol. Some of these products are susceptible to photolysis or reaction with other radicals, resulting in the generation of more radicals that can propagate the oxidation process. In

the toluene-OH reaction mechanism, the hydrogen abstraction pathway leads to the production of benzaldehyde as the final stable product. According to the reaction mechanism reported in MCM, benzaldehyde is produced in 7% of toluene-OH reactions [68].

OH addition can occur as an alternative pathway to hydrogen abstraction. While hydrogen abstraction is the dominant reaction pathway, OH addition to the aromatic ring can lead to the formation of various oxygenated products. In the OH addition pathway, which is also called phenolic route, the hydroxyl radical reacts with toluene by adding to one of the carbon atoms in the aromatic ring. The resulting radicals can further react with indoor oxidants, generating different products including phenols, cresols, and other oxygenated compounds.

$$C_7H_8\ (toluene) + OH \rightarrow C_7H_7OH \tag{5.26}$$

These oxygenated products can participate in additional reactions and contribute to the formation of other secondary pollutants. The total yield is approximately 18% of phenolic route [68]. The overall reaction can generate stable final products as phenol, cresols, and formaldehyde.

It is evident that a significant portion of the reaction pathways are not explained by the above two reaction sequences. The available data indicates that 75% of toluene reactions of OH addition on aromatic ring leading to open the aromatic ring through epoxy and peroxy-bicyclic ring opening channels. In the epoxy and peroxide-bicyclic route, OH radicals and O-atoms are added to the aromatic ring, forming 2,3-epoxy-6-oxo-4-heptenal, glyox, and other peroxy radicals. These ring-opened products then react with OH and HO_2, leading to the production of formaldehyde and inorganic compounds.

Aldehydes

The reaction of aldehydes with hydroxyl radicals plays a significant role in the degradation of aldehydes and the formation of secondary pollutants. Aldehydes are a class of organic compounds that contain a carbonyl group (C = O) bonded to a hydrogen atom and alkyl or an aryl group.

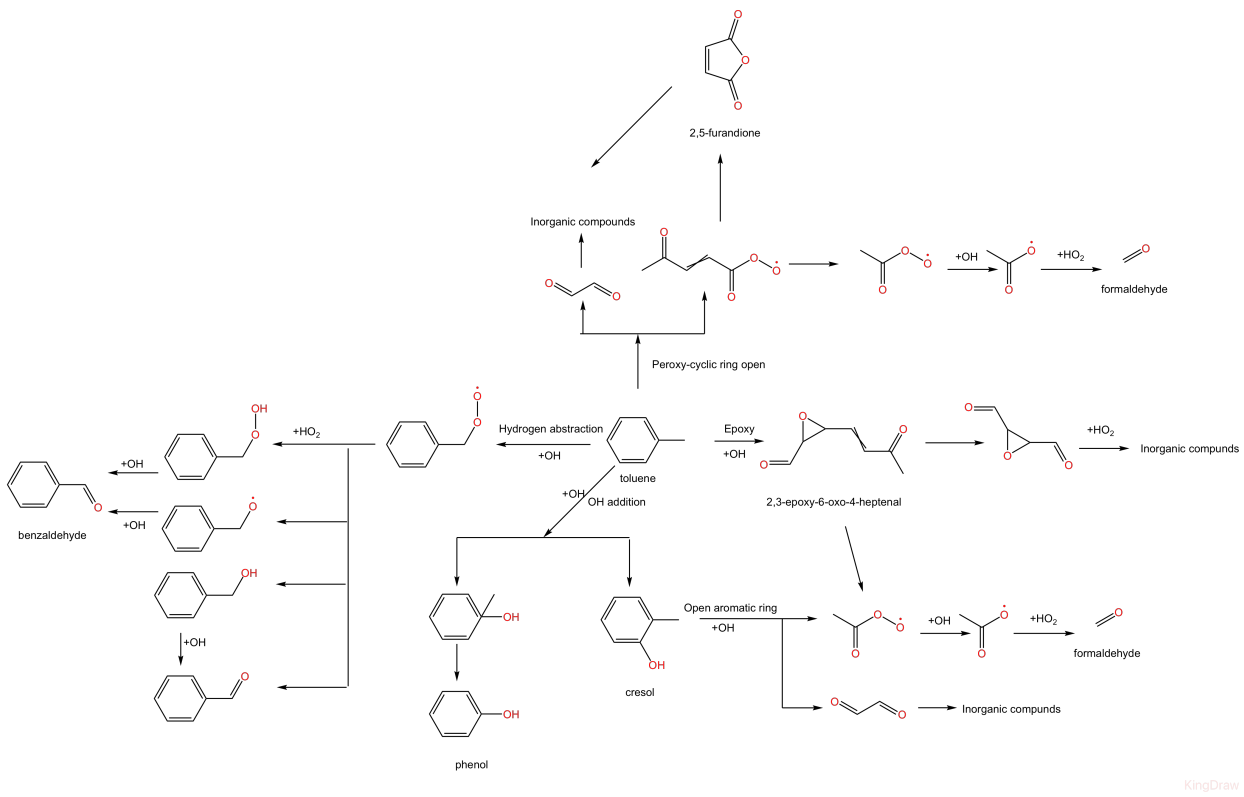

Figure 5.4: Mechanism of toluene OH radical reactions

The general formula for an aldehyde is C_nH_mCHO. The reaction of aldehydes with OH radicals typically follows the mechanism of hydrogen abstraction. The OH radical abstracts a hydrogen atom from the aldehyde, forming an alkoxyl radical (C_nH_mCO).

$$C_nH_mCHO + OH \rightarrow C_nH_mCO\ (alkoxy\ radical) \tag{5.27}$$

The alkoxy radical is highly reactive and can undergo further reactions in the atmosphere. One common reaction is with oxygen, which can form a peroxy radical (C_nH_mCOO).

$$C_nH_mCO + O_2 \rightarrow C_nH_mCOO\ (peroxy\ radical) \tag{5.28}$$

The alkoxy radicals and peroxy radicals can rapidly decompose to yield the alkyl radical and CO_2, which can further react to form aldehydes and alcohol with one less carbon atom in the presence of oxidants ($C_{n-1}H_{m-2}CHO$ and $C_nH_{2n+1}OH$, respectively). The actual reactions involved are more

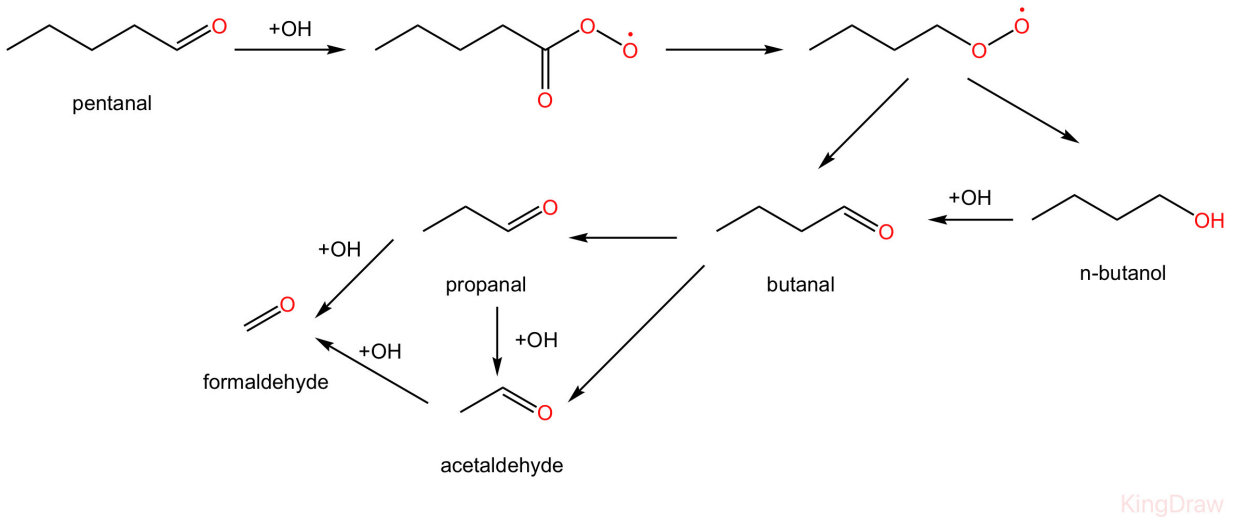

Figure 5.5: Mechanism of pentanal OH radicals reactions

complex, as many unstable radicals are produced during the process. Figure 5.5 provides an example of the reaction mechanism in which pentanal reacts with OH radicals to produce acetaldehyde and formaldehyde.

Alpha-pinene

The primary reaction pathway between α-pinene and OH radicals involves the addition of OH to the double carbon bond. This reaction results in the formation of a cyclic alkyl radical. The newly formed radical can react with oxygen to create a peroxy radical, which can subsequently react with oxygen to produce various oxygenated products, including pinonaldehyde, 2-hydroxy-3-pinanone, and other organic compounds. As depicted in Figure 5.6, these oxygenated products participate in a chain reaction with oxygen to produce stable products such as acetone, formaldehyde, and pinonaldehyde. Pinonaldehyde can further react with oxygen and the alkyl group to produce acetone and formaldehyde. Therefore, the final stable products of IAQ concern from the α-pinene and OH radicals reactions are acetone and formaldehyde.

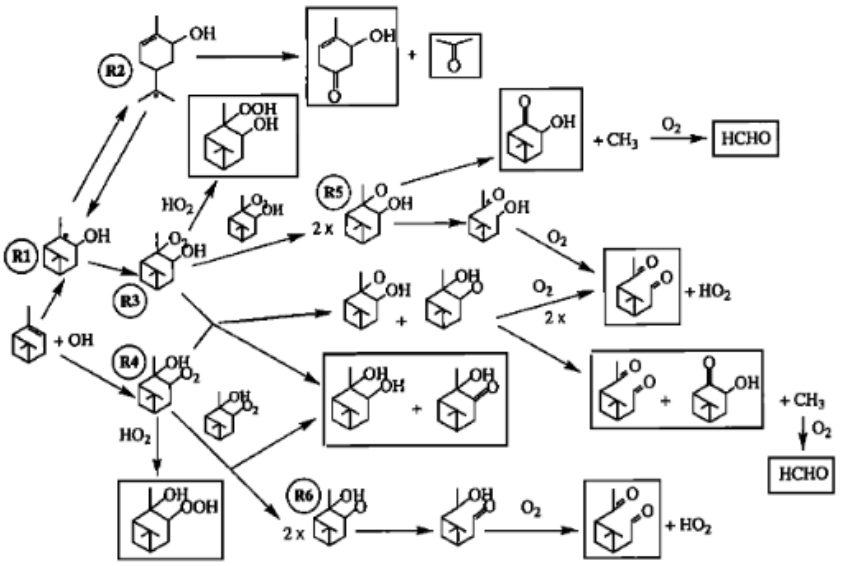

Figure 5.6: Mechanism of alpha-pinene OH radicals reactions [127]

5.3.3 Major or Representative Ozone Induced Reactions Modeled

Ozone is considered as an important indoor oxidant that can react with various organic compounds such as isoprene and styrene. However, the reactions between ozone/toluene and ozone/aldehydes are reported to be very low or even non-existent.

In addition to the gas-phase reactions, ozone are reactive in many indoor surfaces, especially the reactions with carpet, human skin, gypsum board and painting. Clean indoor surfaces have different chemical compositions, but they accumulate surface films with exposure to indoor environments [67, 128]. These surface films tend to be similar both within and across different occupied settings because they are derived from various sources, such as human occupants themselves, occupant activities like cooking and cleaning, and materials containing similar types of semi-volatile additives. This commonality in composition and governing processes potentially simplifies the modeling of chemical transformations that are mediated by indoor surfaces, reducing the large range of different surface types that must be considered when evaluating indoor surface chemistry [67]. In order to investigate the impact of ozone reactions on IAQ, modeling a soiled surface instead of a new clean surface is more reasonable. The organic film on indoor surfaces, which

consists of background VOCs and human skin oil, accumulates over time. As discussed in the gas-phase reactions, ozone reactions with background VOCs of IAQ interest is negligible. The reaction between skin oil and ozone has been extensively studied, and squalene ozonolysis reactions are the major process involved in this reaction [63, 106, 120]. Therefore, in the simplified model, only squalene reactions were considered in the simulation (Figure 5.7). The squalene ozonolysis reac-

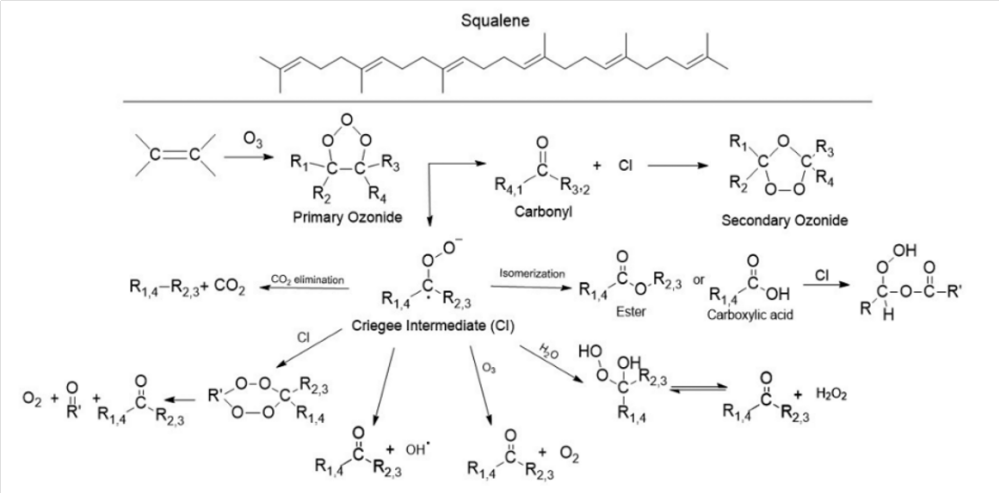

Figure 5.7: Mechanism of squalene ozone reactions [129]

tion is well-established, and the major products include 6-methyl-5-hepten-2-one (14%), acetone (13%), 4-oxopentanal (12%), as well as other hydrocarbons and oxygenates [10].

The ozone-squalene film reactions were modeled by the ozone deposition rate. In a previous ozone decay test, the ozone deposition rate in the same room setting was measured to be approximately 5.5 h^{-1}. The yields of reaction products, such as acetone, 6-MHO, 4-OPA, nonanal, decanal, propanal, and acetaldehyde, were determined based on the study conducted by Wang et al [10]. The gas-phase reactions of these products have been considered in the model.

5.4 Simulation Results and Discussion

Simulations were carried out for the AC-1 and AC-2. The simulation was conducted to represent the chamber test conditions, which is crucial for validating the accuracy of indoor air quality models and gaining a comprehensive understanding of indoor chemical reactions.

5.4.1 Simulation of Chamber Test Condition for AC-1

The stable concentration outcome of the primary emission (refer to Figure 5.8) represented the chamber test results exactly. This is because the net generation rate of VOCs was derived from the measured concentration.

In terms of secondary emissions, simulation results exhibited the same concentration of toluene as observed in the chamber test. This suggests that the estimation of the generation rate of hydroxyl radicals accurately represented the conditions of the chamber test. The toluene-OH reaction led to the production of benzaldehyde and phenol, both of which were detected in the chamber test. However, the simulation reported a smaller quantity of benzaldehyde and phenol in comparison to the chamber test.

The background VOCs were devoid of benzene and p-xylene, both of which fell below the detection threshold. No reactions capable of producing benzene and p-xylene occurred during the chamber test. As such, in the simulation for the air cleaner "ON" state, no additional benzene and p-xylene were generated.

Numerous reactions, including toluene-OH radicals reactions, aldehyde-OH radicals reactions, and squalene-ozone reactions, resulted in the formation of formaldehyde. The squalene-ozone reactions produced acetone and acetaldehyde. The simulated concentrations of formaldehyde, acetaldehyde, and acetone were in strong agreement with the measured data, validating that the simplified IAQ model successfully captured the principal reactions within the chamber.

Based on the alignment between simulation and chamber test findings, the simplified IAQ model has proven its capacity to accurately represent chemical reactions within the test chamber for AC-1. This model is able to evaluate the effects of secondary emissions from AC-1 caused by ozone and OH radical-initiated reactions on indoor air quality.

5.4.2 Simulation of Chamber Test Condition for AC-2

The steady-state concentration result of primary emission (Figure 5.9) showed exactly the same results as the chamber test because the net generation rate of VOCs was obtained from the measured

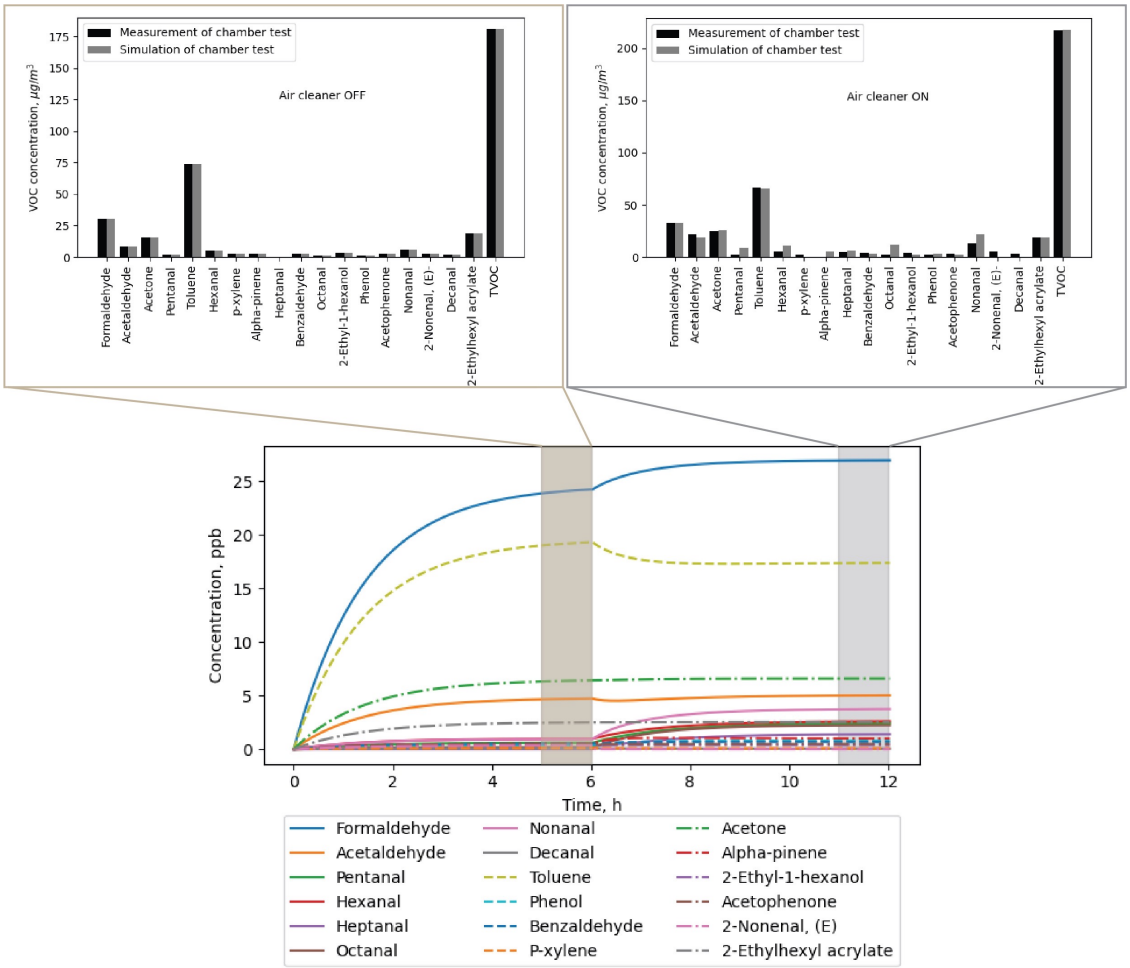

Figure 5.8: Simulated VOC concentrations at transient period and the comparison with measured data at steady state

concentration.

Regarding secondary emission, the simulation results showed that the concentration of toluene was identical to the chamber test results, indicating that the estimation of the generation rate of hydroxyl radicals accurately represented the chamber test conditions. The toluene-OH reaction produced benzaldehyde and phenol, which were detected in the chamber test. However, the simulation showed a lower amount of benzaldehyde and phenol compared to the chamber test. The background VOCs did not contain benzene and p-xylene, which were below the detection limit. During the chamber test, no reactions could have produced benzene and p-xylene. Therefore, no additional benzene and p-xylene were generated in the simulation for the air cleaner "ON" condition. However, the chamber test detected benzene and p-xylene at approximately 2 $\mu g/m^3$ and 1 $\mu g/m^3$, respectively. This phenomenon has been observed in chamber tests of fiber filter based air cleaners which indicating no secondary emission from the air cleaners. Hence, the results for benzene, p-xylene, benzaldehyde and phenol might be due to the uncertainty associated with low concentrations close to the GC-MS detection limit.

Formaldehyde was formed by many reactions including toluene-OH radicals reactions, aldehyde-OH radicals reactions, and squalene-ozone reactions. Acetone and acetaldehyde were produced from the squalene-ozone reactions. The simulated formaldehyde, acetaldehyde and acetone concentrations agree very well with the measured data, which verified that simplified IAQ model captured the major reactions in the chamber.

Based on the comparison of simulation and chamber test results, the simplified IAQ model demonstrated its ability to accurately represent chemical reactions in the test chamber for AC-2. This model is suitable for evaluating the impact of secondary emissions from AC-2 resulting from ozone and OH radical-initiated reactions on IAQ. Furthermore, the parameters obtained from the chamber test can be applied to extend the model to simulate various indoor environments beyond the test chamber conditions.

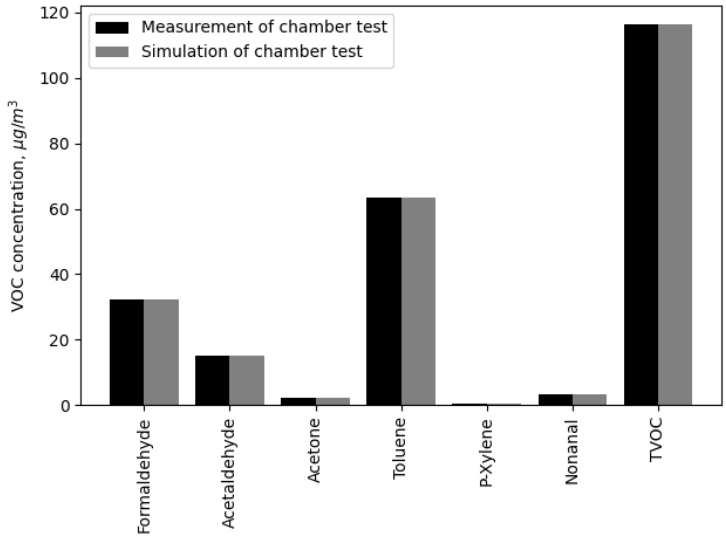

Figure 5.9: VOC concentrations at steady state of the chamber test for AC-2 “OFF” condition

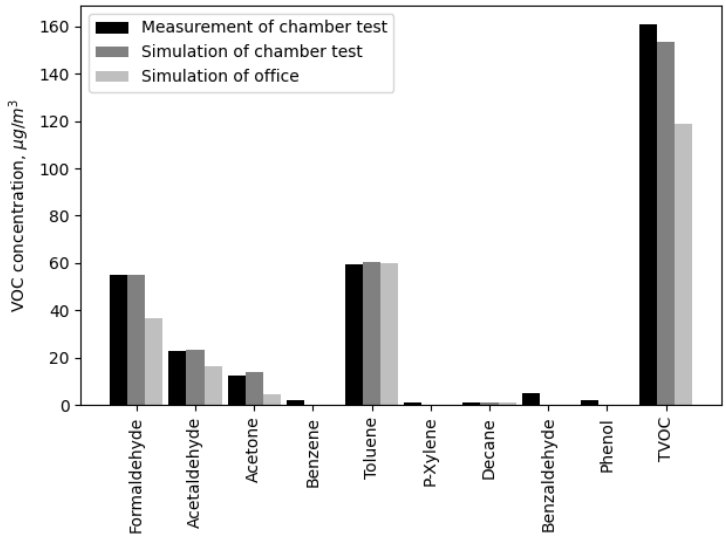

Figure 5.10: VOC concentrations at steady state of the chamber test for AC-2 “ON” condition

5.4.3 Simulation of An Open-plan Office with AC-2

The IAQ model was integrated into the reference case described in the literature for evaluating the airborne transmission of SARS-CoV-2 where an air cleaner can improve IAQ and reduce infection risk [130]. The space had a floor area of 191.9 m^2 with a ceiling height of 2.7 m^3, and the number of occupants and minimum ventilation rate were in compliance with ASHRAE Standard 62.1-2022. According to the installation instruction of AC-2, a minimum duct length of 83 m is required to ensure a safe UV-C exposure level for users if AC-2 is directly connected to an occupied area. The extra sink of ozone by HAVC ducts was simulated by sink model, which quantified the ozone deposition rate associated with duct exposure surface area and Reynolds number, from literature [131]. The duct size and Reynolds number based on the total airflow rate through AC-2 was determined by ASHRAE duct size calculator [132].

The larger surface areas of floor, ceiling, and wall in the office case led to additional ozone deposition compared to the chamber test. The presence of a workstation for each occupant resulted in additional indoor surfaces, which were estimated based on the BIFMA X7.1 Standard 2011 (R2016). By including these additional ozone sinks, the final ozone concentration in the occupied area was approximately 5 ppb. The background VOC concentrations were identical to the chamber test, representing the primary emissions from a typical office room. The formaldehyde and toluene concentrations were higher than typical building pollutant levels, but were chosen to represent a challenging concentration for AC-2.

The simulation results of the office case showed that the ozone-associated reaction products, including formaldehyde, acetaldehyde, and acetone, were much lower than in the chamber test, particularly for acetone, a major product of squalene-ozone reactions (Figure 5.10). This is despite the lower ozone concentration in the office case. The concentration of aromatic compounds, such as toluene, p-xylene, benzene, phenol, and benzaldehyde, were unaffected by the change in ozone concentration because their reactions are OH-radical-initiated. The results demonstrate that the IAQ model can accurately evaluate the impact of secondary emissions from ozone and OH-radical-initiated chemical reactions on IAQ and can be used for further modeling beyond chamber test

conditions with parameters obtained from the chamber test.

5.5 Summary and Conclusion

In conclusion, the conducted chamber test of AC-1 and AC-2 showed significant secondary emissions from the UV light and corona discharge generated by the electrostatic precipitation (ESP) technology. A simplified IAQ model was developed and validated using the chamber test results, which enabled the evaluation of the impact of secondary emissions on indoor air quality. A novel approach for estimating the model parameters based on the concentrations measured at steady states of chamber tests was developed. The estimation of hydroxyl radicals' concentration and net generation rate resulting from toluene reduction needs to emphasize. Direct measuring concentration of OH radicals poses challenges. This research introduced a novel method using toluene as the reference gas. While this approach was successfully validated under chamber test conditions, further research is required to adapt it to actual building environment. The results highlighted that with these specific parameters, the model effectively characterizes both primary and secondary VOC emissions based on a simplified indoor chemistry model. This model is specifically simplified to focus on stable and detectable indoor VOCs which are harmful to human health.

While this study advances the understanding of VOC emissions, additional research remains necessary. Although this study provides a valuable framework for model simplification, the presented simplifications rely on the measurements under these specific experimental conditions. A more extensive exploration of the indoor VOC mixture could pave the way for broader applications of the simplified model, extending its relevance to real-world building conditions.

By implementing simplifications, the computational load and resource requirements have been significantly reduced. This enables the IAQ model to scale up to a building level, accommodating multi-zone models.

CHAPTER 6

CONCLUSION AND RECOMMENDED FUTURE STUDIES

This study has provided a comprehensive examination of primary and secondary emissions in indoor environments, emphasizing the necessary of transitioning laboratory findings to real-world building applications. Due to the vast array of VOC species, building materials, building types, lighting conditions, and indoor thermal conditions, there is a crucial need for systematic approaches for estimating essential model parameters of mechanistic models.

Based on the analysis of the similarity and difference between VOC and water vapor sorption and transport in porous medium, a new correlation has been developed to estimate the VOC partition coefficient based on the water vapor sorption isotherm for the same material. A novel correlation has been proposed between the adsorption energy and monolayer saturation adsorption amount of VOCs and moisture isotherm data of the same material. This relationship facilitates the prediction of partition coefficients for certain VOCs, providing a theoretical foundation for the exploration of VOC behavior in building materials.

Furthermore, this study have analyzed the crucial role of hydrogen peroxide-based housekeeping agents and indoor air purifiers in maintaining air quality, while highlighting the need for caution regarding potential harmful by-products. Comprehensive investigations were conducted for the housekeeping agent and the air purifiers in a test room that represents a typical indoor VOC mixture and interior surfaces. Further investigations on diverse lighting conditions, air purification devices, and secondary VOC emissions have underscored the complex interactions between various factors affecting indoor air quality.

Lastly, a simplified IAQ model that effectively characterizes both primary and secondary VOC emissions has been developed. The simplification reduced the required computation load of modeling indoor chemical reactions and was able to predict the stable VOC by-products from these reactions. The model was verified for specific set of experimental conditions for which the model

was developed. Further validation is needed for different indoor environmental settings including ventilation rate, indoor surface materials and thermal conditions. To further expand its relevance, a more comprehensive study of indoor VOC mixtures is required, which will in turn facilitate its application to a wider range of building conditions.

The findings and methodologies presented in this study will serve as valuable tools for researchers to establish a database for estimating VOC pollution loads of VOC-material and VOC-device pairing, which are needed for IAQ design and control in buildings.

REFERENCES

[1] Yousef Al Horr et al. "Occupant productivity and office indoor environment quality: A review of the literature". In: *Building and environment* 105 (2016), pp. 369–389.

[2] Lidia Morawska and Donald K Milton. "It is time to address airborne transmission of coronavirus disease 2019 (COVID-19)". In: *Clinical Infectious Diseases* 71.9 (2020), pp. 2311–2313.

[3] Nick Wilson, Stephen Corbett, and Euan Tovey. "Airborne transmission of covid-19". In: *bmj* 370 (2020).

[4] Shelly L Miller et al. "Transmission of SARS-CoV-2 by inhalation of respiratory aerosol in the Skagit Valley Chorale superspreading event". In: *Indoor air* 31.2 (2021), pp. 314–323.

[5] Kaiwei Luo et al. "Transmission of SARS-CoV-2 in public transportation vehicles: a case study in Hunan Province, China". In: *Open forum infectious diseases*. Vol. 7. 10. Oxford University Press US. 2020, ofaa430.

[6] Ye Shen et al. "Community outbreak investigation of SARS-CoV-2 transmission among bus riders in eastern China". In: *JAMA internal medicine* 180.12 (2020), pp. 1665–1671.

[7] Leonardo Setti et al. *Airborne transmission route of COVID-19: Why 2 meters/6 feet of inter-personal distance could not be enough*. 2020.

[8] Jianjian Wei and Yuguo Li. "Airborne spread of infectious agents in the indoor environment". In: *American journal of infection control* 44.9 (2016), S102–S108.

[9] Nicolas Castano et al. "Fomite transmission, physicochemical origin of virus–surface interactions, and disinfection strategies for enveloped viruses with applications to SARS-CoV-2". In: *ACS omega* 6.10 (2021), pp. 6509–6527.

[10] Nijing Wang et al. "Emission rates of volatile organic compounds from humans". In: *Environmental Science & Technology* 56.8 (2022), pp. 4838–4848.

[11] Charles J Weschler and Nicola Carslaw. "Indoor chemistry". In: *Environmental Science & Technology* 52.5 (2018), pp. 2419–2428.

[12] Karimatu L Abdullahi, Juana Maria Delgado-Saborit, and Roy M Harrison. "Emissions and indoor concentrations of particulate matter and its specific chemical components from cooking: A review". In: *Atmospheric Environment* 71 (2013), pp. 260–294.

[13] Xiaochen Tang et al. "Volatile organic compound emissions from humans indoors". In: *Environmental science & technology* 50.23 (2016), pp. 12686–12694.

[14] Charles J Weschler. “Changes in indoor pollutants since the 1950s”. In: *Atmospheric environment* 43.1 (2009), pp. 153–169.

[15] Hugo Destaillats et al. “Indoor pollutants emitted by office equipment: A review of reported data and information needs”. In: *Atmospheric Environment* 42.7 (2008), pp. 1371–1388.

[16] S Liu et al. “Contribution of human-related sources to indoor volatile organic compounds in a university classroom”. In: *Indoor Air* 26.6 (2016), pp. 925–938.

[17] Shang Liu et al. “Gas-phase carboxylic acids in a university classroom: Abundance, variability, and sources”. In: *Environmental Science & Technology* 51.10 (2017), pp. 5454–5463.

[18] William W Nazaroff and Charles J Weschler. “Cleaning products and air fresheners: exposure to primary and secondary air pollutants”. In: *Atmospheric environment* 38.18 (2004), pp. 2841–2865.

[19] Mustafa Odabasi. “Halogenated volatile organic compounds from the use of chlorine-bleach-containing household products”. In: *Environmental science & technology* 42.5 (2008), pp. 1445–1451.

[20] Vincent Y Seaman, Deborah H Bennett, and Thomas M Cahill. “Indoor acrolein emission and decay rates resulting from domestic cooking events”. In: *Atmospheric Environment* 43.39 (2009), pp. 6199–6204.

[21] C Stönner, A Edtbauer, and J Williams. “Real-world volatile organic compound emission rates from seated adults and children for use in indoor air studies”. In: *Indoor Air* 28.1 (2018), pp. 164–172.

[22] Xiaochen Tang et al. “Siloxanes are the most abundant volatile organic compound emitted from engineering students in a classroom”. In: *Environmental Science & Technology Letters* 2.11 (2015), pp. 303–307.

[23] Marc O Abadie and Pawel Wargocki. “CR 17: Indoor Air Quality Design and Control in Low-energy Residential Buildings-Annex 68— Subtask 1: Defining the metrics— In the search of indices to evaluate the Indoor Air Quality of low-energy residential buildings”. In: (2017).

[24] JM Logue et al. “Hazard assessment of chemical air contaminants measured in residences”. In: *Indoor air* 21.2 (2011), pp. 92–109.

[25] John C Little, Alfred T Hodgson, and Ashok J Gadgil. “Modeling emissions of volatile organic compounds from new carpets”. In: *Atmospheric Environment* 28.2 (1994), pp. 227–234.

[26] Steven S. Cox, Dongye Zhao, and John C. Little. “Measuring partition and diffusion coefficients for volatile organic compounds in vinyl flooring”. In: *Atmospheric Environment* 35.22 (2001), pp. 3823–3830.

[27] Jinsong Zhang, Jianshun S Zhang, and Qingyan Chen. “Effects of Environmental Conditions on the Sorption of VOCs on Building Materials-Part II: Model Evaluation (RP-1097)”. In: *TRANSACTIONS-AMERICAN SOCIETY OF HEATING REFRIGERATING AND AIR CONDITIONING ENGINEERS* 109.1 (2003), pp. 167–178.

[28] Zhenlei Liu et al. “Development of a procedure for estimating the parameters of mechanistic VOC emission source models from chamber testing data”. In: 14 (2020), pp. 269–282.

[29] Hongyu Huang and Fariborz Haghighat. “Modelling of volatile organic compounds emission from dry building materials”. In: *Building and Environment* 37.11 (2002), pp. 1127–1138.

[30] Yinping Zhang and Ying Xu. “Characteristics and correlations of VOC emissions from building materials”. In: *International Journal of Heat and Mass Transfer* 46.25 (2003), pp. 4877–4883.

[31] Xudong Yang et al. “Numerical simulation of VOC emissions from dry materials”. In: *Building and Environment* 36.10 (2001), pp. 1099–1107.

[32] Baoqing Deng and Chang Nyung Kim. “An analytical model for VOCs emission from dry building materials”. In: *Atmospheric Environment* 38.8 (2004), pp. 1173–1180.

[33] Jianhshun Jensen Zhang, Zhenlei Liu, and Bing Beverly Guo. “Model-based testing and evaluation of VOC emission sources and sinks: theory and application”. In: 609.4 (2019), p. 042015.

[34] JS Zhang et al. “Models for predicting volatile organic compound (VOC) emissions from building materials”. In: *CMEIAQ report* 3 (1999).

[35] N Pétigny et al. “Indoor air depolluting material: Combining sorption testing and modeling to predict product’s service life in real conditions”. In: *Building and Environment* 202 (2021), p. 107838.

[36] G He, X Yang, and CY Shaw. “Material emission parameters obtained through regression”. In: *Indoor and Built Environment* 14.1 (2005), pp. 59–68.

[37] Guoqing He and Xudong Yang. “On regression method to obtain emission parameters of building materials”. In: *Building and environment* 40.9 (2005), pp. 1282–1287.

[38] Jianyin Xiong, Yuan Yao, and Yinping Zhang. “C-history method: rapid measurement of the initial emittable concentration, diffusion and partition coefficients for formaldehyde and VOCs in building materials”. In: *Environmental Science & Technology* 45.8 (2011), pp. 3584–3590.

[39] Jianyin Xiong, Shaodan Huang, and Yinping Zhang. “A novel method for measuring the diffusion, partition and convective mass transfer coefficients of formaldehyde and VOC in building materials”. In: *PloS one* 7.11 (2012), e49342.

[40] Jianyin Xiong et al. “Measuring the characteristic parameters of VOC emission from paints”. In: *Building and environment* 66 (2013), pp. 65–71.

[41] Xiaojun Zhou, Yanfeng Liu, and Jiaping Liu. “Alternately airtight/ventilated emission method: A universal experimental method for determining the VOC emission characteristic parameters of building materials”. In: *Building and Environment* 130 (2018), pp. 179–189.

[42] Awad Saad Bodalal. “Fundamental mass transfer modeling of emission of volatile organic compounds from building materials.” PhD thesis. Carleton University, 1999.

[43] Yanfeng Liu et al. “A prediction model of VOC partition coefficient in porous building materials based on adsorption potential theory”. In: *Building and Environment* 93 (2015), pp. 221–233.

[44] MM i Dubinin. “Physical adsorption of gases and vapors in micropores”. In: *Progress in surface and membrane science*. Vol. 9. Elsevier, 1975, pp. 1–70.

[45] Ke Zhou et al. “Experimental and DFT study on the adsorption of VOCs on activated carbon/metal oxides composites”. In: *Chemical Engineering Journal* 372 (2019), pp. 1122–1133.

[46] Manaschai Kunaseth et al. “A DFT study of volatile organic compounds adsorption on transition metal deposited graphene”. In: *Applied Surface Science* 396 (2017), pp. 1712–1718.

[47] Jing Xu and Jianshun S Zhang. “An experimental study of relative humidity effect on VOCs’ effective diffusion coefficient and partition coefficient in a porous medium”. In: *Building and Environment* 46.9 (2011), pp. 1785–1796.

[48] Jing Xu. “Study of VOCs transport and storage in porous media and assemblies”. PhD thesis. Syracuse University, 2012.

[49] Brett C Singer et al. “Indoor secondary pollutants from cleaning product and air freshener use in the presence of ozone”. In: *Atmospheric Environment* 40.35 (2006), pp. 6696–6710.

[50] Meng Kong et al. “Development of a test method to determine the effectiveness of UVC systems on commercial cooking effluent (RP-1614)”. In: *Science and Technology for the Built Environment* 26.9 (2020), pp. 1285–1300.

[51] Hua Qian et al. “Indoor transmission of SARS-CoV-2”. In: *Indoor Air* 31.3 (2021), pp. 639–645.

[52] Alex WH Chin et al. “Stability of SARS-CoV-2 in different environmental conditions”. In: *The Lancet Microbe* 1.1 (2020), e10.

[53] Neeltje Van Doremalen et al. “Aerosol and surface stability of SARS-CoV-2 as compared with SARS-CoV-1”. In: *New England journal of medicine* 382.16 (2020), pp. 1564–1567.

[54] *Coronavirus disease (COVID-19): Cleaning and disinfecting surfaces in non-health care settings*. https://www.who.int/news-room/questions-and-answers/item/coronavirus-disease-covid-19-cleaning-and-disinfecting-surfaces-in-non-health-care-settings. Accessed May 17, 2023.

[55] *List N Tool: COVID-19 Disinfectants*. https://cfpub.epa.gov/wizards/disinfectants/. Accessed May 17, 2023.

[56] *FILTRATION/DISINFECTION*. https://www.ashrae.org/technical-resources/filtration-disinfection. Accessed May 17, 2023.

[57] Yinping Zhang et al. “Can commonly-used fan-driven air cleaning technologies improve indoor air quality? A literature review”. In: *Atmospheric Environment* 45.26 (2011), pp. 4329–4343.

[58] Alireza Afshari et al. “Electrostatic precipitators as an indoor air cleaner—a literature review”. In: *Sustainability* 12.21 (2020), p. 8774.

[59] Wenhao Chen and Jianshun Jensen Zhang. “Photocatalytic oxidation of multi-component systems–an investigation using toluene/ethylbenzene, octane/decane/dodecane and formaldehyde/acetaldehyde”. In: *Journal of Advanced Oxidation Technologies* 11.1 (2008), pp. 163–173.

[60] Shan Zhou et al. “Hydrogen peroxide emission and fate indoors during non-bleach cleaning: a chamber and modeling study”. In: *Environmental Science & Technology* 54.24 (2020), pp. 15643–15651.

[61] Dan Nørtoft Sørensen and Charles J Weschler. “Modeling-gas phase reactions in indoor environments using computational fluid dynamics”. In: *Atmospheric Environment* 36.1 (2002), pp. 9–18.

[62] CJ Weschler. “Chemistry in indoor environments: 20 years of research”. In: *Indoor Air* 21.3 (2011), pp. 205–218.

[63] Jialei Shen and Zhi Gao. “Ozone removal on building material surface: A literature review”. In: *Building and Environment* 134 (2018), pp. 205–217.

[64] Mingyao Yao and Bin Zhao. “Surface removal rate of ozone in residences in China”. In: *Building and Environment* 142 (2018), pp. 101–106.

[65] Moshood Olawale Fadeyi. “Ozone in indoor environments: Research progress in the past 15 years”. In: *Sustainable Cities and Society* 18 (2015), pp. 78–94.

[66] Roger Atkinson. “Kinetics and mechanisms of the gas-phase reactions of the hydroxyl radical with organic compounds under atmospheric conditions”. In: *Chemical Reviews* 86.1 (1986), pp. 69–201.

[67] Charles J Weschler and William W Nazaroff. “Growth of organic films on indoor surfaces”. In: *Indoor Air* 27.6 (2017), pp. 1101–1112.

[68] C Bloss et al. “Development of a detailed chemical mechanism (MCMv3. 1) for the atmospheric oxidation of aromatic hydrocarbons”. In: *Atmospheric Chemistry and Physics* 5.3 (2005), pp. 641–664.

[69] Sandra M Saunders et al. “Protocol for the development of the Master Chemical Mechanism, MCM v3 (Part A): tropospheric degradation of non-aromatic volatile organic compounds”. In: *Atmospheric Chemistry and Physics* 3.1 (2003), pp. 161–180.

[70] ME Jenkin et al. “Protocol for the development of the Master Chemical Mechanism, MCM v3 (Part B): tropospheric degradation of aromatic volatile organic compounds”. In: *Atmospheric Chemistry and Physics* 3.1 (2003), pp. 181–193.

[71] Michael E Jenkin, Sandra M Saunders, and Michael J Pilling. “The tropospheric degradation of volatile organic compounds: a protocol for mechanism development”. In: *Atmospheric Environment* 31.1 (1997), pp. 81–104.

[72] Golam Sarwar et al. “Hydroxyl radicals in indoor environments”. In: *Atmospheric Environment* 36.24 (2002), pp. 3973–3988.

[73] Golam Sarwar et al. “The significance of secondary organic aerosol formation and growth in buildings: experimental and computational evidence”. In: *Atmospheric Environment* 37.9-10 (2003), pp. 1365–1381.

[74] Nicola Carslaw. “A new detailed chemical model for indoor air pollution”. In: *Atmospheric Environment* 41.6 (2007), pp. 1164–1179.

[75] Xinke Wang, Yinping Zhang, and Jianyin Xiong. "Correlation between the solid/air partition coefficient and liquid molar volume for VOCs in building materials". In: *Atmospheric Environment* 42.33 (2008), pp. 7768–7774.

[76] LS Ettre, C Welter, and B Kolb. "Determination of gas-liquid partition coefficients by automatic equilibrium headspace-gas chromatography utilizing the phase ratio variation method". In: *Chromatographia* 35 (1993), pp. 73–84.

[77] Irving Langmuir. "The adsorption of gases on plane surfaces of glass, mica and platinum." In: *Journal of the American Chemical society* 40.9 (1918), pp. 1361–1403.

[78] Stephen Brunauer et al. "On a theory of the van der Waals adsorption of gases". In: *Journal of the American Chemical society* 62.7 (1940), pp. 1723–1732.

[79] Stephen Brunauer, Jan Skalny, and EE Bodor. "Adsorption on nonporous solids". In: *Journal of Colloid and Interface Science* 30.4 (1969), pp. 546–552.

[80] Jean Rouquerol et al. *Adsorption by powders and porous solids: principles, methodology and applications*. Academic press, 2013.

[81] Zhao Zhenguo. *Application Principle of Adsorption*. Ed. by Zhao Zhenguo. First Edition. Chemical Industry Press, 2005. ISBN: 9787502573683.

[82] Józef Nastaj, Konrad Witkiewicz, and Małgorzata Chybowska. "Modeling of multicomponent and multitemperature adsorption equilibria of water vapor and organic compounds on activated carbons". In: *Adsorption Science & Technology* 34.2-3 (2016), pp. 144–175.

[83] Anh Dung Tran Le et al. "Modeling the similarity and the potential of toluene and moisture buffering capacities of hemp concrete on IAQ and thermal comfort". In: *Building and Environment* 188 (2021), p. 107455.

[84] Jan Skalny and Nataliya Hearn. "Surface area measurements". In: *Handbook of analytical techniques in concrete science and technology, VS Ramachandran and JJ Beaudoin, eds. William Andrew Publishing/Noyes* (2001), pp. 505–527.

[85] Paul H Emmett and Stephen Brunauer. "The use of low temperature van der Waals adsorption isotherms in determining the surface area of iron synthetic ammonia catalysts". In: *Journal of the American Chemical Society* 59.8 (1937), pp. 1553–1564.

[86] Jacob N. Israelachvili. "6 - Van der Waals Forces". In: *Intermolecular and Surface Forces (Third Edition)*. Ed. by Jacob N. Israelachvili. Third Edition. San Diego: Academic Press, 2011, pp. 107–132. ISBN: 978-0-12-375182-9.

[87] HL Pickering and HC Eckstrom. "Physical adsorption of gases on anatase". In: *Journal of the American Chemical Society* 74.19 (1952), pp. 4775–4777.

[88] Aubrey Lester McClellan and HF Harnsberger. "Cross-sectional areas of molecules adsorbed on solid surfaces". In: *Journal of Colloid and Interface Science* 23.4 (1967), pp. 577–599.

[89] Mary Jo Gray et al. "Molecular mechanics and molecular cross-sectional areas: a comparison with molecules adsorbed on solid surfaces". In: *Journal of colloid and interface science* 170.1 (1995), pp. 98–101.

[90] Anthony L Hines and Robert N Maddox. *Mass transfer: fundamentals and applications*. Vol. 434. Prentice-Hall Englewood Cliffs, NJ, 1985.

[91] Elwin Hunter-Sellars et al. "Adsorption of volatile organic compounds by industrial porous materials: Impact of relative humidity". In: *Microporous and Mesoporous Materials* 298 (2020), p. 110090.

[92] Guangyu Cao et al. "Protected zone ventilation and reduced personal exposure to airborne cross-infection". In: *Indoor Air* 25.3 (2015), pp. 307–319.

[93] Meng Kong et al. "Measurements of grease emission and heat generation rates of electric countertop appliances (RP-1631, part 1)". In: *Science and Technology for the Built Environment* 22.6 (2016), pp. 845–865.

[94] Tsung-Hung Li et al. "Indoor hydrogen peroxide derived from ozone/d-limonene reactions". In: *Environmental Science & Technology* 36.15 (2002), pp. 3295–3302.

[95] Zhihua Fan et al. "Co-formation of hydroperoxides and ultra-fine particles during the reactions of ozone with a complex VOC mixture under simulated indoor conditions". In: *Atmospheric Environment* 39.28 (2005), pp. 5171–5182.

[96] Manolis N Romanias, Atallah El Zein, and Yuri Bedjanian. "Heterogeneous interaction of H2O2 with TiO2 surface under dark and UV light irradiation conditions". In: *The journal of physical chemistry A* 116.31 (2012), pp. 8191–8200.

[97] Yue Zhao et al. "Kinetics and mechanisms of heterogeneous reaction of gaseous hydrogen peroxide on mineral oxide particles". In: *Environmental science & technology* 45.8 (2011), pp. 3317–3324.

[98] Zhishi Guo. "Development of a Windows-based indoor air quality simulation software package". In: *Environmental Modelling & Software* 15.4 (2000), pp. 403–410.

[99] Ademir A Prata Jr et al. "A critical review on liquid-gas mass transfer models for estimating gaseous emissions from passive liquid surfaces in wastewater treatment plants". In: *Water Research* 130 (2018), pp. 388–406.

[100] Marzio Invernizzi et al. “Assessment of the chemical-physical variables affecting the evaporation of organic compounds from aqueous solutions in a sampling wind tunnel”. In: *Chemosphere* 220 (2019), pp. 353–361.

[101] Dustin Poppendieck, Heidi Hubbard, and Richard L Corsi. “Hydrogen peroxide vapor as an indoor disinfectant: removal to indoor materials and associated emissions of organic compounds”. In: *Environmental Science & Technology Letters* 8.4 (2021), pp. 320–325.

[102] Charles J Weschler and Helen C Shields. “Production of the hydroxyl radical in indoor air”. In: *Environmental science & technology* 30.11 (1996), pp. 3250–3258.

[103] Daniel Stone, Lisa K Whalley, and Dwayne E Heard. “Tropospheric OH and HO 2 radicals: field measurements and model comparisons”. In: *Chemical Society Reviews* 41.19 (2012), pp. 6348–6404.

[104] Argyro Lagoudi, Maria Loizidou, and Demosthenes Asimakopoulos. “Volatile organic compounds in office buildings: 1. Presence of volatile organic compounds in the indoor air”. In: *Indoor and Built Environment* 5.6 (1996), pp. 341–347.

[105] Catherine H Stephens and Eric M Breitung. “Impact of volatile organic compounds (VOCs) from acrylic double-sided pressure-sensitive adhesives (PSAs) on metals found in cultural heritage environments”. In: *Polymer Degradation and Stability* 193 (2021), p. 109738.

[106] AC Rai et al. “Ozone reaction with clothing and its initiated VOC emissions in an environmental chamber”. In: *Indoor air* 24.1 (2014), pp. 49–58.

[107] Jiangyao Chen et al. “OH radicals determined photocatalytic degradation mechanisms of gaseous styrene in TiO2 system under 254 nm versus 185 nm irradiation: Combined experimental and theoretical studies”. In: *Applied Catalysis B: Environmental* 257 (2019), p. 117912.

[108] Ilho Kim and Hiroaki Tanaka. “Photodegradation characteristics of PPCPs in water with UV treatment”. In: *Environment international* 35.5 (2009), pp. 793–802.

[109] Kristin Zoschke, Hilmar Börnick, and Eckhard Worch. “Vacuum-UV radiation at 185 nm in water treatment–a review”. In: *Water research* 52 (2014), pp. 131–145.

[110] David R Crosley et al. “Gas-phase photolytic production of hydroxyl radicals in an ultraviolet purifier for air and surfaces”. In: *Journal of the Air & Waste Management Association* 67.2 (2017), pp. 231–240.

[111] Jennifer A Logan et al. “Tropospheric chemistry: A global perspective”. In: *Journal of Geophysical Research: Oceans* 86.C8 (1981), pp. 7210–7254.

[112] David J Creasey, Dwayne E Heard, and James D Lee. “Absorption cross-section measurements of water vapour and oxygen at 185 nm. Implications for the calibration of field instruments to measure OH, HO2 and RO2 radicals”. In: *Geophysical Research Letters* 27.11 (2000), pp. 1651–1654.

[113] Christopher S Foote et al. *Active oxygen in chemistry*. Vol. 2. Springer Science & Business Media, 1998.

[114] B Eliasson and U Kogelschatz. “Ozone generation with narrow–band UV radiation”. In: (1991).

[115] Manfred Salvermoser, Daniel E Murnick, and Ulrich Kogelschatz. “Influence of water vapor on photochemical ozone generation with efficient 172 nm xenon excimer lamps”. In: *Ozone: Science and Engineering* 30.3 (2008), pp. 228–237.

[116] K Watanabe, Edward CY Inn, and Murray Zelikoff. “Absorption coefficients of oxygen in the vacuum ultraviolet”. In: *The Journal of Chemical Physics* 21.6 (1953), pp. 1026–1030.

[117] Holger Claus. “Ozone generation by ultraviolet lamps”. In: *Photochemistry and photobiology* 97.3 (2021), pp. 471–476.

[118] Andrew S Viner et al. “Ozone generation in DC-energized electrostatic precipitators”. In: *IEEE transactions on industry applications* 28.3 (1992), pp. 504–512.

[119] A Goldman and J Amouroux. “Plasma chemistry”. In: *NATO Advanced Study Institute (ASI) Series B* 89 (1983), p. 293.

[120] Charles J Weschler. “Ozone in indoor environments: concentration and chemistry”. In: *Indoor air* 10.4 (2000), pp. 269–288.

[121] Michael S Waring and J Raymond Wells. “Volatile organic compound conversion by ozone, hydroxyl radicals, and nitrate radicals in residential indoor air: Magnitudes and impacts of oxidant sources”. In: *Atmospheric Environment* 106 (2015), pp. 382–391.

[122] José Albaladejo et al. “A PLP–LIF kinetic study of the atmospheric reactivity of a series of C4–C7 saturated and unsaturated aliphatic aldehydes with OH”. In: *Atmospheric environment* 36.20 (2002), pp. 3231–3239.

[123] Heidi Hellén et al. “Carbonyl compounds in boreal coniferous forest air in Hyytiälä, Southern Finland”. In: *Atmospheric chemistry and physics* 4.7 (2004), pp. 1771–1780.

[124] Julia Hurst Bowman, Dennis J Barket, and Paul B Shepson. “Atmospheric chemistry of nonanal”. In: *Environmental science & technology* 37.10 (2003), pp. 2218–2225.

[125] Rui Zhang et al. “Effects of moisture content, temperature and pollutant mixture on atmospheric corrosion of copper and silver and implications for the environmental design of data centers (RP-1755)”. In: *Science and Technology for the Built Environment* 26.4 (2020), pp. 567–586.

[126] *Nitrogen Dioxide’s Impact on Indoor Air Quality*. https://www.epa.gov/indoor-air-quality-iaq/nitrogen-dioxides-impact-indoor-air-quality. Accessed Aug 20, 2023.

[127] Barbara Nozière, Ian Barnes, and Karl-Heinz Becker. “Product study and mechanisms of the reactions of α-pinene and of pinonaldehyde with OH radicals”. In: *Journal of Geophysical Research: Atmospheres* 104.D19 (1999), pp. 23645–23656.

[128] Clara MA Eichler et al. “Modeling the formation and growth of organic films on indoor surfaces”. In: *Indoor Air* 29.1 (2019), pp. 17–29.

[129] Breann Coffaro and Clifford P Weisel. “Reactions and products of squalene and ozone: A review”. In: *Environmental Science & Technology* 56.12 (2022), pp. 7396–7411.

[130] Jialei Shen et al. “A systematic approach to estimating the effectiveness of multi-scale IAQ strategies for reducing the risk of airborne infection of SARS-CoV-2”. In: *Building and environment* 200 (2021), p. 107926.

[131] Glenn C Morrison et al. “Indoor air quality impacts of ventilation ducts: ozone removal and emissions of volatile organic compounds”. In: *Journal of the Air & Waste Management Association* 48.10 (1998), pp. 941–952.

[132] *ASHRAE Duct Size Calculator*. https://www.ashrae.org/about/news/2016/new-duct-sizing-calculator-available. Accessed May 20, 2022.

VITA

Zhenlei Liu

Education

Ph.D., *Mechanical and Aerospace Engineering*, Syracuse University, USA Jan 2018 – Aug 2023
M.S., *Mechanical and Aerospace Engineering*, Syracuse University, USA Sep 2015 – Dec 2017
B.S., *Building Environment and Energy Engineering*, Shandong Jianzhu University, China Sep 2008 – July 2012

Work Experiences

Luneng Group Co., Ltd **Beijing, China**
Senior MEP Engineer Jul 2012 – Jun 2015

- Led multiple engineering teams to design MEP systems for a high-rise tower building complex with shopping malls, offices, apartments, and hotels at Beijing CBD.
- Simulated energy consumption by EnergyPlus for applying LEED Gold certification.
- Simulated temperature and air flow distribution of a lobby by STARCCM to ensure thermal comfort in summer and winter.
- Collaborated with a third-party vendor for the architecture of an Energy Management System.

Projects

Ph.D. Thesis: VOC Pollution Loads and Their Impacts on Indoor Air Quality
Oct 2021 – Aug 2023

- Developed an integrated indoor air quality (IAQ) model considering the synergistic effects of primary and secondary emission sources, ventilation, air purification, and chemical reactions of IAQ concern. Solve the model numerically in Python program
- Conducted full-scale experiments to characterize the secondary emissions from hydroxyl radicals and ozone-initiated chemistry under a pre-defined realistic reference office setting.
- Collected the categories and concentrations of VOCs by using the Gas Chromatography-Mass Spectrometry (GC-MS) and High Performance Liquid Chromatography (HPLC)
- Statistical analysis for VOCs samples' data with/without oxidants (hydroxyl radicals and ozone) in Python. It showed the pollutant load of the primary and secondary emission.
- Participate in Annex86 program and presented the related studies in their conference.
- Developed a similarity approach to estimate the diffusion and partition coefficients of building materials. It involved the storage and transport properties of materials, such as moisture isotherm curve and moisture transport.

A Comprehensive Test Method for Evaluating the Performance and Efficiency of Various Types of Air Cleaning/Purification Technologies under Realistic Room Environmental Settings
Mar 2021 – Present

- Developed a novel test method to evaluate air cleaning technologies under a realistic indoor setting with simulated constant emission sources
- Performed the measurements and analysis of VOCs, particles (SMPS and APS) and virus surrogate (PFU and qPCR).
- Studied the statistical correlation for describing the relationship between the concentration of the virus-laden particle and viral load in the air.
- Evaluated the pollutant removal efficiency, energy consumption, and noise level of different air cleaners.

- Predicted the performance of air cleaners and their impact on IAQ beyond the standard test condition by applying the IAQ model.

IEA-EBC Annex68: Indoor Air Quality Design and Control in Low Energy Residential Buildings Sep 2016 – Oct 2020

- Used indoor air quality modeling software, such as Indoor Air Quality and Inhalation Exposure (IAQX) to predict IAQ performance in the low-energy consumption reference residential building. Evaluated building energy consumption by DesignBuilder.
- Defined a reference residential building prototype for evaluating indoor air quality and energy efficiency strategies according to B10 Benchmark from NREL and a prototype designed for cold climate zone
- Developed a standard method for estimating diffusion coefficient, partition coefficient, and initial concentration in the material from the results of a standard chamber test with multivariate non-linear regression with MATLAB code

Chamber and Modeling Study of Hydrogen Peroxide Emission and Fate Indoors during Non-Bleach Cleaning May 2018 – Jan 2020

- Designed a reference test room to represent a typical indoor environment with carpeted floor, painted gypsum board walls and ceiling within a full-scale environmental controlled chamber
- Performed chamber tests to identify and quantify emissions from a commercial hydrogen peroxide based cleaning agent in the reference test room
- Collaborated with multiple research teams to investigate the impacts of light conditions (dark, artificial light, simulated sunlight) on formation of hydroxyl radicals

Smartphone App for Screening Formaldehyde Level in Residential Buildings Jan 2018 – Oct 2018

- Tested formaldehyde color-changing badges with various formaldehyde concentrations, humidity levels, and exposure times
- Correlated and calibrated the formaldehyde exposure amount (formaldehyde concentration multiples by exposure time) with RGB values of color-changing badges captured by various cameras

Skills

Laboratory techniques: GC/MS, HPLC, PTR-MS, SMPS, APS
Modeling tools: Designbuilder, EnergyPlus, CONTAM, Fluent, Solidworks, MATLAB, AutoCAD
Programming languages: C++, Python, R, Git/Terminal

Activities

President of the ASHRAE Syracuse University Student Branch Oct 2019 – Oct 2022

Publications

Journal paper

- **Liu, Z.**, Nicolai, A., Abadie, M., Qin, M., Grunewald, J., and Zhang, J. (2021). Development of a procedure for estimating the parameters of mechanistic VOC emission source models from chamber testing data. Building Simulation, 14(2), 269–282. https://doi.org/10.1007/s12273-020-0616-3
- Tran Le, A. D., Zhang, J. S., and **Liu, Z.** (2021). Impact of humidity on formaldehyde and moisture buffering capacity of porous building material. Journal of Building Engineering, 36, 102114. https://doi.org/10.1016/j.jobe.2020.102114

- Tran Le, A. D., Zhang, J. S., **Liu, Z.**, Samri, D., and Langlet, T. (2021). Modeling the similarity and the potential of toluene and moisture buffering capacities of hemp concrete on IAQ and thermal comfort. Building and Environment, 188, 107455. https://doi.org/10.1016/j.buildenv.2020.107455
- Kong, M., Zhang, J., Han, K., Guo, B., and **Liu, Z.** (2020). Development of a test method to determine the effectiveness of UVC systems on commercial cooking effluent (RP-1614). Science and Technology for the Built Environment, 26(9), 1285–1300. https://doi.org/10.1080/23744731.2020.1763144
- Zhou, S., **Liu, Z.**, Wang, Z., Young, C. J., VandenBoer, T. C., Guo, B. B., Zhang, J., Carslaw, N., and Kahan, T. F. (2020). Hydrogen Peroxide Emission and Fate Indoors during Non-bleach Cleaning: A Chamber and Modeling Study. Environmental Science and Technology, 54(24), 15643–15651. https://doi.org/10.1021/acs.est.0c04702
- Zhang, S., Shapiro, N., Gehrke, G., Castner, J., **Liu, Z.**, Guo, B., Prasad, R., Zhang, J., Haines, S. R., Kormos, D., Frey, P., Qin, R., and Dannemiller, K. C. (2019). Smartphone App for Residential Testing of Formaldehyde (SmART-Form). Building and Environment, 148, 567–578. https://doi.org/10.1016/j.buildenv.2018.11.029

Conference paper

- Rode, C., Grunewald, J., **Liu, Z.**, Qin, M., and Zhang, J. (2020). Models for residential indoor pollution loads due to material emissions under dynamic temperature and humidity conditions. E3S Web of Conferences, 172, 11002. https://doi.org/10.1051/e3sconf/202017211002
- Zhang, J., **Liu, Z.**, and Guo, B. (2019). Model-based testing and evaluation of VOC emission sources and sinks: Theory and application. IOP Conference Series: Materials Science and Engineering, 609, 042015. https://doi.org/10.1088/1757-899X/609/4/042015
- **Liu, Z.**, Nicolai, A., Abadie, M., Qin, M., and Zhang, J. (2018). Development of a Procedure for Estimating the Parameters of Mechanistic Emission Source Models from Chamber Testing Data. Healthy, Intelligent and Resilient Buildings and Urban Environments, 1193–1198. https://doi.org/10.14305/ibpc.2018.ms-7.02